Chairman:	Prof. Dr. Marlies Vanbael, Hasselt University
Promoter:	Prof. Dr. Tanja Junkers, Monash University – Hasselt University
Copromoter:	Prof. Dr. Dirk Vanderzande, Hasselt University
Members of the jury:	Dr. Neomy Zaquen, Lapinus BV
	Dr. Jasper Michels, Max Planck Institute for Polymer Research Mainz
	Dr. Evelien Baeten, Hogeschool Zuyd
	Prof. Dr. Simon Kuhn, Katholieke Universiteit Leuven

Table of Contents

Chapter 1

Introduction

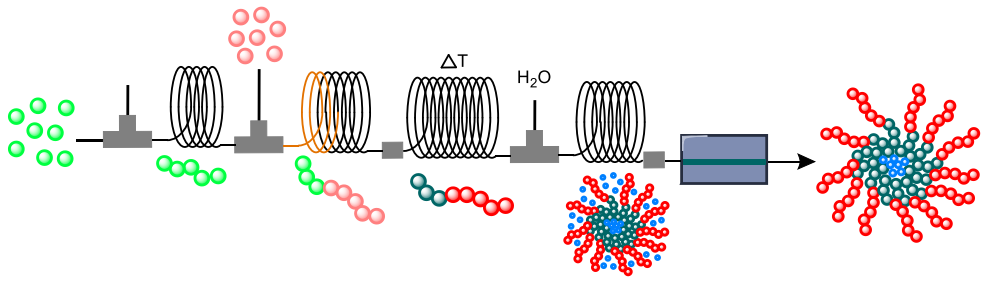

1.1. Polymer history

A polymer is a molecule with a high relative molecular weight and is built up out of smaller repeating units, called monomers. Polymers can be divided in natural and synthetic polymers. Nature bears a great variety of polymers, think about cellulose, sugar and rubber. And also in our bodies there are polymers present like our DNA and proteins. The first synthetic polymer was discovered by Leo Baekeland in 1907 with the synthesis of bakelite (poly(oxybenzyl methylene glycol anhydride): a hard moldable plastic out of phenol and formaldehyde.[1] This polymer was used worldwide as a plastic in for example telephones, electronic devices and toys. The start was made for the usage and synthesis of polymers for a variety of applications up to the present day. In 1920, Herman Staudinger published what is called the landmark paper, "Über Polymerization" and together with Jacob Fritschi they introduced in 1922 for the first time the concept of a macromolecule.[2,3] They presented experimental evidence that rubber is a macromolecule and therefore is a high molecular weight hydrocarbon with many ethylene bonds.[4] Another pioneer worth mentioning is Charles Goodyear who invented the vulcanization of rubber in 1839, long before the actual 'discovery' of polymer science.[5]

1.1.1. Start of the 'plastic' generation

A few years after the publication of Staudinger's landmark paper, the growth of the polymer field kicked off leading to more understanding and studies on polymerizations. Synthetic polymers and polymer techniques were discovered which are still used nowadays. One of the inventors of these polymers and techniques is Wallace Carothers. He invented nylon and laid the foundations of the discovery of neoprene. Carothers team was able to produce polyesters with a high molecular weight and therefore the first silk was synthesized. Carothers looked further into the polymerization technique of condensation polymers that are formed by step-growth polymerization and inspired on his turn a lot of polymer scientists. One of them was Paul Flory who discovered the way polymers are dissolved in a solvent. Moreover, he was one of the founders of living polymers (besides Szwarc[6]) due to his predication on the lack of termination in a polymerization which leads to a Poisson molecular weight distribution.[7] Lastly, two names that cannot be forgotten are Karl Ziegler and Giulio Natta who developed the use of catalysts for polymerization reactions.[8,9] With this the start of the modern plastic industry was made and a variety of polymer products was developed.

Nowadays, synthetic polymers can be found not only in these widely used plastics, but also specialty polymers gain more and more interest due to the extensive research performed on polymer chemistry. These specialty polymers can find their applications in for example: electronics, batteries, automotive and even in data storage and the biomedical field (e.g. drug delivery and bioimaging). The application of specialty polymers in the biomedical field will be further addressed in this thesis.

1.2. Polymerization techniques

Polymerization reactions can proceed via different mechanisms, with the step-growth and chain-growth as the most prominent ones. In step-growth polymerizations, which mostly require a catalyst, the polymer will grow by stepwise addition of monomers in time. At the start of the reaction mostly monomers are available, therefore they will first react with each other leading to very short polymer chains. Carothers derived an equation (given below) for a step-growth polymerization which shows that to achieve a high degree of polymerization, a high monomer conversion is required.[10]

$$X_n = \frac{1}{1-p}$$

X_n is the number average degree of polymerization and p is the monomer to polymer conversion.

Accordingly, the development of high molecular weight products is only possible at high conversions. A multitude of commercial polymers such as polyamides (nylon), polyesters and polyurethanes are synthesized via step-growth polymerization (e.g. polycondensation or polyaddition).

Otherwise, in chain-growth polymerizations, an initiator is used to start the reaction and high molecular weight polymers are directly achieved. A chain-growth reaction such as free radical polymerization, usually consists out of four stages: initiation, propagation, chain transfer and termination, as shown in Scheme 1.

Firstly, decomposition of an initiator molecule, which is mostly activated by heat or light, takes place. The initiator falls apart in two species with an electron deficiency, called radicals. These free radicals are very reactive and have therefore a short lifetime. The second step of the initiation takes place when the free radical of the initiator reacts with the monomer. A new free radical species is formed and will in turn react with another monomer molecule, this is the propagation step which will go on until a termination reaction takes place. There are two types of termination: recombination and disproportionation. Recombination happens when two radicals of the growing chains (or a growing chain and an active initiator) react with each other and a longer, stable polymer chain is formed. Disproportionation occurs when one growing chain transfers a hydrogen atom to another growing chain and two stable polymer chains are formed. Lastly, chain transfer reactions can occur where the active centre of the growing chain is transferred to another molecule, this can be a monomer, a polymer chain, a solvent or a chain transfer agent.

Decomposition	I_2	$\xrightarrow{k_d}$	$2\ I^{\bullet}$
Initiation	$I^{\bullet} + M$	$\xrightarrow{k_i}$	$R_1^{\bullet}$
Propagation	$R_i^{\bullet} + M$	$\xrightarrow{k_p}$	$R_{i+1}^{\bullet}$
Chain transfer	$R_i^{\bullet} + X$	$\xrightarrow{k_{tr}}$	$P_i + X^{\bullet}$
Termination	$R_i^{\bullet} + R_j^{\bullet}$	$\xrightarrow{k_t}$	P_{i+j} and/or $P_i + P_j$

Scheme 1: General overview of the different reactions occurring in free radical polymerization

If no chain transfer or termination occurs during the polymerization reaction, a living polymerization is achieved. In a living polymerization, the amount of polymer chains that are produced is equal to the amount of initiator, all chains will keep growing until all the monomers are consumed and the polymer chain end will stay active during the polymerization, Figure 1.

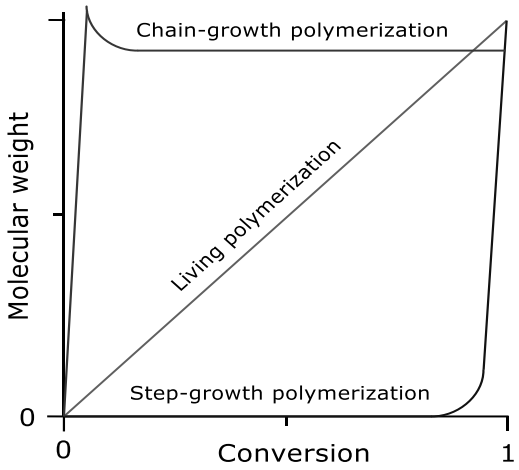

Figure 1: Molecular weight for increasing monomer conversion for general chain-growth, step-growth and living polymerization mechanisms

A polymerization can be classified as living when following criteria are fulfilled: (i) the number average molecular weight is controlled by the monomer conversion and the ratio between the monomer and initiator concentration (the degree of polymerization), (ii) no termination or chain transfer is allowed which extends the lifetime of the propagating chain, (iii) the rate of initiation is fast which leads to narrow dispersities. When all these criteria are fulfilled, a linear relationship between the molecular weight and the monomer conversion is achieved. In the next sections some specific (living) polymerization reactions are highlighted.

1.2.1. Reversible-deactivation radical polymerizations

In radical polymerizations, termination reactions can never be completely avoided. Therefore, it is incorrect to use the term living or controlled radical polymerization when termination reactions are occurring. Hence, the term reversible-deactivation radical polymerization (RDRP) is introduced to define these reactions.[11] In order to minimize chain transfer and termination events, the lifetime of the radicals need to be elongated. The mechanism of this polymerization technique requires a dormant species (P_n-X) which can be activated to a radical species (P_n^*) that can undergo propagation, see Scheme 2 where the mechanism of an atom transfer radical polymerization (ATRP) is given as an example of an RDRP reaction. When the reaction equilibrium is shifted towards the dormant species, less active radical species are present and the termination (radical-radical coupling) is minimized.

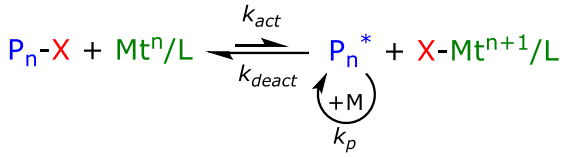

Scheme 2: Reaction mechanism of atom transfer radical polymerization with P_n the polymer chain, X a halogen, Mt a metal (mostly copper) and L a ligand. K_{act}, k_{deact} and k_p represent respectively the activation, deactivation and propagation rate constants

Shifting the equilibrium towards the dormant species can be realized by deactivating the radical species. The most prominent reaction mechanisms with these properties are atom transfer radical polymerizations (ATRP)[12], nitroxide-mediated polymerizations (NMP)[13] and reversible addition-fragmentation chain

transfer polymerizations (RAFT)[14]. The RDRP reactions used in this thesis can be classified under the copper(0)-mediated RDRP which also includes ATRP, it is therefore interesting to elucidate a bit more on this specific reaction type. The first ATRP reaction was catalysed with a copper complex and was first reported in 1995 by Jin-Shan Wang and Krzysztof Matyjaszewski.[15] It quickly became one of the most used and effective methods of RDRP. Two years later, in 1997, Matyjaszewski introduced for the first time an RDRP reaction with Cu(0) and suitable ligands.[16] However, almost ten years later in 2006, Virgil Percec proposed a Cu(0)-mediated RDRP with a very different mechanism (Scheme 3), single electron transfer living radical polymerization (SET-LRP).[17] In ATRP the alkyl halide (P_n-X) reacts with a lower oxidized transition metal (Cu(I)) to form the higher oxidized transition metal (Cu(II)) and the radical ($P_n^{\cdot}$), since this is an equilibrium also the reverse reaction occurs. In SET-LRP the alkyl halide is activated by Cu(0) and forms the radical and Cu(I), which spontaneously disproportionate into Cu(0) and Cu(II). Cu(0) again rapidly activates the alkyl halide and Cu(II) deactivates the radical. There are several other types of ATRP, but these will not be discussed in this thesis.

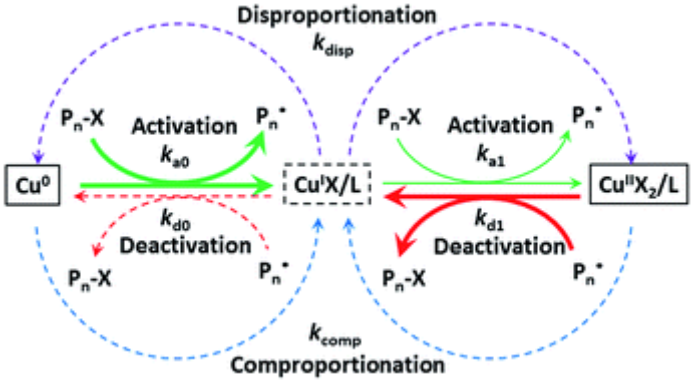

Scheme 3: Mechanism of SET-LRP reaction[18]

1.2.2. Anionic and cationic polymerizations

Another type of polymerizations used in this thesis can be classified under ionic polymerizations, it is therefore interesting to elucidate a bit more on this specific reaction type. Ionic polymerization reactions proceed via a chain-growth mechanism, the propagation species can be anionic or cationic, see Scheme 4. These polymerization reactions require stabilization of the active ion. In anionic polymerizations, the active anion can be stabilized by electron-withdrawing substituents (or via delocalization of the negative charge) on the monomer. Cationic polymerizations require the stabilization of the cation, by electron-donating substituents on the monomer. Ring opening polymerizations (ROP) of heterocyclic monomers also proceed via an ionic mechanism.

Commonly, ionic polymerizations can be depicted as living polymerization as the molecular weights increase linearly with the conversion and the termination reactions are reduced. Generally, ionic polymerizations are very sensitive to impurities or oxygen, so the reactions need to be carried out with high reagent purities and inert reaction conditions.[19]

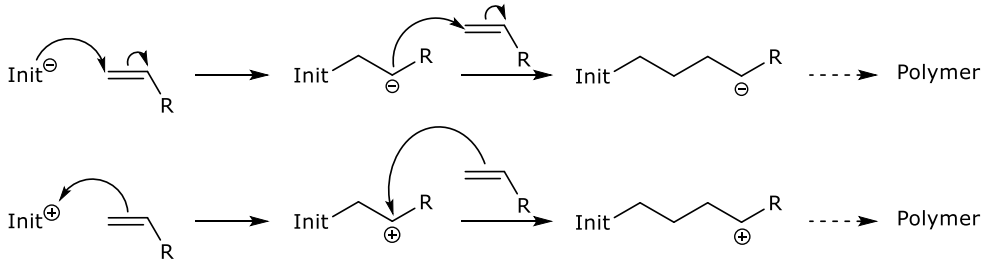

Scheme 4: General reaction scheme for the anionic and cationic polymerization

1.3. Polymer architectures

The properties of polymers are determined by their macromolecular structure, making it possible to achieve control over for example the solubility and critical solution temperatures. Complex architectures can be designed due to the development of the living polymerization techniques with tailored monomers and initiators. The polymer architecture can be classified by its composition, topology and functionality, see Figure 2.

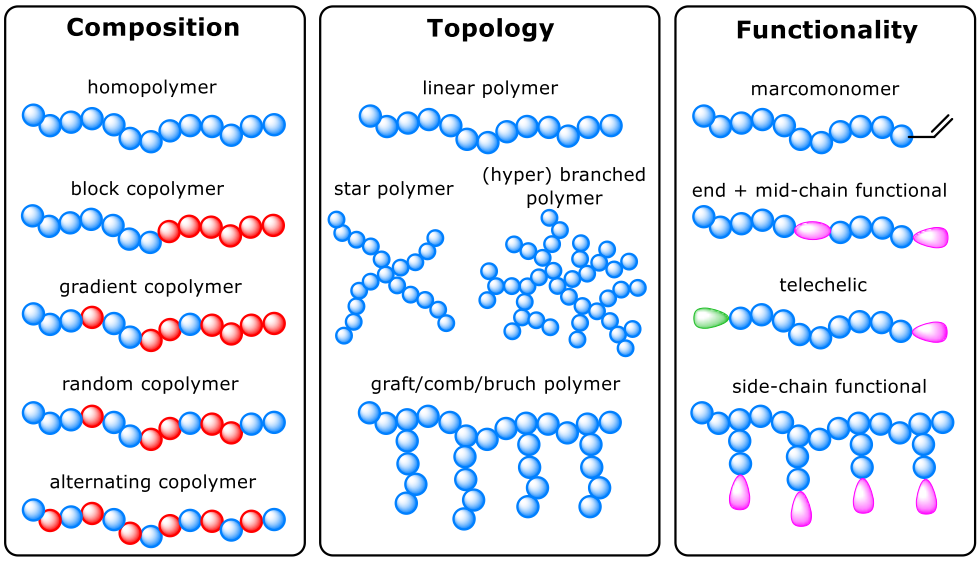

Figure 2: Classification of polymer architectures by composition, topology and functionality

The composition of the polymer is determined by the order wherein the monomers are arranged in the (co)polymer. If only one monomer is used in the polymerization a homopolymer is formed, if two or more different monomers are used a copolymer is formed. The copolymer composition includes block-, random/statistical-, periodic-, gradient/tapered- and graft copolymers.[20]

Another classification can be made by the topology, which is determined by the shape of the polymers. The architecture of the polymer can be varied and structures such as linear, star, comb/brush and (hyper)branched can be distinguished. A linear polymer is the simplest topology a polymer can have. Otherwise, star polymers are composed of a multifunctional initiator which forms the core and linear polymers which are the arms. These star polymers can be constructed via the core-first, arm-first and grafting onto approach.[21] Comb/brush polymers consist of two or more blocks that are grafted through the backbone of the polymer. Lastly, (hyper)branched polymers are – as its name suggests – polymer structures with two or more branching points. All the different kinds of polymer topologies can give the synthesized polymer various properties that are contrasting with the linear homopolymer.

The functionality of the polymers is determined by the presence and position of a functional group. Functionalities can be introduced by initiators and functional monomers at one end (chain-end), both ends (telechelic), in the middle (mid-chain) or at the side (sidechain) of the polymer chain.

In a next step, the polymer architecture can become more complex by the spontaneous organization of the polymers into stable structures with non-covalent interactions, also called self-assembly. The non-covalent interactions that hold these structures together are often specific secondary interactions such as hydrogen bonding, van der Waals interactions, π-π interactions, hydrophobic and hydrophilic interactions.[22] Block copolymers are well-known for their self-assembly when the different blocks have distinct properties. Amphiphilic block copolymers are a special kind which have a hydrophobic block and a hydrophilic block that tend to self-assemble in different architectures depending on the

characteristics of the blocks and the environment. In aqueous solutions, the contact of the hydrophobic block with water is minimized by the hydrophilic block that forms the coronae. Different morphologies such as micelles, vesicles or tubes can be obtained by the nature and lengths of the particular blocks. Their architecture is determined by the packing parameter (p), which is dependent on the volume (v) and length (l_c) of the hydrophobic block and the contact area (a_0) of the hydrophilic block. A schematic diagram is depicted in Figure 3.

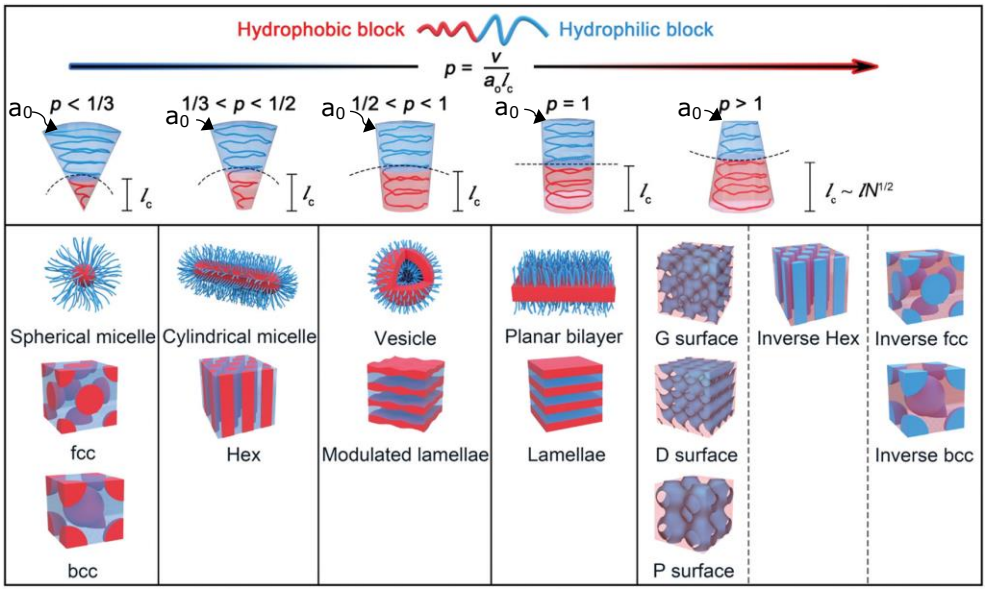

Figure 3: Schematic diagram of block copolymer self-assembly[23]

1.4. Continuous flow chemistry

1.4.1. General overview of continuous flow chemistry

Continuous flow chemistry is used in chemical engineering for over a century. The first flow reactors that were built by engineers were often complex modular units or silicon chips.[24] More recent, flow chemistry is scaled down and has become very interesting as a tool for organometallic and organic synthesis and is known for solving complex chemical problems.[25] Microflow reactors are one example of continuous flow reactors, feature micrometer dimensions, and have an enhanced control of the reaction conditions. Flow chemistry has already proven a lot of benefits towards the synthesis of natural products, heterocycles and in the field of photochemistry.[26,27,28] It is typically used because its superiority towards batch reactors in terms of mass- and heat transfer. Moreover, small hold-up volumes, excellent residence time control and easy scale up possibilities (*e.g.,* numbering-up) emphasize the paradigm shift in recent chemical research.[29] In this thesis the benefits of flow chemistry become clear by using flash chemistry for anionic polymerizations and self-assembly of block copolymers with their in-line purification in continuous flow reactors. The continuous flow tubular reactors used in this thesis consist of polytetrafluoroethylene (PTFE) or perfluoroalkoxy copolymers (PFA) tubing. The reagents used in the flow reaction are introduced into the reactor via a pumping mechanism and are performed using a relatively inexpensive syringe pump or a HPLC pump.

Flow reactions can be performed in all the different states of matter (gas, liquid and solid), off course different states need different approaches on the design of the continuous flow system. Many chemical reactions involve multiple phases such as gas-liquid, liquid-liquid or solid-liquid reactions.[30] To perform these reactions

with high reactivity, various mixing strategies are employed. This mixing can be subdivided into micro-, meso- and macro-mixing. Micro-mixing is defined as diffusive mass transfer, which is the movement of a substance from high to low concentration. On the micro-mixing level, substances are mixed on the molecular scale where chemical reactions take place. Macro-mixing is the largest mixing scale present in the reactor and mainly realizes macroscopic convective turbulent transport of substances, where convection is the movement of a substance with the bulk flow.[31,32] Lastly, meso-mixing takes place on the scale between micro- and macro-mixing, where molecular and viscous diffusion are important and wherein the turbulent exchange between the incoming substance stream and the environment is described.[33]

Further, the flow regimes accompanied with the above explained different phase systems can be diverse, most prominent regimes for gas-liquid reactions are slug flow (Tayler flow)[34], bubble flow and annular flow. Liquid-liquid systems are mostly characterized by laminar flow, turbulent flow or slug flow regimes and lastly, for solid-liquid reactions packed beds are frequently used. Since this thesis only covers miscible liquid phase systems, the other systems will not be discussed in more detail. The flow regimes of miscible liquids involve mostly laminar and turbulent flow profiles. A laminar flow profile can be defined by liquid layers flowing past each other with almost no mixing. The laminar flow regime is most prominent when the flowrate is low and is characterized by a parabolic flow profile, see Figure 4. This profile is caused by the lower flow rate of the liquids close to the tubing wall compared to the liquids in the center of the tubing due to frictional forces between the liquid layer and the tubing. This parabolic flow profile must be considered when expecting a laminar flow because it can cause residence time distributions which can be problematic for some reactions and product grade. On

the other hand, turbulent flow is, as the name suggests, a flow regime where much more lateral mixing occurs.

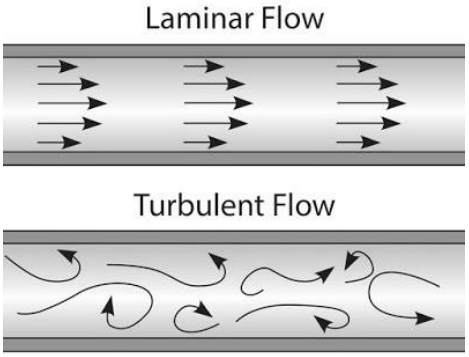

Figure 4: Laminar and turbulent flow regimes[35]

Which of the two takes place depends on the flow rate of the fluids and is determined by the Reynolds number.[36] The Reynolds number (Re), described by the equation below, is dependent on the density (ρ) and characteristic velocity (v) of the fluid, the dimensions of the reactor tubing (d) and the dynamic viscosity (μ) of the reaction mixture. If the Reynolds number is equal to or less then 2100, a laminar flow regime is most prominent and above 4000, turbulent flow will be mostly pronounced.[37]

$$Re = \frac{\rho v d}{\mu}$$

1.4.2. Advantages and challenges of continuous flow chemistry

Continuous flow chemistry brings a lot of advantages to organic and polymer synthesis, part of these advantages are highlighted here. Efficient mixing on the millisecond scale can be ensured by the constant motion of the reagents in the continuous flow reactor, which is in strong contrast with batch processes where mixing happens typically on a second's scale. In fact, the efficient mixing indicates that the concentration gradient is minimized in continuous flow processing and

therefore the formation of byproducts is suppressed.[38,39] The stoichiometry in flow reactions can be adjusted more easily than in batch reactions. In batch reactions the stoichiometry is determined by the initial concentration of chemical reagents, while in flow reactors the stoichiometry can be easily varied by changing the ratio of the flow rates from the reagents.[40] In this way, reaction conditions can be easily screened and optimized. Flow chemistry is also typically used because its superiority towards batch reactors in terms of mass-and heat transfer. Highly controlled and fast heat transfer can be accomplished due to the small reactor volumes related to the size of the reactor channels, leading to a high surface to volume ratio of continuous flow reactors in comparison with batch reactors.[41] This leads to almost ideal isothermal reaction conditions throughout the whole reactor, whereby less side reactions, higher product yields and polymers with highest performance are achieved.[42]

The flow rate and therefore also the residence time can be easily varied and perfectly controlled, this is for example a major advantage for the regulation over the dispersity and molecular weight in polymer synthesis.[43,44] Due to the uniform heat transfer, very good mixing and excellent residence time control, continuous flow chemistry is very reliable and reproducible.

Safety of operation can be assured in flow reactors due to the closed reaction environment and is especially advantageous when using highly exothermic, explosive or toxic reagents.[45] Moreover, microreactors retain small hold-up volumes, which ensures minimized risk on reactor failing. By performing the reaction under harsh conditions, such as superheated and supercritical conditions, the reactivity of the reaction can be increased under perfectly controllable conditions, also called chemical intensification, resulting in shorter residence times with higher product yields.[46] Also flash chemistry can be seen as a kind of chemical

intensification and will be used in chapter 3. In flash chemistry extremely fast reactions are performed with high reaction process control which would not be possible to maintain in batch.[47]

Besides temperature-controlled reactions, electrochemical or photochemical reactions could also largely benefit from continuous flow processing. The small channel dimensions of the flow reactor make the travel distance of the light really small, therefore less light is absorbed by the reaction medium then in common batch reactors.[48]

The scale up of the reaction can be achieved by several different ways. Firstly, reactor tubing/channels can be made longer in order to increase the total reactor volume while respecting the same residence time (increase in flow rate). Alternatively, a numbering-up system can be introduced where reactors are coupled in parallel in order to increase throughput, without altering any reaction parameters. Or another way is to simply let the reaction run for a longer period of time (scale-out principle) and let the reactors operate continuously.[38] This is possible since only minimal supervision is necessary when flow reactors are operating in a steady state regime. Multi-step synthesis where several reactors can be coupled in series is also possible.[49]

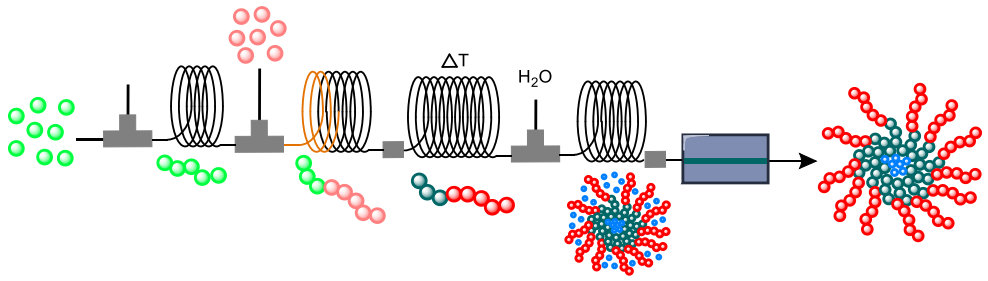

Figure 5: Example of a cascade of reactors with different properties for each reactor like length, temperature and tubing

Figure 5 shows a possible cascade of reactors specifically for this thesis where the different chapters considering flow polymerization, block copolymerization, micellation and purification are combined. However, this figure is somewhat simplistic since solvent changes and dilution effects must be considered. Inline purification techniques make continuous flow processing very attractive due to the time efficiency and the integration of multi-step synthesis, which will be further discussed in chapter 5. Automation allows for better control over time-sensitive synthetic reactions and easier and more rapid reaction optimization, including in situ reaction monitoring.[50,51]

Despite the rapid development of continuous flow chemistry, a lot of organic and polymer chemistry is still being carried out in a very traditional way. Reactions are typically performed in standardized glassware and compounds are synthesized batchwise. However, chemists are learning new ways of thinking because time and costs determine today's laboratory work more and more. An issue for industry is the big initial investment they may have to make in order to start using flow chemistry. But they must keep in mind that in order to scale-up the process, batch reactors need to be replaced, while flow chemistry can be scaled-up by numbering-up procedures, as mentioned before. However, some aspects of flow chemistry need to be further explored, *e.g.,* the automation is still in its infancy and there are also some major limitations arising when using flow chemistry. The most important one is the formation of solids during the reaction. Due to the small dimensions of the flow reactor, clogging of the reactor can occur. Solutions to overcome solid encounters in micro flow reactors can be ultra-sound, increased flow velocity, use of gas-liquid flow and the usage of fixed beds to adopt immobilized reagents or catalysts.[46]

1.5. Conjugated polymers

Conjugated polymers play a very important role in many different disciplines in chemistry, due to their remarkable (opto)electronic properties they possess.[52] These polymers have large domains of delocalized, polarizable π-electrons which make them excellent candidates for the use in devices such as light-emitting diodes (LEDs), organic photovoltaics (OPVs) and field-effect transistors (FETs).[53,54,55] The first conducting polymer was reported by H. Shirakawa[56], A.G. MacDiarmid[57] and A.J. Heeger[58]. They found that the conductivity of intrinsically semiconducting polyacetylene increased upon doping the polymer with electron-withdrawing compounds.[59,60] This discovery was the start of the investigation and development of a variety of conjugated polymers of which some very prominent ones are shown in Figure 6.[52] The conductivity of these conjugated polymers is induced by charge carriers, which make these polymers semiconducting materials. As a result, the combination of the properties of traditional polymers and the electrical and optical properties of these semiconductors, a whole new field can be explored.

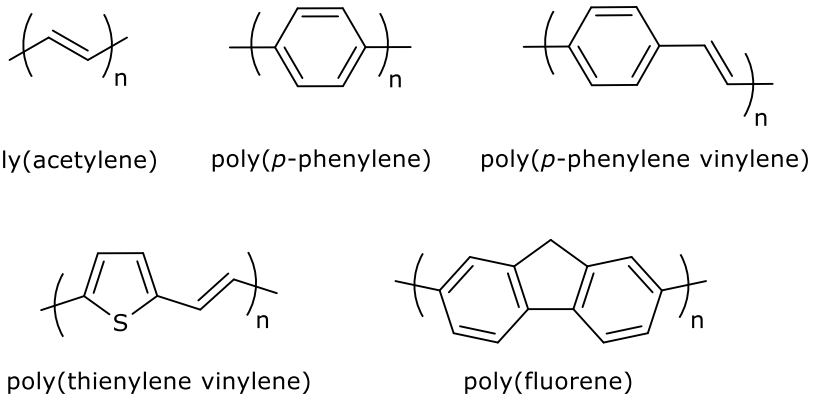

poly(acetylene) poly(*p*-phenylene) poly(*p*-phenylene vinylene)

poly(thienylene vinylene) poly(fluorene)

Figure 6: Examples of some very common conjugated polymers

1.5.1. Electronic properties

The conductivity in these conjugated polymers is induced by their π-conjugation (delocalization of electrons along the polymer backbone) and makes that these polymers are semiconducting materials. In order to achieve conductive materials, oxidation or reduction (doping) of the materials should occur, leading to transport of the charges along the polymer backbone (interchain mobility) or between backbones of different polymer chains (interchain hopping).[61] Upon doping, charges are generated that can be delocalized over the π-orbitals and depending on whether oxidation or reduction occurs, respectively p-type (creation of holes) or n-type conductive materials (creation of valence electrons) can be obtained. In semiconducting materials electrons can be transported from a lower energy bonding π orbital to a higher energy antibonding π* orbital, see Figure 7. The energy difference between the HOMO (highest occupied molecular orbital) and the LUMO (lowest unoccupied molecular orbital) is called the band gap (E_g) and determines the electrical properties of the material (conductor, semiconductor, insulator). The bandgap of semiconducting polymers is stretched between 0.5 and 4 eV. The HOMO and LUMO levels (and thereby also the bandgap) of conjugated polymers can be changed by modifying the monomer structure, disruption of the conjugation length, steric hindrance from side chains or by defects in the polymer chain.[62] A lower band gap can for example be achieved by increasing the conjugation length of the polymer.

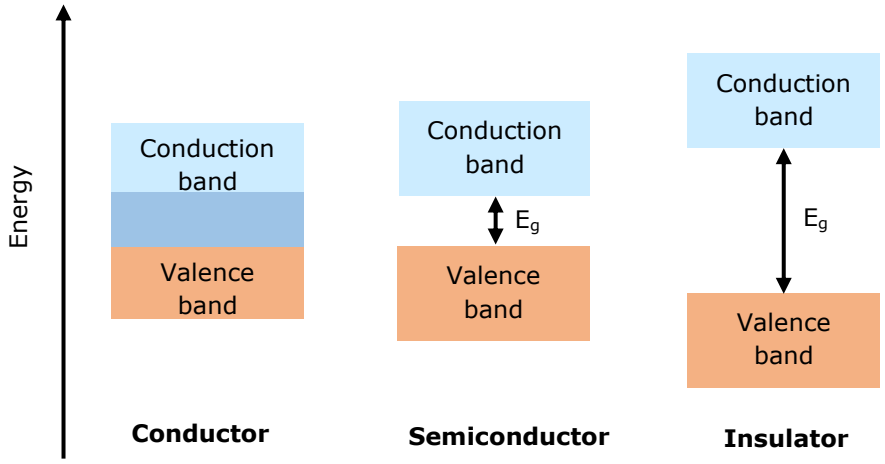

Figure 7: Band gap diagram of different materials (conductor, semiconductor and insulator)

1.5.2. Optical properties

The bandgap of conjugated polymers gives them not only interesting electrical properties, also their optical properties are appealing. Depending on the size of the bandgap photons with different energy can be absorbed and emitted, leading to distinct colors. A photon can be absorbed by the polymer and when it has enough energy, it can excite an electron from the HOMO level into the LUMO level (Figure 8). The excitation can be triggered by light (photoluminescence) or by electrical charges (electroluminescence). An exciton is created which can fall back to the ground state via several routes. When the emission of the photon occurs between states of the same spin (via internal conversion), the process is called fluorescence. When the emission of the photon occurs between two different spin states (via intersystem crossing), the process is called phosphorescence.

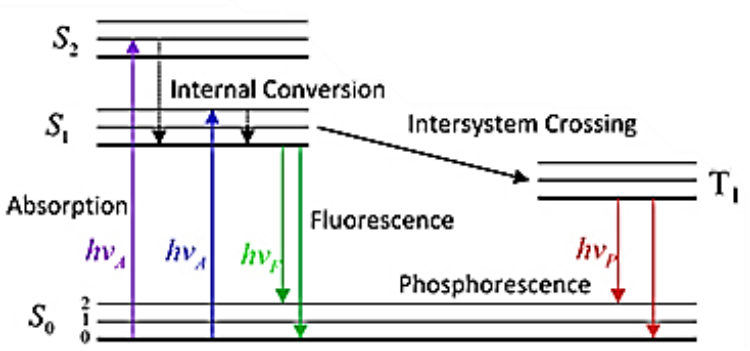

Figure 8: Jablonski diagram[63]

1.6. Poly(*p*-phenylene vinylenes) (PPVs)

Poly(arylene-vinylene)s (PAVs) are an interesting class of conjugated polymer materials due to their electroluminescent properties. The first organic light emitting device (OLED) was derived from poly(*p*-phenylene vinylene) (PPV) (Figure 6), one of the most widely studied PAVs due to their excellent electrical and optical properties.[53] Nevertheless, PPVs have lost some significance in the last years due to new generations of conjugated polymers being developed. Yet, PPV and its derivatives are among the most common types of conjugated polymer materials due to their robustness, high reproducibility and relatively simple reaction scale up.[64] The substantial improvements of controlled synthesis procedures and subsequent characterization promoted PPV for the use in a variety of complex polymer architectures. Despite their use in optoelectronics being decreased, PPVs remain interesting and are ideal candidates for the use in biomedical applications (see section 1.7.1.) due to their excellent fluorescent properties, high reproducibility in synthesis and non-toxic character.[65,66] In order to synthesize these conjugated polymer materials, different synthesis routes were developed. A distinction can be made between two major classes of synthesis routes for PAVs: direct and indirect/precursor routes. In the direct routes, the conjugated polymer is formed in one step, whereas in the precursor routes a *p*-quinodimethane species is polymerized into the precursor polymers, which in a second step can be converted into the conjugated polymer structure. Ring opening metathesis polymerizations (ROMP) belong to the indirect polymerization methods as well, but these polymerizations will not be discussed further in this thesis.

1.6.1. Synthesis of PPVs *via* direct routes

Synthesis of PPVs *via* the direct route follow a step-growth mechanism. Prominent reactions for the step-growth synthesis of PPVs are the Wittig,[67] Horner,[67,68] McMurry,[69] Knoevenagel[70,71] and Siegrist[72] polycondensations or the palladium-catalyzed Heck,[73,74] Stille[75] and Suzuki[76] cross-coupling reactions. Although most of these direct routes are easy to carry out, only low molecular weight polymers can be achieved since they are polymerized via the step-growth mechanism. As a result, polymers with a higher molecular weight and more complex architectures require the use of chain-growth polymerization methods.[77,78]

1.6.2. Synthesis of PPVs *via* the precursor routes

In the last decades, many efforts have been made to synthesize PPVs in a controllable manner. In order to overcome the disadvantages of the direct step-growth synthesis of PPVs, the indirect/precursor routes, which follow a chain-growth mechanism, are introduced. This allows to create – in principle – well-defined end groups and chain lengths due to the relatively fast and cost-effective synthesis approach.[19] Especially the precursor routes take an important role here. In these methods, disubstituted xylenes are activated by a base to form a quinodimethane derivative that can then undergo polymerization. Conjugation of the polymer chain is only achieved in a last step, when the polarizer group is eliminated. Different precursor routes were established, depending on the choice of the so-called leaving group and polarizer. The symmetrical premonomers are employed in the Gilch[79], Wessling[80,81], Xanthate[82,83] and dithiocarbamate[84,85] routes. Remarkably, an asymmetric premonomer is used in the sulfinyl (also known as Vanderzande) route, which makes it possible to completely decouple the polymerization process from the elimination of the polarizer group, see

Scheme 5. [86,87,88] This results in polymers with very low defect levels and thereby leading to the synthesis of distinct polymer materials with excellent optical properties.[89,90]

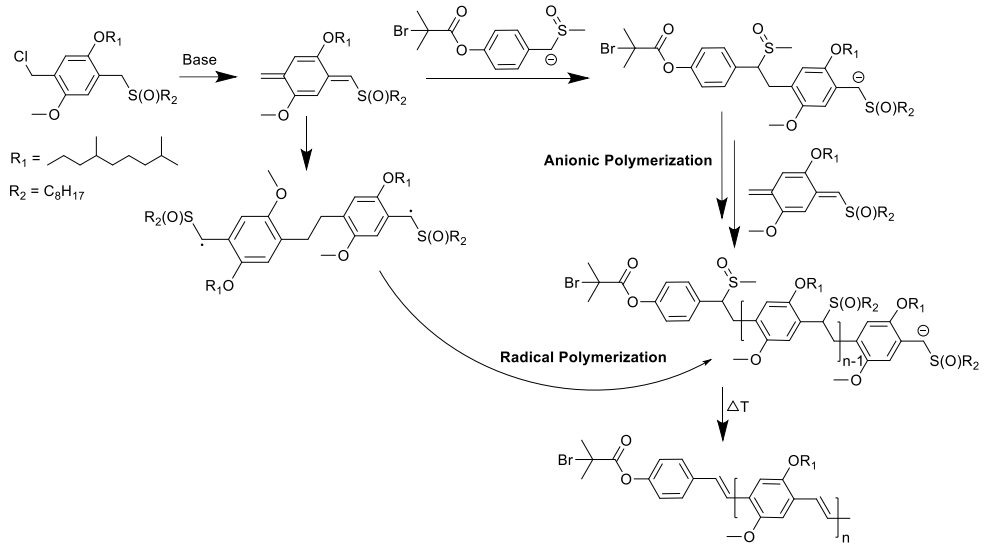

Scheme 5: Radical and anionic polymerization mechanism of the sulfinyl precursor route towards MDMO-PPV

Another remarkable advantage of the Vanderzande route is that the polymers can be formed either via radical or anionic polymerization, depending on the choice of solvent and base.[91,92] Both pathways start with the abstraction of a proton from the premonomer with a base, followed by the 1,6-elimination of the leaving group to enable the formation of a *p*-quinodimethane system. This *p*-quinodimethane system is the actual (unstable) monomer which can, via two different pathways, be polymerized into the precursor polymer. In most precursor routes, the active monomer is polymerized via self-initiation of monomer dimers, leading to the propagation via a radical pathway. In the anionic route, however, the base not only forms the active monomer species, but also deprotonates an anionic chain

initiator after which chains will grow until all the monomer has been consumed. In this way, specific functional groups can be introduced during the anionic polymerization. The anionic polymerization pathway is preferred due to its living character, while the radical pathway is known for its high molecular weight polymers and greater tolerance to reaction conditions. Whether the radical or the anionic pathway is followed, is depending on the type of base and solvent used during the reaction. To exclusively follow the anionic pathway, the sterically hindered lithium bis(trimethylsilyl)amide (LHMDS) must be used as the base and THF is typically chosen as the solvent, due to its aprotic character and its ability to stabilize the anionic chain ends. [93,94] In a last step, the conjugated polymer can be formed via elimination of the polarizer group by thermal or base induced treatment.[78]

Concerning the solubility of the precursor and conjugated polymers in organic solvents, long and flexible side chains are introduced on the aromatic core of the premonomers.[95] A few examples of some very interesting PPV derivatives are poly[2-methoxy-5-(3',7'-dimethyloctyloxy)-1,4-phenylenevinylene] (MDMO-PPV), poly[2-methoxy-5-(2'-ethylhexyloxy)-1,4-phenylenevinylene] (MEH-PPV), poly[2,5-bis(2'-ethylhexyloxy)-1,4-phenylenevinylene] (BEH-PPV), poly[2-methoxy-5-(carboxypentyloxy)-1,4-phenylenevinylene] (CPM-PPV) and poly[(2,5-dicyano)-1,4-phenylenevinylene] (CN-PPV) of which MDMO-PPV is the most studied one in this thesis.

1.6.3. Synthesis of PPV containing block copolymers

In order to synthesize complex polymer architectures with the rather stiff PPV polymer, a flexible second block can be introduced. PPVs and other conjugated polymers are rigid and have limited solubility due to their delocalized electronic structures and interchain π-π interactions. When a flexible polymer block is covalently bonded to the PPV block, a rod-coil block copolymer is obtained and hereby a variety of morphologies and nanostructured materials become available, like presented in Figure 3.[96] Such block copolymers are mostly reported to be synthesized via the Siegrist polycondensation method.[72] In this method an aldehyde end group was introduced that could easily be coupled with an anion or another suitable linker. Block copolymers such as PPV-*b*-PS (polystyrene)[97,98], PPV-*b*-PLA (poly(lactic acid))[99], PPV-*b*-PI (polyisoprene)[100], PPV-*b*-PBA (poly(butyl acrylate))[101] and PPV-*b*-PMMA (poly(methyl methacrylate))[102] can be synthesized. Another method for the synthesis of soluble PPV block copolymer materials is ROMP, which also gives access to PPVs with a living character. However, since the accessibility of these specific PPV cyclic monomers is rather low, this method is not been studied in high detail.[103,104] More recently, PPV block copolymers were obtained via the synthesis of highly tailored PPVs via the living anionic sulfinyl precursor route. In this polymerization reaction an anionic initiator is used to create an end group functionality that can produce the block copolymer in a second step. More specifically, a bromine end group could be introduced which can be used to connect a second polymer block either via single electron transfer-living radical polymerization (SET-LRP) or atom transfer radical polymerization (ATRP).[105,106,107,108] Classical ATRP is mostly carried out at elevated temperatures which could enable premature elimination of the precursor polymer and could therefore hinder block copolymer formation. Accordingly, executing

polymerizations under milder reaction conditions – as typically described for SET-LRP – is preferred when using PPV macroinitiators. Block copolymers synthesized *via* this re-initiation method were for example PPV-*b*-P*t*BuA (poly(*tert*-butyl acrylate))[109,110] and PPV-*b*-PEG (poly(ethylene glycol))[111]. Interestingly, when PPV, most of the time strongly hydrophobic, is extended with a water-soluble polymer, amphiphilic block copolymers can be obtained that are able to self-assemble. Previous work has already shown that amphiphilic block copolymers were obtained by the treatment of PPV-*b*-P*t*BuA with trifluoroacetic acid in order to yield PPV-*b*-PAA (poly(acrylic acid)). And later on, amphiphilic PPV block copolymers were directly synthesized by the use of hydrophilic acrylate blocks to create for example: PPV-*b*-PEGMA (poly(ethylene glycol methyl ether methacrylate)), PPV-*b*-PHEA (poly(2-hydroxyethyl acrylate)) and PPV-*b*-PHPMA (poly(2-hydroxypropyl methacrylate)).[112] These block copolymers can in a next step be self-assembled into micelles leading to new applications for PPV materials with complex architectures.

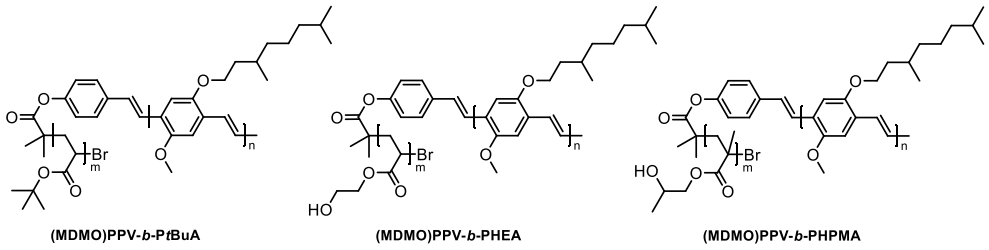

Figure 9: Chemical structure of PPV containing block copolymers with acrylates as the second block

1.7. Applications of PPV materials

Initially, PPVs were very interesting for the use in electronic applications,[113] but over the years their use in optoelectronics has decreased due to their lower performance when compared to other conjugated polymer systems.[114] Despite their lower efficiency, studies still involve PPV for the production of thin-films due to their excellent solubility properties.[115] Also, PPVs show excellent optical properties, making them ideal candidates for the use in the biomedical field (e.g. bioimaging or drug delivery).[116]

1.7.1. Biomedical applications

Nowadays, quantum dots (QDs) and fluorescent dyes are mostly used in the biomedical field for bioimaging. Although organic dyes have been widely investigated, they are associated with severe limitations such as photo bleaching and low photo stability.[117] QDs on the other hand exhibit resistance to photo bleaching and possess a high quantum yield, allowing for a strong fluorescence signal.[118] As a significant downside, the practical use of QDs *in vivo* is still an issue due to their cytotoxicity. In recent years, polymer shell-covered and surface-modified QDs have been prepared to improve their biocompatibility, which requires, however, tedious synthesis procedures.[119] Lately, encapsulation of conjugated polymers in nano-objects have also been reported.[120] Although the latter is a promising alternative to the fluorescent dyes or QDs, they still require advanced synthesis steps, often accompanied with physical or chemical crosslinks to ensure encapsulation of the material. Interestingly, conjugated polymers can themselves be used as shell material, which in principle simplifies the above concept. Also, in this way a conventional payload can be encapsulated, while

retaining the inherent fluorescent properties without further modification. PPVs possess excellent resistance to photo bleaching, strong fluorescence and are non-toxic, and hence are ideal to be used in such approach. Previous work has already shown that amphiphilic PPV-containing block copolymers show excellent self-assembly and payload uptake, and that these are ideal inherently fluorescent carriers for potential biomedical application (Figure 10).[121] Such nanoaggregates are able to penetrate into cancer cells and release their encapsulated drug payload.

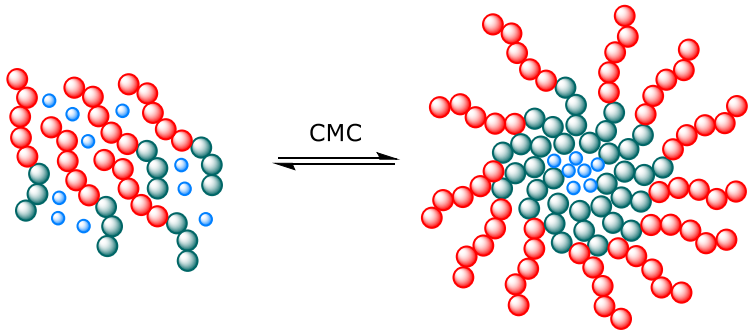

Figure 10: PPV containing micelles which can be used in bioimaging and drug delivery applications. Left are the block copolymers (green = PPV, red = hydrophilic acrylate block) and drug molecules (blue); right are the drug-loaded micelles

Interestingly, the block copolymers show fluorescence, however, when self-assembled, the fluorescence is quenched due to the organization of the conjugated chain segments.[121] Only upon cell uptake the fluorescence becomes visible again, since the micelle is decomposed back into the block copolymers. This is a useful feature that can be employed to closely monitor the cell uptake and later to determine the fate of the micelle materials over a longer period.

PPV-derivatives can also be used to form conjugated polymer nanoparticles (NPs) which are highly interesting for bioimaging in the field of nanomedicine.[122] A statistical copolymer 2-(5'-methoxycarbonylpentyloxy)-5-methoxy-1,4-phenylenevinylene (CPM-MDMO-PPV) is synthesized and the ester groups on the NPs surface are hydrolyzed into carboxylic acid groups, this allows for biomolecule conjugation. Due to the high fluorescent brightness and photostability of the NPs, they were *in vitro* tested as potential nanoprobes for studying cell populations within the central nervous system.[118] The NPs showed biocompatibility and surface charge dependent cellular uptake, making them highly promising for the use in bioimaging applications.

1.7.2. MDMO-PPV thin-film polymer light emitting diodes

The interest in using conjugated polymers for organic electronics is visible in the extensive research performed over the past decades towards polymer-based light emitting diodes (PLEDs). The main attractions of PLEDs are the easy processability, light weight and flexibility which boosted the research for these applications.[123] Their processing techniques involve the formation of thin-films, which can be easily performed via spin-coating, drop-casting and printing, amongst other deposition techniques.[124] PPV played a major role in the development of these organic electronics, since it was the first PLED reported in 1990, by Holmes *et al.*[125]

The efficiency of PLEDs is defined by the film morphology of the polymer active layer since charges need to be transported from one electrode to the other through the polymer layer, see Figure 11. Therefore, the structure of the polymer layer plays a major role in the transport of holes and electrons which is crucial for the efficiency of the device. This transport can be interrupted by so called trap

states, which are locations in the polymer layer that restrict the movement of holes and electrons such as impurities or structural defects.[126] The trapping of the electrons is often tackled by blending the conjugated polymer with an insulating polymer. Unfortunately, due to the immiscibility of both polymers, macrophase separation occurs. To overcome this problem, both homopolymers can be covalently bonded to form a block copolymer wherein only microphase separation can occur. This topic will be further elucidated in chapter 6.

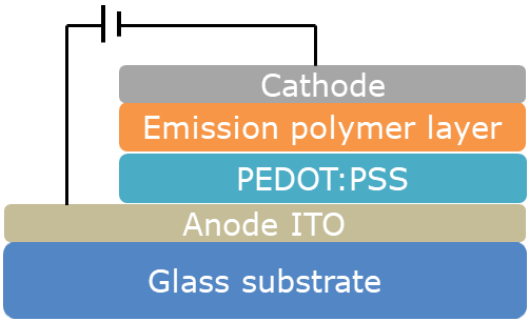

Figure 11: General structure of a PPV containing PLED on a glass substrate, with a cathode (often aluminum), the active polymer layer, the hole transport layer which is poly(3,4-ethylenedioxythiphene):poly(styrene sulfonate) (PEDOT:PSS) and the anode indium tin oxide (ITO)

1.8. Outline of the thesis

This thesis presents a further in-depth study of the synthesis and polymerization of poly[2-methoxy-5-(3′,7′-dimethyloctyloxy) -1,4-phenylenevinylene] (MDMO-PPV). Continuous flow techniques are used for the anionic polymerization of MDMO-PPV, block copolymer synthesis, self-assembly of MDMO-PPV containing block copolymers and the inline purification thereof. Lastly, thin films of PPV containing block copolymers are formed and their nanoscale structural organization is investigated for the use in polymer light emitting diode (PLED) applications.

In **Chapter 2**, low dispersity MDMO-PPV with well-defined end groups is made available by performing the anionic polymerization in a continuous tubular reactor under flash chemistry conditions. For the first time premature termination of PPV anionic polymerization could be observed leading to control over the microstructure and the dispersity. Due to the efficient mixing in the tubular reactors, dispersities of 1.2 could be reached at such low residence times, which are unachievable in conventional batch-wise chemistry. In a second step, a block copolymer was formed of the precursor PPV and *tert*-butyl acrylate (*t*BuA), which is further converted into an amphiphilic block copolymer of PPV with poly(acrylic acid) (PAA).

In **Chapter 3,** the PPV containing block copolymer synthesis using single electron transfer-living radical polymerization (SET-LRP) in continuous flow reactors is explored. First, the optimal reaction conditions are determined using a benchmark methyl acrylate (MA) polymerization. Lastly, high temperature SET-LRP was used for the block copolymerization of MDMO-PPV and MA in continuous tubular reactors. This chapter presents for the first time the PPV block copolymer synthesis in a continuous flow reactor.

Chapter 4 describes the kinetically stable micelles which are formed from block copolymers using continuous flow techniques by turbulent mixing of water with a polymer solution in THF. The formation of well-defined micelles in continuous flow reactors is used to show the well-controlled conditions of the PPV polymerization step. The PPV self-assembly *via* continuous flow is the novelty presented in this chapter.

In **Chapter 5**, purified micelle solutions are made available by the inline dialysis of the organic solvent, which are used to dissolve the block copolymers for micelle formation in continuous flow. The purification was performed using custom-made dialysis units with a cellulose membrane. Eventually, the integration of the method into a full synthesis line to produce encapsulated micelles directly from block copolymer solutions is demonstrated. DLS measurements proved the presence and good quality of the micelles at the end of the purification.

Chapter 6 represents the formation of thin-films from MDMO-PPV containing block copolymers for the use in PLED applications. The block copolymer thin-films are deposited via spin-coating on a PEDOT:PSS layer which was spin-coated on an indium-tin oxide (ITO) containing glass substrate. The nanoscale structural organization of the block copolymer thin-films was then examined using atomic force microscopy (AFM), temperature-controlled scanning probe microscopy (SPM) and small-angle x-ray scattering (SAXS).

At the end of the thesis, general experimental procedures and the used materials and characterization methods are collected in **chapter 7**. A summary of the thesis is given in **chapter 8** and a **list of the used abbreviations** is given together with an overview of the **publications and poster contributions** on conferences. At the very end, the **acknowledgment** is dedicated to everyone who helped me throughout this PhD.

1.9. References

[1] L. Baekeland, *Ind. Eng. Chem*. **1909**, 1, 202.

[2] H. Staudinger, *Ber. Dtsch. Chem. Ges.* **1920**, 53, 1073 —1085.

[3] H. Staudinger, J. Fritschi, *Helv. Chim. Acta* **1922**, 5, 785 —806.

[4] H. Frey, T. Johann, *Polym. Chem.* **2020**,11, 8-14.

[5] J. A. Calzonetti, C. J. Laursen, *Rubber Chem. Technol.* **2010**, 83, 303-321.

[6] B. J. Schwartz, *Ann. Rev. of Phys. Chem.* **2003**, 54, 141-172.

[7] P. J. Flory, *J. Am. Chem. Soc.* **1940**, 62, 1561-1565.

[8] K. Ziegler, E. Holzkamp, H. Breil, H. Martin, *Angew. Chem. Int. Ed.* **1955**, 67, 541−547.

[9] G. Natta, P. Pino, P. Corradini, F. Danusso, E. Mantica, G. Mazzanti, G. Moraglio, *J. Am. Chem. Soc.* **1955**, 77, 1708−1710.

[10] W. H. Carothers, *Trans. Faraday Soc.* **1936**, 32, 39-49.

[11] A. D. Jenkins, R. G. Jones, G. Moad, *Pure Appl. Chem.* **2010**, 82, 483-491.

[12] K. Matyjaszewski, J. H. Xia, *Chem. Rev.* **2001**, 101, 2921-2990.

[13] J. Nicolas, Y. Guillaneuf, C. Lefay, D. Bertin, D. Gigmes, B. Charleux, *Prog. Polym. Sci.* **2013**, 38, 63.

[14] R. T. A. Mayadunne, E. Rizzardo, J. Chiefari, Y. K. Chong, G. Moad and S. H. Thang, *Macromolecules* **1999**, 32, 6977-6980.

[15] J. Wang, K. Matyjaszewski, *J. Am. Chem. Soc*. **1995**, 117, 5614-5615.

[16] K. Matyjaszewski, S. Coca, S. G. Gaynor, M. Wei, B. E. Woodworth, *Macromolecules* **1997**, 23, 7348-7350.

[17] V. Percec, T. Guliashvili, J. S. Ladislaw, A. Wistrand, A. Stjerndahl, M. J. Sienkowska, M. J. Monteiro, S. Sahoo, *J. Am. Chem. Soc*. **2006**, 128, 14156-14165.

[18] Y. Gao, T. Zhao, W. Wang, *RSC Adv*. **2014**, 4, 61687-61690.

[19] G. Odian, *Principles of polymerization*, 4th ed; Wiley–Interscience, **2004**, Chapter 3.

[20] K. Matyjaszewski, N. V. Tsarevsky, *Nat. Chem*. **2009**, 1, 276-288.

[21] J. M. Ren, T. G. McKenzie, Q. Fu, E. H. H. Wong, J. Xu, Z. An, S. Shanmugam, T. P. Davis, C. Boyer, G. G. Qiao, *Chem. Rev.* **2016**, 116, 6743–6836.

[22] C. E. Carraher Jr., *Polymer chemistry, 6th ed*; Marcel Cekker Inc. **2003**, Chapter 15.

[23] C. Li, Q. Li, Y. V. Kaneti, D. Hou, Y. Yamauchi, Y. Mai, *Chem. Soc. Rev.* **2020**, 49, 4681-4736.

[24] D. T. Mcquade, P.H. Seeberger, *J. Org. Chem* **2013**, 78, 6384-6389.

[25] J. Bao, G. K. Tranmer, *Tetrahedron Lett*. **2016**, 57, 654–657.

[26] J. C. Pastre, D. L. Browne, S. V. Ley, *Chem. Soc. Rev*. **2013**, 42, 8849.

[27] M. Baumann, I. R. Baxendale, S. V. Ley, *Mol. Diversity* **2011**, 15, 613–630.

[28] N. J. W. Straathof, H. P. L. Gemoets, X. Wang, J. C. Schouten, V. Hessel, T. Noël, *ChemSusChem* **2014**, 7, 1612–1617.

[29] N. Zaquen, M. Rubens, N. Corrigan, J. Xu, P. B. Zetterlund, C. Boyer, T. Junkers, *Prog. Polym. Sci.* **2020**, 107, 101256.

[30] M. B. Plutschack, B. Pieber, K. Gilmore, P. H. Seeberger, *Chem. Rev.* **2017**, 117, 11796-11893.

[31] Z. Mao, C. Yang, *Chin. J. Chem. Eng*. **2017**, 25, 381–390.

[32] L. Ray, J. J. Iliff, J. J. Heys, Fluids and Barriers of the CNS, 16, **2019**.

[33] M. Barrett, D. O'Grady, E. Casey, B. Glennon, *Chem. Eng. Sci.* **2011**, 66, 2523-2534.

[34] P. Angeli, A. Gavriilidis, *Taylor Flow in Microchannels. In Encyclopedia of Microfluidics and Nanofluidics*; Li, D., Ed.; Springer: Boston, MA, **2008**, 1971−1976.

[35] M. Botma, *Targeting a Specific y+ Value for your Turbulent Flow CFD Simulation (Part 1)*, **2019**.

[36] B. Rehm, J. Schubert, A. Haghshenas, A. S. Paknejad, J. Hughes, *Managed Pressure Drilling*, Gulf Publishing Company, **2008**, 39-80.

[37] P. J. LaNasa, E. L. Upp, in Fluid Flow Measurement (Third Edition), **2014**.

[38] K. Geyer, J. D. C. Code´e, P. H. Seeberger, *Chem. Eur. J.* **2006**, 12, 8434-8442.

[39] K. Jähnisch, V. Hessel, H. Löwe, M. Baerns, *Angew. Chem. Int. Ed*. **2004**, 43, 406-446.

[40] J. Wegner, S. Ceylan, A. Kirschning, *Chem. Commun*. **2011**, 47, 4583–4592.

[41] V. Hessel, D. Kralisch, N. Kockmann, T. Noël, Q. Wang, *ChemSusChem* **2013**, 6, 746-789.

[42] D. Wilms, J. Klos, H. Frey, *Macromol. Chem. Phys*. **2008**, 209, 343-356.

[43] J. Wegner, S. Ceylan, A. Kirschning, *Chem. Commun*. **2011**, 47, 4583-4592.

[44] J. Morsbach, A. H. E. Muller, E. Berger-Nicoletti, H. Frey, *Marcomolecules* **2016**, 49, 5043-5050.

[45] T. Noel, S. L. Buchwald, *Chem. Soc. Rev*. **2011**, 40, 5010–5029.

[46] V. Hessel, D. Kralisch, N. Kockmann, T. Noël, Q. Wang, *ChemSusChem* **2013**, 6, 746–789.

[47] J. Yoshida, *Flash Chemistry in: Basics of Flow Microreactor Synthesis,* Springer, **2015**, 73-77.

[48] S. Railian, B. Wenn, T. Junkers, *J. Flow Chem.* **2016**, 6, 260-267.

[49] T. Junkers, *J. Flow Chem*. **2017**, 7, 106–110.

[50] C. F. Carter, H. Lange, S. V. Ley, I. R. Baxendale, B. Wittkamp, J. G. Goode, N. L. Gaunt, *Org. Process Res. Dev*. **2010**, 14, 393.

[51] M. Rubens*, J.H. Vrijsen*, J. Laun, T. Junkers, *Angew. Chem. Int. Ed.*, **2019**, 58, 3183.

[52] Z. Qiu, B.A.G. Hammer, K. Mullen, *Prog. Polym. Sci.* **2020**, 100, 101179.

[53] J.H. Burroughes, D.D.C. Bradley, A.R. Brown, R.N. Marks, K. Mackay, R.H. Friend, et al., *Nature* **1990**, 347, 539–541.

[54] H. Sirringhaus, N. Tessler, R.H. Friend, *Science* **1998,** 280, 1741–1744.

[55] A. Facchetti, *Chem Mater* **2011**, 23, 733–758.

[56] H. Shirakawa, *Angew. Chem., Int. Ed.* **2001**, 40, 2574–2580.

[57] A. G. MacDiarmid, *Angew. Chem., Int. Ed*. **2001**, 40, 2581–2590.

[58] A. J. Heeger, *Angew. Chem., Int. Ed*. **2001**, 40, 2591–2611.

[59] H. Shirakawa, E. J. Louis, A.G. MacDiarmid, C.K. Chiang, A. J. Heeger, *J. Chem. Soc., Chem. Commun*. **1977**, 578–580.

[60] P. Morin, T. Bura, M. Leclerc, *Mater. Horiz.* **2016**, 3, 11-20.

[61] A. J. Heeger, *Synthetic Met.* **2001**, 125, 23-42.

[62] D. F. Schriver, P. W. Atkins, C. H. Langford, *Inorganic Chemistry*, 2nd ed., Oxford University Press, Oxford, **1994**, 91.

[63] G. Popescu, *Principles of Biophotonics, Volume 2*, **2019**, 5.1-5.8.

[64] R. H. Friend, R. W. Gymer, A. B. Holmes, J. H. Burroughes, R. N. Marks, C. Taliani, D. D. C. Bradley, D. A. Dos Santos, J. N. Bredas, M. Logdlund, W. R. Salaneck, *Nature* **1999**, 397, 121-128.

[65] K. H. Hendriks, W. Li, M. M. Wienk, R. A. J. Janssen, *J. Am. Chem. Soc*. **2014**, 136, 12130-12136.

[66] W. Zhang, H. Sun, S. Yin, J. Chang, Y. Li, X. Guo, Z. Yuan, J. *Mater. Sci*. **2015**, 50, 5571-5577.

[67] A. P. Davey, A. Drury, S. Maier, H. J. Byrne, W. J. Blau, *Synth. Met.* **1999**, 103, 2478–2479.

[68] S. Pfeiffer, H.-H. Hörhold, *Macromol. Chem. Phys.* **1999**, 200, 1870–1878.

[69] M. Rehahn, A. D. Schlüter, *Macromol. Chem., Rapid Commun.* **1990**, 11, 375–379.

[70] N. C. Greenham, S. C. Moratti, D. D. C. Bradley, R. H. Friend, A. B. Holmes, *Nature* **1993**, 365, 628–630.

[71] S. C. Moratti, R. Cervini, A. B. Holmes, D. R. Baigent, R. H. Friend, N. C. Greenham, J. Grüner, P. J. Hamer, *Synth. Met.* **1995**, 71, 2117–2120.

[72] H. Kretzschmann, H. Meier, *Tetrahedron Lett.* **1991**, 32, 5059–5062.

[73] Z. Bao, Y. Chen, R. Cai, L. Yu, *Macromolecules* **1993**, 26, 5281–8286.

[74] M. Pan, Z. Bao, L. Yu, *Macromolecules* **1995**, 28, 5151–5153.

[75] F. Babudri, S. R. Cicco, G. M. Farinola, F. Naso, A. Bolognesi, W. Porzio, *Macromol. Rapid Commun.* **1996**, 17, 905–911.

[76] F. Koch, W. Heitz, *Macromol. Chem. Phys.* **1997**, 198, 1531–1544.

[77] M. C. Scharber, D. Wuhlbacher, M. Koppe, P. Denk, C. Waldauf, A. J. Heeger, C. L. Brabec, *Adv. Mater*. **2006**, 18, 789-794.

[78] T. Junkers, J. Vandenbergh, P. Adriaensens, L. Lutsen and D. Vanderzande *Polym. Chem.* **2012**, 3, 275-285.

[79] H. G. Gilch, W. L. Weelwright, *J. Polym. Sci. Polym. Chem.* Ed. **1966**, 4, 1337-1349.

[80] R. A. Wessling, R. G. Zimmerman, *US Patent* 3401152, **1968**.

[81] F. R. Denton, A. Serker, P. M. Lathi, R. O. Garay, F. E. Karasz, *J. Polym. Sci. Part A: Polym. Chem.* **1992**, 30, 2233-2240.

[82] S. Son, A. Dodabalapur, A. J. Lovinger, M. E. Galvin, *Science* **1995**, 269, 376–378.

[83] E. Kesters, S. Gilissen, F. Motmans, L. Lutsen, D. Vanderzande, *Macromolecules* **2002**, 35, 7902–7910.

[84] A. Henckens, I. Duyssens, L. Lutsen, D. Vanderzande, T. Cleij, *Polymer* **2006**, 47, 123–131.

[85] A. Henckens, L. Lutsen, D. Vanderzande, M. Knipper, J. Manca, T. Arnouts, J. Poortman, *J. Proc. SPIE Int. Soc. Opt. Eng*. **2004**, 5464, 52–59.

[86] F. Louwet, D. Vanderzande, J. Gelan, *Synth. Met.* **1995**, 69, 509-510.

[87] A. Van Breemen, D. Vanderzande, P. Adriaensens, J. Gelan, *J. Org. Chem.* **1999**, 64, 3106-3112.

[88] L. Lutsen, A. Van Breemen, W. Kreuder, D. Vanderzande, J. Gelan, *Helv. Chem. Acta* **2000**, 83, 3113-3121.

[89] A. Issaris, D. Vanderzande, J. Gelan, *Polymer* **1997**, 38, 2571–2574.

[90] J. Wiesecke, M. Rehanh, *Angew. Chem. Int. Ed*. **2003**, 42, 567–570.

[91] L. Hontis, V. Vrindts, L. Lutsen D. Vanderzande, J. Gelan, *Polymer* **2001**, 42, 5793-5796.

[92] L. Hontis, V. Vrindts, D. Vanderzande, L. Lutsen, *Macromolecules* **2003**, 36, 3035-3044.

[93] I. Cosemans, L. Hontis, D. Van Den Berghe, A. Palmaerts, J. Wouters, T. Cleij, L. Lutsen, W. Maes, T. Junkers, D. Vanderzande, *Macromolecules* **2011**, 44, 7610-7616.

[94] I. Cosemans, J. Wouters, T. Cleij, L. Lutsen, W. Maes, T. Junkers, D. Vanderzande, *Macromol. Rapid Commun.* **2012**, 33, 242-247.

[95] I. Van Severen, M. Breselge, S. Fourier, P. Adriaensens, J. Manca, L. Lutsen, T. J. Cleij, D. Vanderzande, *Macromol. Chem. Phys.* **2007**, 208, 196–206.

[96] A. de Cuendias, R. C. Hiorns, E. Cloutet, L. Vignau, H. Cramail, *Polym. Int.* **2010**, 59, 1452–1476.

[97] N. Sary, R. Mezzenga, C. Brochon, G. Hadziioannou, J. Ruokolainen, *Macromolecules* **2007**, 40, 3277–3286.

[98] C. Brochon, N. Sary, R. Mezzenga, C. Ngov, F. Richard, M. May, G. Hadziioannou, *J. Appl. Polym. Sci.* **2008**, 110, 3664–3670.

[99] C. H. Braun, B. Schopf, C. Ngov, C. Brochon, G. Hadziioannou, E. J. W. Crossland, S. Ludwigs, *Macromol. Rapid Commun.* **2011**, 32, 813–819.

[100] B. D. Olsen, R. A. Segalman, *Macromolecules* **2005**, 38, 10127–10137.

[101] U. Stalmach, B. de Boer, A. D. Post, P. F. van Hutten, G. Hadziioannou, *Angew. Chem. Int. Ed.* **2001**, 40, 428–430.

[102] C.-C. Ho, Y.-H. Lee, C.-A. Dai, R. A. Segalman, W.-F. Su, *Macromolecules* **2009**, 42, 4208–4219.

[103] M. Porz, D. Mäker, K. Brödner, U. W. F. Bunz, *Macromol. Rapid Commun.* **2013**, 34, 873-876.

[104] B. J. Lidster, J. M. Behrendt, M. L. Turner, *Chem. Commun*. **2014**, 50, 11867-11870.

[105] N. H. Nguyen, M. E. Levere, V. Percec, *J. Polym. Sci. Part A: Polym. Chem*. **2012**, 50, 860–873.

[106] N. H. Nguyen, V. Percec, *J. Polym. Sci. Part A: Polym. Chem*. **2010**, 48, 5109-5119.

[107] G. Lligadas, S. Grama, V. Percec, *Biomacromolecules* **2017**, 18, 1039−1063.

[108] A. Anastasaki, C. Waldron, P. Wilson, R. McHale, D. M. Haddleton, *Polym. Chem.* **2013**, 4, 2672-2675.

[109] I. Cosemans, J. Vandenbergh, V. S. D. Voet, K. Loos, L. Lutsen, D. Vanderzande, T. Junkers, *Polymer* **2013**, 54, 1298-1304.

[110] I. Cosemans, J. Vandenbergh, L. Lutsen, D. Vanderzande, T. Junkers, *Polym. Chem.* **2013,** 4, 3471-3479.

[111] I. Cosemans, J. Vandenbergh, L. Lutsen, D. Vanderzande, T. Junkers, *Eur. Polym. J.* **2014**, 55, 114-122.

[112] N. Zaquen, H. Lu, T. Chang, R. Mamdooh, L. Lutsen, D. Vanderzande, M. Stenzel, T. Junkers, *Biomacromolecules* **2016**, 17, 4086-4094.

[113] A. P. Kulkarni, C. J. Tonzola, A. Babel, S. A. Jenekhe, *Chem. Mater*. **2004**, 16, 4556-4573.

[114] K. H. Hendriks, W. Li, M. M. Wienk, R. A. J. Janssen, *J. Am. Chem. Soc*. **2014**, 136, 12130-12136.

[115] B. Gündüz, *Polym. Bull.* **2015**, 72, 3241–3267.

[116] W. Zhang, H. Sun, S. Yin, J. Chang, Y. Li, X. Guo and Z. Yuan, J. *Mater. Sci*. **2015**, 50, 5571-5577.

[117] Y.-P. Ho, K. W. Leong, *Nanoscale* **2010**, 2, 60–68.

[118] U. Resch-Genger, M. Grabolle, S. Cavaliere-Jaricot, R. Nitschke and T. Nann, *Nat. Methods* **2008**, 5, 763–775.

[119] M. Walling, J. Novak, J. R. E. Shepard, *Int. J. Mol. Sci*. **2009**, 10, 441–491.

[120] D. K. Tiwari, T. Jin, J. Behari*, Int. J. Nanomed*. **2011**, 6, 463–475.

[121] N. Zaquen, H. Lu, T. Chang, R. Mamdooh, L. Lutsen, D. Vanderzande, M. Stenzel, T. Junkers, *Biomacromolecules* **2016**, 17, 4086-4094.

[122] M. Peters, N. Zaquen, L. D'Olieslaeger, H. Bové, D. Vanderzande, N. Hellings, T. Junkers, A. Ethirajan, *Biomacromolecules* **2016**, 17, 2562-2571.

[123] Y. Xu, Z. Xie, *Advanced Nanomaterials for Solar Cells and Light Emitting Diodes*, Elsevier, **2019**, 457-476.

[124] C. Deibel, V. Dyakonov, *Rep. Prog. Phys*. **2010**, 73, 096401.

[125] J. H. Burroughes, D. D. C. Bradley, A. R. Brown, R. N. Marks, K. Mackay, R. H. Friend, P. L. Burns, A. B. Holmes, *Nature* **1990**, 347, 539.

[126] D. Abbaszadeh, A. Kunz, N. B. Kotadiya, A. Mondal, D. Andrienko, J. J. Michels, G.-J. A. H. Wetzelaer, P. W. M. Blom, *Chem. Mater*. **2019**, 31, 6380−6386.

Chapter 2

Flash-Synthesis of Low Dispersity PPV *via* Anionic Polymerization in Continuous Flow Reactors and Block Copolymer Synthesis

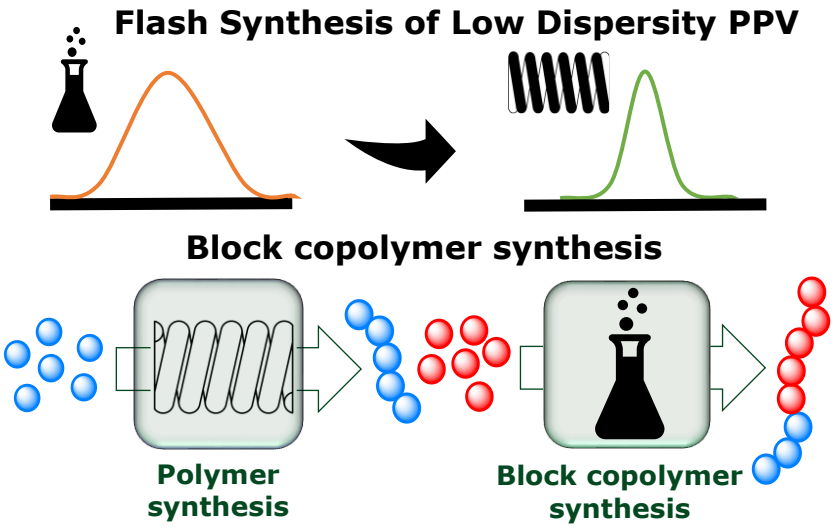

K. Verstraete, N. Zaquen, T. Junkers, *Polym. Chem.*, **2020**, 11, 7094-7103.

2.1. Abstract

Low dispersity poly[2-methoxy-5-(3',7'-dimethyloctyloxy)]-1,4-phenylenevinylene (MDMO-PPV) with well-defined end-groups is made available by performing the anionic polymerization in a continuous tubular reactor under flash chemistry conditions. The anionic polymerization was carried out via the sulfinyl (Vanderzande) precursor route, following a protocol previously established. Flash flow chemistry allowed now to not only control the microstructure, but also the disperisty of the PPV efficiently. Further, this is the first time that premature termination of PPV anionic polymerization could be observed. Only at ultra-low reaction times in the order of tens of milliseconds, products can be observed that have not reached full monomer conversion, rendering this type of polymerization one of the fastest polymerizations known. Due to the efficient mixing in the tubular reactors, dispersities of 1.2 could be reached at such low residence times, which is unachievable in conventional batch-wise chemistry. In a second step, a block copolymer was formed of the precursor PPV and tert-butyl acrylate (*t*BuA), which is further converted into an amphiphilic block copolymer of PPV with poly(acrylic acid) (PAA).

2.2. Introduction

In the last decades, many efforts have been made to synthesize PPVs in a controllable manner. They stick out as they are synthesized in a chain-growth polymerization. This allows to create them – in principle – with well-defined end-groups and chain lengths. Especially the sulfinyl (also known as Vanderzande) precursor route is of very high interest due to the decoupling of the polymerization and elimination process, see Scheme 1.[1,2,3] This results in polymers with very low defect levels and excellent optical properties.[4,5] Another remarkable advantage of the Vanderzande route is that the polymers can be formed either via radical or anionic polymerization, depending on the choice of solvent and base (explained in chapter 1).[6,7] Although more control over the reaction is gained by using the anionic polymerization route, it is still a challenge to tune the desired polymeric properties, such as the molecular weight and the dispersity since the reaction is extremely fast.

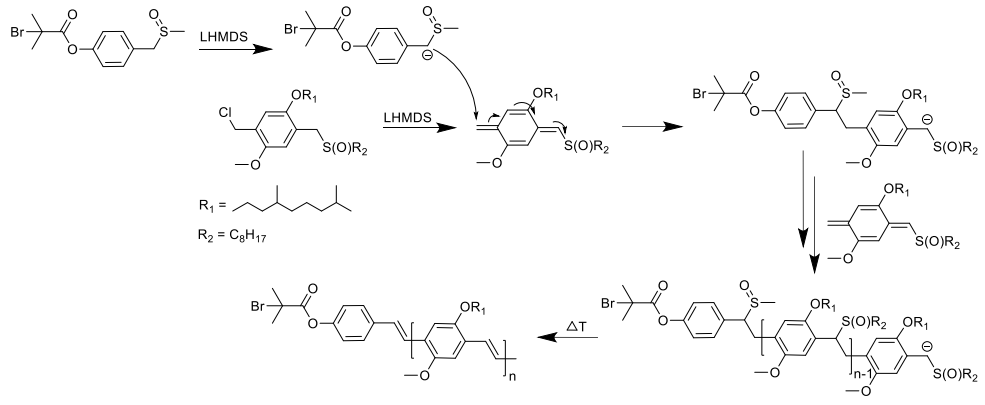

Scheme 1: Mechanism of the anionic sulfinyl polymerization of the MDMO premonomer

Previous studies had already shown that polymerizations proceed on the timescale of mixing of all components, and hence reaches full conversion below 1 second even at dry ice temperature conditions. In order to tune polymer properties more efficiently, continuous flow techniques can be employed.[8] Research already showed the possibility to radically polymerize conjugated PPVs in a continuous flow reactor, but tubular reactors have, to the best of our knowledge, not yet been used for the anionic polymerization of PPV.[9,10] Since mixing of the starting materials has been identified as the largest limitation with respect to molecular weight distribution control in the classical batch anionic PPV polymerization, these polymerizations could largely benefit from flow processing.[11] As demonstrated by the work of Takahashi and Nagaki, anionic polymerizations are advantageous to perform in continuous flow reactors.[12] They explained that fast reactions generally greatly benefit from what they termed "flash chemistry", due to the control that is gained by reducing the residence time.[13] Further, flow flash chemistry allows to perform reactions that usually would require very low temperatures at room temperature, removing the need for tedious temperature control. The flow rate and therefore also the residence time can be easily varied and perfectly controlled, therefore regulation over the dispersity and molecular weight of the polymers can be gained and especially the very short reaction times are of high value for the PPV polymerization, even on timescales below one second.[14,15] Batch chemistry is not able to provide such reaction process control on this timescale, and in fact flash chemistry has been identified as one key method to control the dispersity of a polymer product.[16,17] On the other hand, with respect to PPV synthesis, microflow chemistry is also limited in the sense that PPV is inherently difficult to dissolve, and leads quickly to reactor fouling. Only low concentrations can be

tolerated in flow channels. Also, lithium bases can quickly lead to blockages of the reactor, which makes such synthesis not that straightforward.

The formation of highly tailored PPVs via living anionic polymerization make them readily available for further applications like the development of (amphiphilic) block copolymers, synthesized via single electron transfer living radical polymerization (SET-LRP).[18,19,20] When PPV, which is hydrophobic, is extended with a water-soluble polymer, amphiphilic block copolymers can be obtained that are able to self-assemble.

In here, the synthesis of low dispersity MDMO-PPV via the anionic sulfinyl precursor route in continuous flow reactors will be discussed. So far, it had not been possible to achieve narrowly dispersed materials of this kind, and to the best of our knowledge, this is the first report on low dispersity PPV made in a consistent and reproducible fashion. Improved control over the molecular weight and low dispersity MDMO-PPV polymers are obtained by the use of flash chemistry, and hence display one of the cases where the engineering approach to a reaction - here flow chemistry with very low residence times – yields a synthetic result that otherwise would be inaccessible. Reactions are all performed at room temperature (ignoring adiabatic heat up), for simplicity of the process and to use the advantage of the flash chemistry concept. Optimization of the precursor polymer from the MDMO premonomer in continuous flow reactors will be highlighted as well as the design of the reactor and the reaction conditions. Block copolymer synthesis is described, streamlining the synthesis of PPV-containing block copolymers under highly reproducible conditions.

2.3. Experimental Section

2.3.1. General flow reactor setup for the polymerization of the precursor MDMO-PPV

Scheme 2 represents the general flow reactor setup for the polymerization of the precursor MDMO-PPV. The continuous tubular flow reactions were performed in a self-made PFA tubular reactor with an internal diameter of 0.75 mm and varying reactor volumes from 1.7 µL (dead volume, Y-Piece) to 0.5 mL. The polymerization reactions were performed at room temperature. The reagent solutions (premonomer, initiator and base) were injected into the reactor through two gastight syringes (SGE) and a Y-piece (PEEK Y for 1/16" OD tubing, thru-hole = 0.020") to ensure mixing of both solutions. An extra gastight syringe (SGE) containing 1 M HCl was added via a Y-piece at the end of the reactor and serves as a quenching line. The flow rates were controlled via two syringe pumps (Chemyx) and vary between 1 mL·min^{-1} and 31 mL·min^{-1} (for each syringe), the residence times corresponding to these flow rates depend on the reactor used. The end of the reactor was connected to a vial which could be easily switched in order to collect different samples for screening of the residence time and reactor volume.

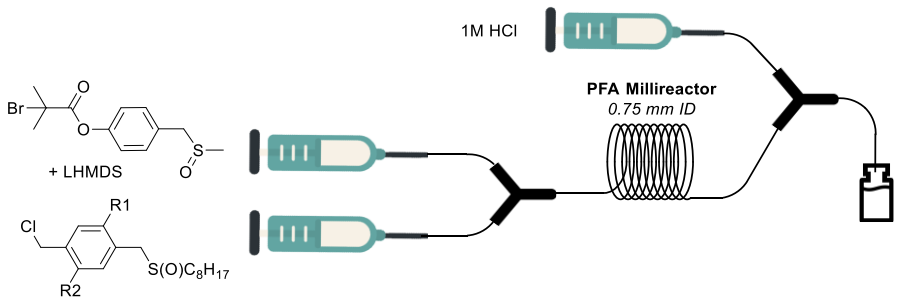

Scheme 2: Schematic representation of the precursor MDMO-PPV polymerization in continuous flow

2.3.2. General method for the synthesis of the MDMO-PPV precursor polymer in a tubular flow reactor

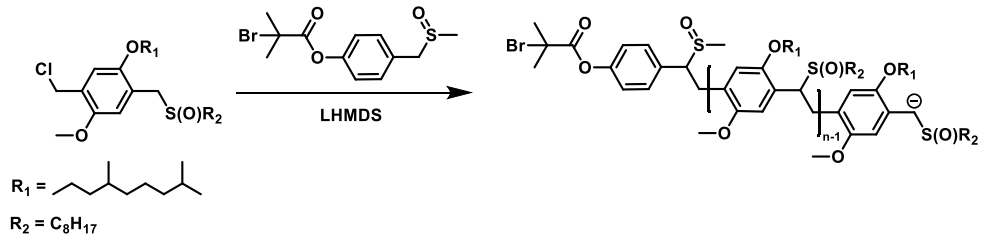

Scheme 3: Precursor MDMO-PPV synthesis via the anionic sulfinyl polymerization

The MDMO premonomer (585 mg, 1.2 mmol, 1 equiv) and the initiator (76.6 mg, 0.24 mmol, 0.2 equiv) were added into separate vials and both were transferred into the glovebox where the compounds were dissolved in THF (20 mL and 18.44 mL respectively). The base LHMDS (1M in THF) (261 mg, 1.56 mL, 1.56 mmol, 1.3 equiv) was added to the vial containing the initiator. The monomer-initiator-base ratio of 1/0.2/1.3 was chosen because this initiator concentration gives generally the lowest dispersity and the LHMDS base needs to activate both the MDMO premonomer and the initiator. Two 25 mL gastight syringes were filled with the solutions which were then connected to the Y-piece that was capped with a stopper at the end. Everything was transferred out of the glovebox and the Y-piece was connected to the reactor together with the quenching line. The reagent solutions were pumped into the reactor with the syringe pumps and the polymer was formed at room temperature. The precursor polymer was collected as a yellow viscous oil and was poured into H_2O (40 mL) before extraction with CH_2Cl_2 (3 x 50 mL). The solvent was evaporated and the precursor polymer was precipitated in cold MeOH (40 mL). Filtration on a Teflon® filter resulted in the purified precursor polymer as a bright yellow sticky oil.

2.4. Results and Discussion

2.4.1. Polymerization of MDMO-PPV in flow reactors

The ability to polymerize PPVs exclusively via the anionic precursor route has been extensively investigated for batch polymerization, but due to the fast polymerization, control over molecular weight and dispersity could not really be achieved so far. Some molecular weight control could be realized, yet dispersities were typically high, and no example is known yet where this polymerization could be quenched before reaching full conversion. It is also due to this limitation, that until recently even the mechanism of PPV polymerization was under debate. We hypothesized that this limitation could be overcome in continuous flow reactors, where residence times are better controlled, and mixing is achieved on much faster timescale. First, the MDMO-premonomer and initiator were combined in one syringe in THF and another syringe was filled with LHMDS in THF. The base needs to deprotonate the premonomer and the initiator. A small further excess (0.1 equiv.) was added to make sure that the deprotonation goes to completion. Both syringes were combined in a Y-piece after which it was connected to a 1 mL reactor. At the exit of the reactor (the same was done in all following experiments), the reaction mixture is directly quenched with 1 M HCl solution to stop any further reaction and thus to rule out that further polymerization occurs in the vessel in which the product is collected, see Scheme 2. PPV precursor polymer was successfully formed, but unfortunately, varying the residence times did not show any variation in the molecular weight or dispersity (see Table 1). Further, in total 4 different reactor designs were tested, the first one with a 1 mL reactor volume, the second one with 0.5 mL and two designs without any reactor, only a Y-piece or a static mixing tee, see Table 1.

Due to the fast reaction kinetics of this polymerization a rather small reactor volume was chosen to start with, the 1 mL reactor with a Y-piece. PPV precursor polymer could be synthesized successfully but varying the residence time did not reveal any variation in molecular weight nor dispersity, Figure 1. Since the variation in residence times was still quite low (between 60 and 10 seconds), it was chosen to reduce the reactor volume to 0.5 mL in order to go to even shorter residence times (from 20 seconds to 1 second). It is clearly evident that even at a residence time of 1 second the precursor PPV polymer is formed, but still (almost) no variation in polymer length was achieved. Since the reactor volume had almost no influence on the polymeric properties, a design was chosen without any tubular residence unit at all, and hence only consisted of a Y-piece to bring both solutions together. The same results were still seen as for the designs with a reactor connected, despite the residence time being practically zero after mixing.

Table 1: Overview of the different reactors and residence times of the MDMO precursor polymer synthesized via the first reactor set-up in continuous flow

Residence time / sec	M_n g·mol^{-1}	M_w g·mol^{-1}	$Đ$	Residence time / sec	M_n g·mol^{-1}	M_w g·mol^{-1}	$Đ$	Residence time*/ sec	M_n g·mol^{-1}	M_w g·mol^{-1}	$Đ$
	1 mL reactor				0.5 mL reactor				Only Y-piece/mixing tee		
60	1900	2700	1.4	20	2200	3400	1.6	0.10	1900	2600	1.4
40	1900	2700	1.4	10	2100	3300	1.6	0.05	1900	2600	1.4
30	1900	2700	1.4	5	2100	3300	1.6	0.026	1900	2600	1.4
15	1900	2600	1.4	2	2200	3200	1.4	0.020	1900	2600	1.4
10	1800	2600	1.4	1	2200	3200	1.5	0.017	1900	2600	1.4

*residence times are estimated from the flow rate and the dead volume of the Y-piece, the [MDMO premonomer]/[initiator]/[LHMDS] ratio = 1/0.2/1.3

Lastly, also a design with a static mixing tee could not change the molecular weight or dispersity of the precursor PPV polymers.

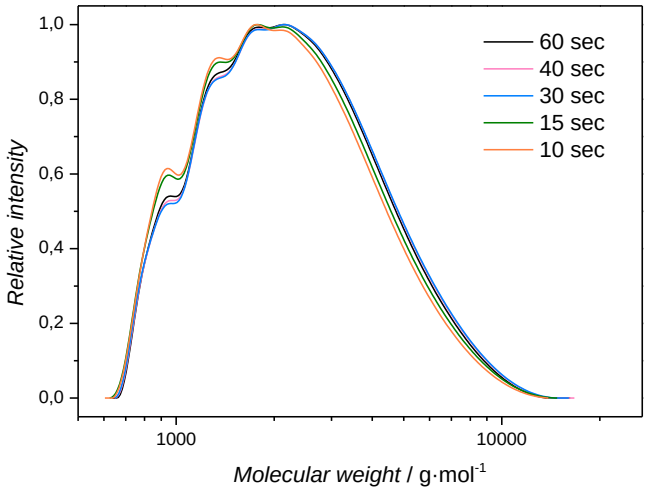

Figure 1: Molecular weight distributions obtained for PPV precursor polymers synthesized in the 1 mL reactor

Since the reactor design or mixing units couldn't provide a solution, the composition of the starting solutions was changed. Monomer and base cannot be mixed, as this triggers spontaneous polymerization, even in absence of the dedicated initiator. Thus, the system was changed to the first syringe only containing the premonomer in THF and the second syringe containing the initiator and base LHMDS in THF, see Scheme 2. In this way, the LHMDS base could already activate/ deprotonate the initiator before it encountered the monomer. In this way, the initiation of the anionic polymerization will be faster and be decoupled from the mixing process. Initiation and chain growth can happen immediately when active quinodimethane monomer is formed. With this setup, PPV precursor polymer could be synthesized successfully in a 0.5 mL reactor with a number

average molecular weight (M_n) of 3400 g·mol^{-1} and a dispersity of 1.4 (determined using SEC). To examine if the different compositions of the syringes influenced the polymerization length, again different reactor lengths were investigated, see Table 2. Three reactor designs were tested, a 0.5 mL reactor, 0.13 mL reactor and a design with only a Y-piece to bring both solutions together. With the 0.5 mL reactor volume, the residence time could be easily varied between 10 and 0.5 seconds (flow rate varied between 3 mL·min^{-1} and 60 mL·min^{-1}). The molecular weights that were obtained range from 3400 g·mol^{-1} to 3000 g·mol^{-1} and the dispersities decreased from 1.5 to 1.2. Thus, when the residence time is lowered, the molecular weight and the dispersity decrease as well, even if only in limits. At higher flow rates (lower residence times), shorter polymer chains were formed because the polymer chain has less time to grow and more chains are initiated.

Table 2: Overview of the different reactors and residence times of the MDMO polymer synthesized in continuous flow

Residence time / sec	M_n g·mol^{-1}	M_w g·mol^{-1}	$Đ$	Residence time / sec	M_n g·mol^{-1}	M_w g·mol^{-1}	$Đ$	Residence time*/ sec	M_n g·mol^{-1}	M_w g·mol^{-1}	$Đ$
0.5 mL reactor				0.13 mL reactor				Only Y-piece			
10	3400	4700	1.4	2	3100	4600	1.5	0.05	3900	5200	1.3
5	3100	4600	1.5	1	3100	4400	1.4	0.026	3800	5200	1.4
2.5	3200	4500	1.4	0.5	3000	4000	1.3	0.013	3900	5200	1.3
1	3000	3900	1.3	0.25	3000	3700	1.2	0.0064	3800	4800	1.3
0.5	3100	3800	1.2	0.12	2800	3500	1.2	0.0032	3200	3800	1.2

*residence times are estimated from the flow rate and the dead volume of the Y-piece, the [MDMO premonomer]/[initiator]/[LHMDS] ratio = 1/0.2/1.3

Remarkably, in literature this trend is not visible for the anionic polymerizations of PPV in batch and this is the first time, to the best of our knowledge, where a premature termination of the PPV chain growth could be observed. In batch polymerization, it is seen that even at "0" minutes of reaction time polymer is formed to high conversion, indicating once more how fast this polymerization is. Encouraged by these results, the residence time was further reduced. A shorter reactor with an internal volume of 0.13 mL was employed. In this way, the residence times could be varied between 2 seconds and 0.12 seconds (flow rate varied between 3.9 $mL \cdot min^{-1}$ and 63.7 $mL \cdot min^{-1}$), leading to molecular weights that range from 3100 $g \cdot mol^{-1}$ to 2800 $g \cdot mol^{-1}$ with a dispersity decreasing from 1.5 to 1.2.

Still at these low residence times PPV prepolymer can be formed, showing that the reaction is even faster than anticipated. Again, the same trend of decreasing molecular weight and dispersity with decreasing residence times is seen, even if within rather narrow limits. It should be mentioned here that the determination of monomer conversion in PPV polymerization is non-trivial due to the inherent instability of the monomer once it is formed in the elimination step. Thus, shorter chain lengths must serve as sufficient proof for reaching lower conversions before chain growth is terminated. The previous results show that even at very low residence times PPV precursor polymer is already formed with high conversion. Therefore, in the next step the two reagent solutions were connected with a Y-piece and the polymer sample was directly collected without a tubular reactor unit. The residence times were changed from 0.05 seconds to 0.0032 seconds (residence times are estimated from the flow rate and the dead volume of the Y-piece) displaying the same (although rather small) trend as seen in the previous experiments, namely the molecular weight that decreases from 3900 $g \cdot mol^{-1}$ to

3200 g·mol^{-1} and the dispersity ranges from 1.4 to 1.2, see Figure 2. For this reactor type there can although be seen that the decrease in molecular weight only start to be really visible from 0.006 to 0.003 seconds. Nevertheless, it shows that the process is a true flash chemistry reaction, not necessitating any residence unit to produce PPV precursor polymer in flow. Mixing of reactants is the only rate determining step.[11]

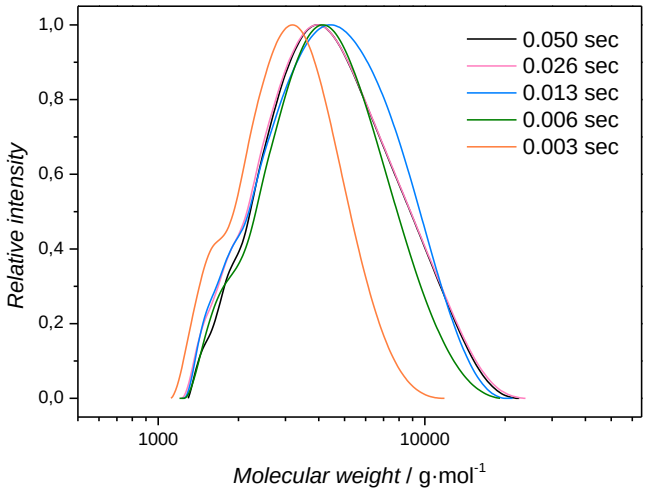

Figure 2: Molecular weight distributions for the PPV precursor polymers synthesized with only the Y-piece were determined via SEC without the impurities at low molecular weight

Having said that, a reaction time of only 3.2 msec is truly remarkable for any polymerization to occur, explaining also why previous attempts (with longer reaction times) at flow polymerization had not been successful. When being carried out at higher starting monomer concentration, the exotherm cannot be dissipated, and the reaction accelerates further, leading to fouling and reactor blockages. As for the polymerization itself, it is of only small consequence if a

reactor residence unit is used or not (even though not negligible). All reactors show the same decrease in molecular weight and dispersity within an experimental series. Even if the reaction is finished when exiting the mixer unit, no further polymerization occurs anymore, explaining why all three reactors summarized in Table 2 show similar results. Yet, we found that a residence unit does have a beneficial effect (as seen by the inter-reactor variation summarized in Table 2), probably by increasing back pressure and hence leading to more stable flow conditions. It may be interesting to elucidate the exact influence of mixer geometries and backpressure. Yet, the results obtained here are already satisfactory and much more precise than any synthesis effort before.

2.4.2. Varying the initiator concentration

Varying the molecular weight is usually achieved by changing the initiator concentration.[11] Also here, batch reactions showed only limited success in controlling the residual polymer chain length. For our flow setup, these experiments were performed in 2 reactors since the length of the reactor has a small influence on the molecular weight, as described above. First, the 0.5 mL reactor with a residence time of 0.5 seconds was chosen since this reactor type and residence time gave low dispersities. Concerning the testing for different initiator concentrations, different amounts of initiator are brought in separate syringes and consecutively connected to the reactor. When the initiator concentration is reduced, the molecular weight should increase because less chains will be initiated and therefore longer chains are formed. This trend is also seen in this experiment where the initiator concentration was varied from 0.25 equivalents (relative to the monomer) to 0.05 equivalents, see Table 3. For

this variation, the molecular weight increases from 6600 g·mol^{-1} to 7800 g·mol^{-1} and the dispersity ranges from 1.3 to 1.5, see Figure 3.

Table 3: Variation of the initiator concentration of the MDMO precursor polymerization in continuous flow

equiv initiator	M_n g·mol^{-1}	M_w g·mol^{-1}	$Đ$	equiv initiator	M_n g·mol^{-1}	M_w g·mol^{-1}	$Đ$
	0.5 mL reactor				0.13 mL reactor		
0.25	6600	8600	1.3	0.25	4800	6800	1.4
0.20	6300	8200	1.3	0.20	4700	6400	1.3
0.15	6900	9500	1.4	0.15	5900	8600	1.5
0.10	7500	10800	1.4	0.10	6700	10200	1.5
0.05	7800	12000	1.5	0.05	6900	11000	1.6

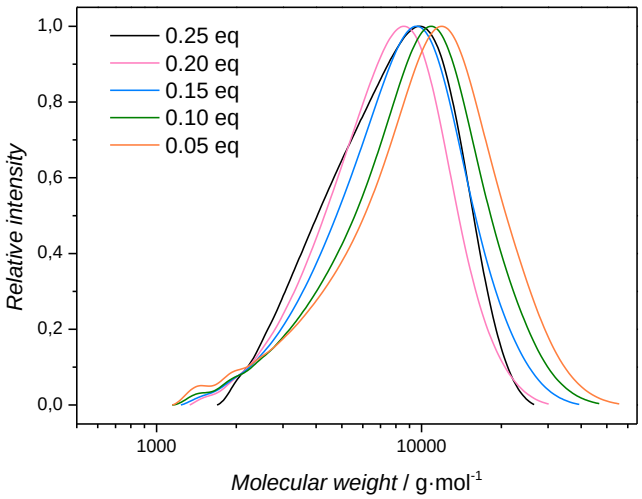

Figure 3: Variation of the initiator concentration in the MDMO precursor polymerization in continuous flow for a 0.5 mL tubular reactor

The same trend is seen when a 0.13 mL reactor with a residence time of 0.25 seconds was used to investigate the molecular weight changes when the initiator concentration was varied. For this reaction setup, the molecular weight increases from 4800 g·mol^{-1} to 6900 g·mol^{-1} and the dispersity ranges from 1.3 to 1.6 (with initiator concentrations decreasing from 0.25 equivalents to 0.05 equivalents), see Figure 4.

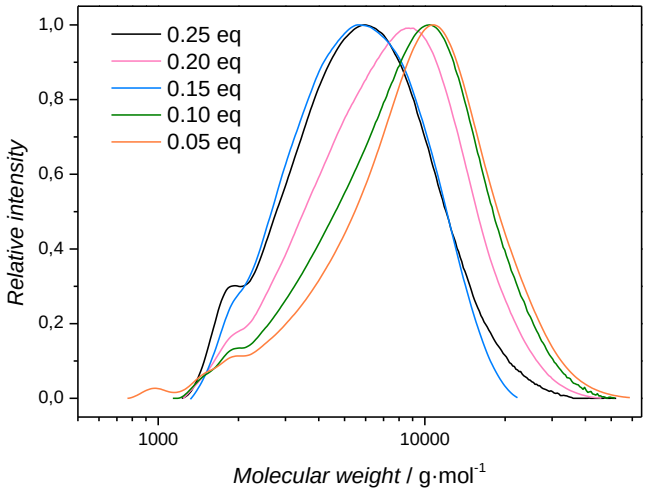

Figure 4: Variation of the initiator concentration in the MDMO precursor polymerization in continuous flow for a 0.13 mL tubular reactor

As can be observed, the molecular weights are lower than for the 0.5 mL reactor (like it was also the case when the different reactor volumes were investigated), and the same trend of increasing molecular weight and broadening of the dispersity is visible with the decrease of the initiator concentration. The broadening of the dispersity and the increase in molecular weight is often seen in batch reactions when the amount of initiator is reduced.[11]

Obviously, the variation in molecular weight, even with the small reactor, is not as large as one would expect from the initiator to monomer concentration ratios. Less initiator decelerates the overall initiation rate (given by the concentration of initiator and monomer), hence leading to conditions where initiation and propagation progressively occur simultaneously. This corrupts the molecular weight control and leads to the observation of progressively broader distributions being produced. Yet, within limits the molecular weight can be changed, while retaining the low dispersity of the polymer. Interestingly, in recent years increasing attention is given in the polymer synthesis field to controlling the dispersity of polymers, as this affects physical properties and self-assembly behaviour of polymers significantly.[17] In this sense, the choice of flow rate and/or mixing of the reaction streams gives access to PPVs with controllable dispersity, which may pose a significant advantage in future studies.

2.4.3. Block copolymer synthesis in batch

Now that PPV polymers with different molecular weights are readily available, chain extensions can be performed to form block copolymers. This serves as a facile application of the method, but also is used to further underpin the well-controlled flash polymerization procedure. Only if high endgroup fidelity is obtained in the initiation, successful block copolymer formation will be achievable. The second block can be grown from the Br end-group introduced via the anionic initiator on the PPV precursor polymer by SET-LRP. This approach had been described before, but then for more disperse PPVs. The Br-containing end-group is effectively build in in the polymer, as can be observed by NMR, see Figure 5. The two CH_3 groups adjacent to the terminal bromine appear at 2.06 and 2.08 ppm.

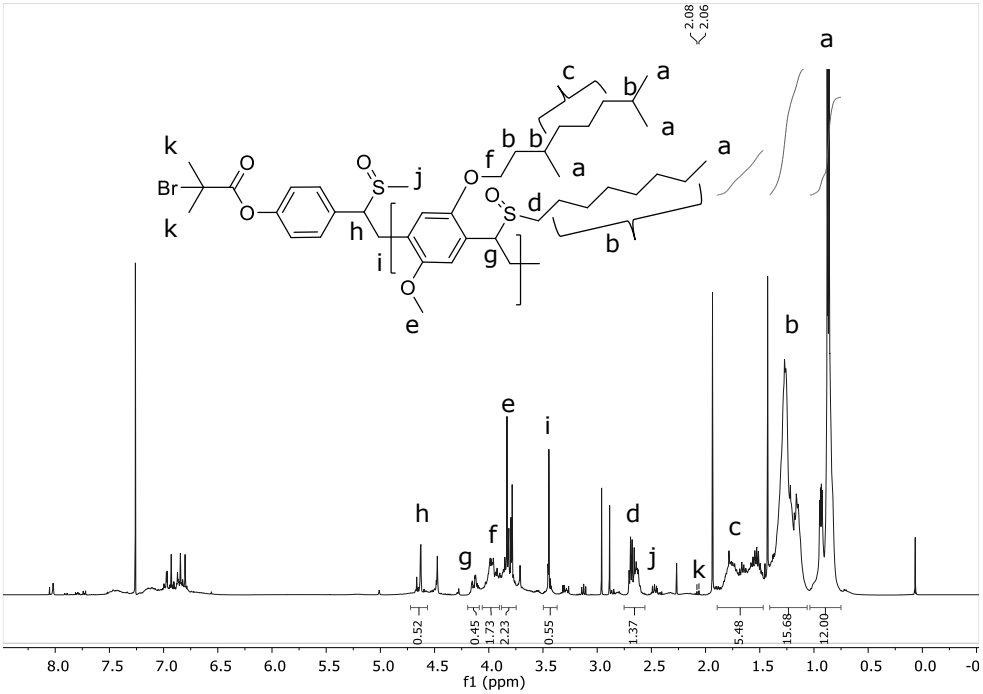

Figure 5: ^{1}H NMR of the PPV precursor polymer with a flow reactor of 0.5 mL and a residence time of 10 seconds

For SET-LRP, tert-butyl acrylate (*t*BuA) is chosen as the second block, as it allows to hydrolyse the acrylate block later to form amphiphilic material.[21] In order to perform the SET-LRP with *t*BuA, tris[2-(dimethylamino)ethyl]amine (Me_6TREN) and DMF were added to the precursor polymer. This mixture was admitted to five freeze pump thaw cycles before it was transferred into the glovebox where Cu(0) was added and the mixture was stirred for 4 h at 50 °C. At the end of the reaction, the mixture was taken out of the glovebox and exposed to air which quenches the reaction. Next, the block copolymer was dissolved in a small amount of chloroform and applied on a plug with basic alumina to remove all copper species. The chloroform was evaporated and the precursor block copolymer was dissolved in

toluene and refluxed at 110 °C for 3 hours. Afterwards, the solvent was evaporated and the block copolymer was purified by precipitation in a cold methanol/water (4/1) mixture. After filtration, the purified block copolymers were obtained and analysed using SEC. Since it can be expected that the acrylate has polymerized to full conversion in this time, different PPV to acrylate monomer concentration ratios were employed to vary the block copolymer composition. As expected, a shift in the SEC chromatograms is observed for the chain extensions. Unfortunately, the elongation itself is not clearly visible for the series of PPV-*b*-P*t*BuA block copolymers, see Figure 6.

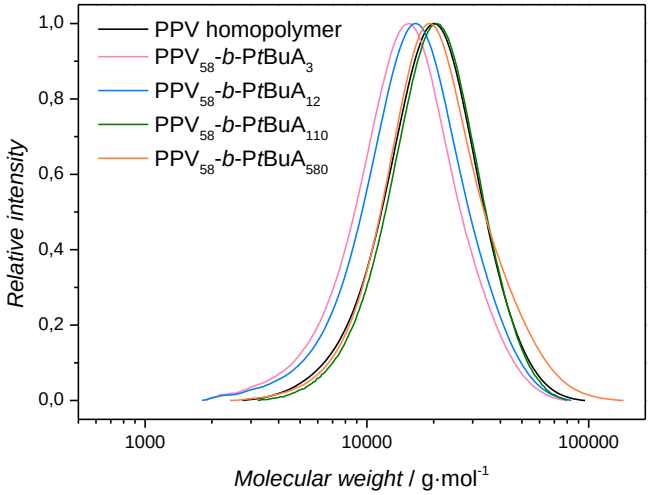

Figure 6: Molecular weight distributions of the PPV homopolymer and the different PPV-*b*-P*t*BuA block copolymers

This is somewhat unusual, but has been observed before, especially for PPV polymers. It can be explained by the low change in hydrodynamic volume when the block copolymer is formed. PPV-*b*-P*t*BuA is a rod-coil like block copolymer, where PPV is the rod-like polymer segment and *t*BuA is the coil-like polymer

segment. When these polymer segments are connected, the coil-like *t*BuA polymer segment is convoluted around the rod-like PPV polymer segment, making it difficult to follow any change in block length via size exclusion chromatography. SEC is simply not able to separate these polymers correctly. Further, since PPV is fluorescent, light scattering cannot be used for the determination of M_w, and Mark-Houwink parameters for the PPV homopolymer were used, also leading to a slight misinterpretation of the results. Other methods for testing the success of the reactions had thus to be found. Examination on the presence of the *t*BuA polymer can be done via ^{1}H NMR analysis, see Figure 7.

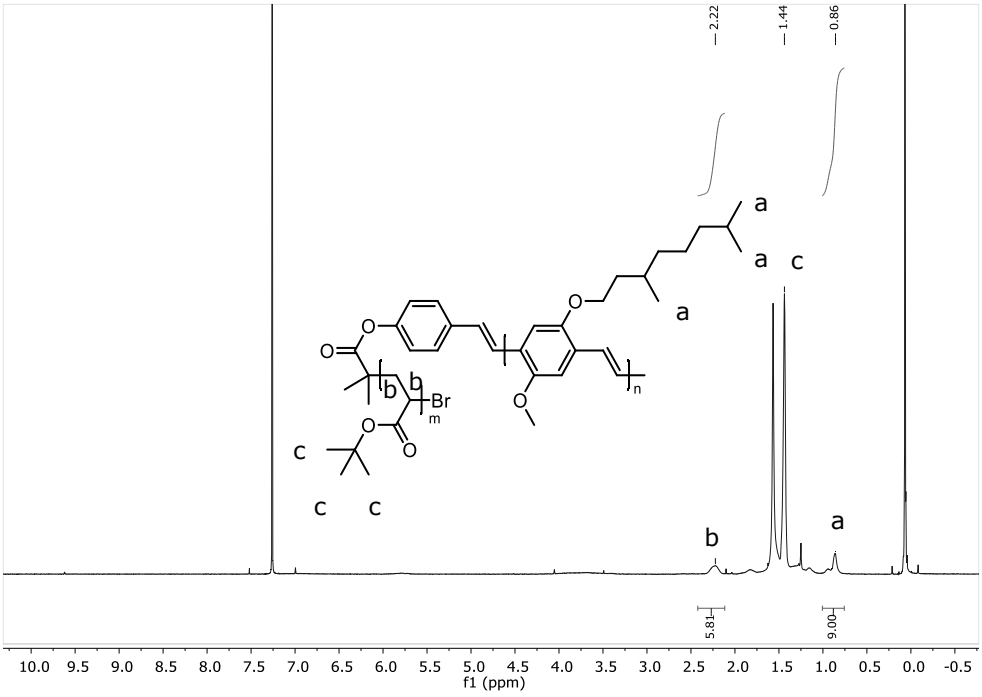

Figure 7: ^{1}H NMR of the PPV-*b*-P*t*BuA block copolymer

The ^{1}H NMR graphs indicate clearly the presence of the protons originating from the *t*BuA polymer block. The protons of the tertiary butyl group are present at 1.44 ppm, and the protons of the acrylate backbone are located at 2.22 ppm together with the two methyl groups originating from the initiator chain-end, see Figure 7. The ^{1}H NMR spectra can also be used to quantitatively analyse the degree of polymerization of the SET-LRP and therefore also an estimation of the molecular weight can be made, see Table 4. For the calculation of the molecular weight of the block copolymers via ^{1}H NMR, the peaks integrated in Figure 7 are used. The signal at 0.86 ppm corresponds to the 3 CH_3 groups of MDMO-PPV and the integration is therefore set at 9 relative numbers (rel). The signal at 2.22 ppm corresponds to 3 protons that belong to the *t*BuA polymer. In this example this peak integrates for 5.81 relative numbers, to define the degree of polymerization for the *t*BuA block the following calculation is done:

$$\frac{5.81\ rel}{3\ rel} = 1.9$$

This means there are 1.9 times more *t*BuA blocks in the block copolymer then PPV blocks.

The molecular weight of the PPV block is determined using SEC and is 16700 g·mol^{-1} and the molecular weight of one block is 288 g·mol^{-1}, the degree of polymerization (*DP*) is:

$$\frac{16700\ g \cdot mol^{-1}}{288\ g \cdot mol^{-1}} = 58\ PPV\ units$$

The *DP* for the *t*BuA block is therefore:

$$1.9 \cdot 58\ units = 110\ \text{tBuA units}$$

The molecular weight of the *t*BuA block is:

$$110\ \text{tBuA units} \cdot 128\ \text{g} \cdot mol^{-1} = 14100\ g \cdot mol^{-1}$$

This means the total molecular weight of the block copolymer is:

$$16700\ g \cdot mol^{-1} + 14100\ g \cdot mol^{-1} = 30800\ g \cdot mol^{-1}$$

Using this calculation method for all block copolymers, the different degrees of polymerization for the second block were achieved ranging from 3 till 580, corresponding to molecular weights ranging from 17 100 g·mol^{-1} to 90 900 g·mol^{-1}.

Table 4: Overview of the molecular weight, dispersity and λ_{max} of the PPV-*b*-PtBuA block copolymers

PPV/P*t*-BuA *DP* [a]	$M_{n,T}$ [b] g·mol^{-1}	M_n [c] g·mol^{-1}	M_w [c] g·mol^{-1}	*Đ*	λ_{max} [e]
58 [d]		16700	21700	1.30	489
58/3	17100	12500	17100	1.37	450
58/12	18200	13400	18400	1.37	467
58/110	30800	17500	22000	1.26	489
58/580	90900	17200	23500	1.36	485

[a] *DP* is the theoretical degree of polymerization, [b] $M_{n,T}$ is the theoretical molecular weight calculated via ^{1}H NMR, [c] M_n is the number average molecular weight, M_w the weight average molecular weight and *Đ* represents the dispersity of the molecular weight distribution. Measurements were performed via SEC. [d] *DP* for the PPV homopolymers is calculated from the M_n measured via SEC, [e] λ_{max} was determined using chloroform as solvent.

To further analyse the block copolymers their λ_{max} was measured using UV-VIS spectrometry, Figure 8. It can be noticed that there is only a small change in the λ_{max} of the different block copolymers and the PPV homopolymer, Table 4. This is also seen before in batch polymerizations of PPV with *t*BuA.[22] The (small) shift in λ_{max} occurs due to variations in the conjugation length of the PPV polymer around the values of the actual conjugation length.

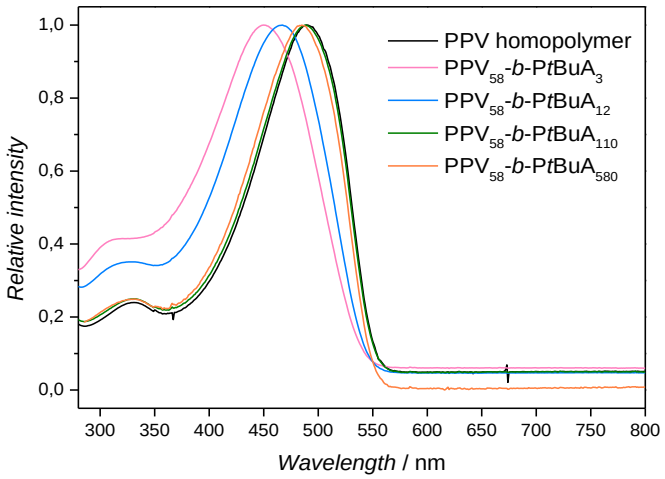

Figure 8: UV-VIS of the PPV homopolymer and PPV-b-P*t*BuA dissolved in chloroform

Another way to elucidate if the block copolymer is present is by performing a FT-IR measurement. In Figure 9, the comparison is made between the spectra of the MDMO precursor polymer and the precursor PPV-*b*-P*t*BuA block copolymer. The C=O ester peak (1728 cm^{-1}) of the acrylate is clearly present in the spectrum of the block copolymer.

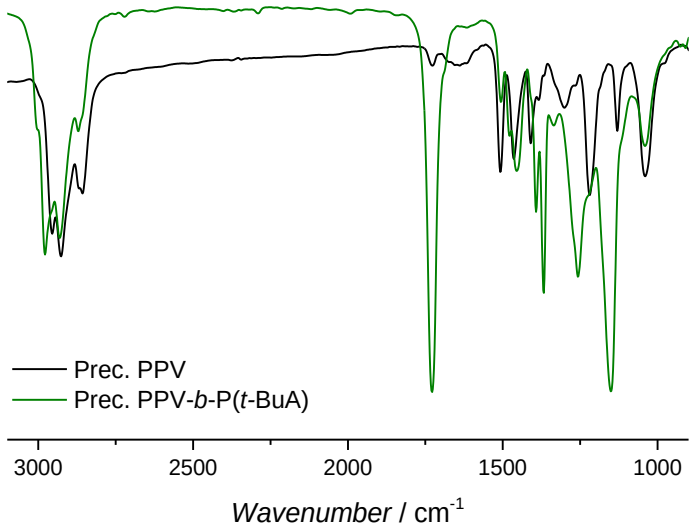

Figure 9: FT-IR of the PPV precursor homopolymer and the precursor PPV-*b*-P*t*BuA block copolymer

The techniques presented above give all indications that the PPV-*b*-P*t*BuA block copolymer is formed. Yet, NMR and FT-IR cannot distinguish between a polymer blend and a block copolymer, even if a block copolymer is the only reasonable explanation, since no other ATRP initiator (and hence source of Br) was present in the polymerization other than the PPV polymer. A solid confirmation for the existence of a block copolymer is self-assembly, this will be further elucidated in chapter 4.

2.5. Conclusions

A flash chemistry approach to the anionic polymerization of MDMO-PPV via precursor Vanderzande-route polymerization in continuous flow reactors is presented. The polymerization was accomplished in very fast reaction times on the timescale of milliseconds and polymers with low dispersity of 1.2 were achieved for the first time. The molecular weight of the PPV polymers could be changed by tuning the reactor setup or changing the amount of initiator used for the polymerization. A second polymer block was coupled to the PPV precursor polymer via SET-LRP and in this way PPV-*b*-P*t*BuA was obtained. As mentioned, the main advantage of the flow process is to reduce the dispersity of the PPV to levels typically observed for living or controlled polymerization, as much as giving more insights on the mechanism and kinetics of the precursor polymerization.

2.6. References

[1] F. Louwet, D. Vanderzande, J. Gelan, *Synth. Met.* **1995**, 69, 509-510.

[2] A. Van Breemen, D. Vanderzande, P. Adriaensens, J. Gelan, *J. Org. Chem.* **1999**, 64, 3106-3112.

[3] L. Lutsen, A. Van Breemen, W. Kreuder, D. Vanderzande, J. Gelan, *Helv. Chem. Acta* **2000**, 83, 3113-3121.

[4] A. Issaris, D. Vanderzande, J. Gelan, *Polymer* **1997**, 38, 2571–2574.

[5] J. Wiesecke, M. Rehanh, *Angew. Chem. Int. Ed*. **2003**, 42, 567–570.

[6] L. Hontis, V. Vrindts, L. Lutsen D. Vanderzande, J. Gelan, *Polymer* **2001**, 42, 5793.

[7] L. Hontis, V. Vrindts, D. Vanderzande, L. Lutsen, *Macromolecules* **2003**, 36, 3035.

[8] N. Zaquen, M. Rubens, N. Corrigan, J. Xu, P. B. Zetterlund, C. Boyer, T. Junkers, *Prog. Polym. Sci.* **2020**, 107, 101256.

[9] N. Zaquen, E. Baeten, J. Vandenbergh, L. Lutsen, D. Vanderzande, T. Junkers, *Chem. Eng. Technol.* **2015**, 38, 1749-1757.

[10] N. Zaquen, P. H. M. Van Steenberge, D. R. D'Hooge, M.-F. Reyniers, G. B. Marin, J. Vandenbergh, L. Lutsen, D. Vanderzande, T. Junkers, *Macromolecules* **2015**, 48, 8294-8306.

[11] I. Cosemans, J. Vandenbergh, V. S. D. Voet, K. Loos, L. Lutsen, D. Vanderzande, T. Junkers, *Polymer* **2013**, 54, 1298-1304.

[12] Y. Takahashi, A. Nagaki, *Molecules* **2019**, 24, 1532.

[13] J. Yoshida, A. Nagaki, T. Yamada, *Chem. Eur. J.* **2008**, 14, 7450-7459.

[14] J. Wegner, S. Ceylan, A. Kirschning, *Chem. Commun*. **2011**, 47, 4583-4592.

[15] J. Morsbach, A. H. E. Muller, E. Berger-Nicoletti, H. Frey, *Marcomolecules* **2016**, 49, 5043-5050.

[16] R. Whitfield, N.P. Troung, D. Massmer, K. Parkatzidis, M. Rolland, A. Anastasaki, *Chem. Sci.* **2019**, 10, 8724-8734.

[17] T. Junkers, Macromol. *Chem. Phys* **2020**, 221, 2000234.

[18] N. Zaquen, J. Vandenbergh, M. Schneider-Baumann, L. Lutsen, D. Vanderzande, T. Junkers, *Polymers* **2015**, 7, 418-452.

[19] G. Lligadas, S. Grama, V. Percec, *Biomacromolecules* **2017**, 18, 1039-1063.

[20] V. Percec, T. Guliashvili, J. Ladislaw, A. Wistrand, A. Stjerndahl, M. Sienkowska, M. Montiero, S. Sahoo, *J. Am. Chem. Soc*. **2006**, 128, 14156-14165.

[21] I. Cosemans, J. Vandenbergh, L. Lutsen, D. Vanderzande, T. Junkers, *Polym. Chem.* **2013**, 4, 3471.

[22] A) A. Sokolova, J. Christoforidis, A. Eltobaji, J. Barnes, F. Darmann, A. E. Whitten, L. de Campo, *Neutron News* **2016**, 27, 9-13; b) A. Sokolova, A. E. Whitten, L. de Campo, J. Christoforidis, A. Eltobaji, J. Barnes, F. Darmann, A. Berry, *J. Appl. Crystallogr*. **2019**, 52, 1-12.

Chapter 3

High Temperature SET-LRP in Continuous Flow Reactors

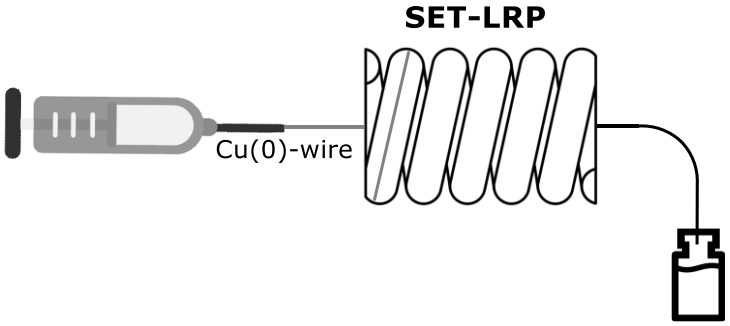

3.1. Abstract

The block copolymer synthesis of poly[2-methoxy-5-(3',7'-dimethyloctyloxy)-1,4-phenylenevinylene] (MDMO-PPV) and poly(methyl acrylate) (PMA) via single electron transfer-living radical polymerization (SET-LRP) in a continuous flow reactor is presented. A PFA tubular reactor with a copper(0)-wire is used to perform the SET-LRP reactions in continuous flow. First, the optimal reaction conditions for the benchmark polymerization of methyl acrylate (MA) with ethyl-2-bromoisobutyrate (EBiB) are determined. The residence times are varied and different polymers are synthesized with diverse degrees of polymerization. SET-LRP will be performed at elevated temperatures, to further accelerate the polymerization. There was chosen to not use ATRP for this reaction because this chapter was based on earlier research performed by Haddleton *et al.* and since in the previous chapter the block copolymerization was also performed *via* SET-LRP. Lastly, the optimal reaction conditions are converted towards the block copolymerization of MDMO-PPV and MA in continuous tubular reactors. The research of Haddleton *et al*. was based on MA, therefore this second block was used as well for the block copolymerization instead of the earlier used *t*BuA.

3.2. Introduction

In Chapter 2, low dispersity MDMO-PPV with well-defined end-groups is made available by performing the anionic polymerization in continuous flow reactors.[1] The anionic polymerization is carried out *via* the sulfinyl (Vanderzande) precursor route, following a protocol previously established.[2,3] Dispersities of 1.2 are reached, due to the efficient mixing in the tubular reactors with such low residence times that are unachievable in conventional batch-wise chemistry. In a second step, a block copolymer is formed of the precursor PPV and *tert*-butyl acrylate (*t*BuA) in batch. The formation of PPV block copolymers is of high interest, especially when amphiphilic block copolymers are synthesized, since they tend to self-assemble upon the addition of water.[4] These micelles are inherently-fluorescent and have therefore great potential to be used in biomedical applications, more of the micelle synthesis and properties are elucidated in chapter 4. It will be of great interest to perform the block copolymerization in continuous flow reactors as well, since coupling of reactions will become accessible and the reaction time can be reduced. The block copolymer synthesis of PPV and various acrylates are already well investigated in previous studies.[5] These block copolymers are synthesized via single electron transfer-living radical polymerization (SET-LRP).[6,7] The mechanism, proposed by Percec *et al.*, is explained in chapter 1 and involves Cu-sources as catalyst to perform the polymerization. The advantages of SET-LRP include the high molecular weight polymers which can be synthesized with a high chain-end functionality at high conversion.[8,910] But, the batch-wise performance of SET-LRP also involves limitations, such as the batch-to-batch variations caused by the induction times that can be observed. This is one of the reasons why SET-LRP reactions greatly

benefit from continuous flow processing. Another hurdle of SET-LRP is the exothermicity of the reaction, but this can be solved by the good heat transfer of flow reactors. Other advantages of performing SET-LRP in flow reactors are the potential to use heterogeneous catalysts and the simple reaction scale up. Moreover, the synthesis of poly(acrylates) via SET-LRP in continuous flow reactors is investigated earlier. Hutchinson *et al.* performed SET-LRP in a copper tubular reactor and later, Haddleton *et al.* performed the reaction in a PTFE reactor equipped with a copper wire.[11,12] Methyl acrylate was polymerized in DMSO *via* SET-LRP with narrow molecular weight distributions and a high degree of livingness, simultaneously with high conversions and short residence times. The advantage of using a copper reactor is that it serves both as the reactor and the catalyst. The copper tubing is also inexpensive and readily available, but on a long term the copper tubing could dissolute. Therefore, Haddleton *et al*. constructed a PTFE reactor with a simpler copper wire inside of the tubing to be used as catalyst.

In this work, poly(methyl acrylate) (PMA) is synthesized *via* SET-LRP in DMF and in a second step, a block copolymer of PPV and MA is formed. A normal PFA tubing is used with a Cu(0)-wire inside the first part of the reactor, the reactor setup is shown in Scheme 1. First, MA is polymerized at room temperature and later at elevated temperatures, to reduce the residence time even more. When optimal reaction conditions are established for the polymerization of MA, the block copolymerization of MDMO-PPV and MA is performed.

3.3. Experimental Section

3.3.1. General flow reactor setup for the SET-LRP reactions

Scheme 1 represents the general flow reactor setup for the SET-LRP reactions described in this chapter. The continuous flow reactions were performed in a self-made PFA tubular reactor with an internal diameter of 0.75 mm and a reactor volume of 1 mL. In the first part of the reactor tubing a 35 cm Cu(0)-wire, with a diameter of 0.22 mm, was inserted. This length was chosen since it resembles the surface area of the Cu(0)-wire used by Percec *et al*. The polymerization reactions were performed at temperatures ranging from room temperature till 100 °C. At 100 °C, a back-pressure regulator of 25 PSI was installed to prevent the solvent dimethylformamide (DMF) from boiling. The reagent solution (monomer, initiator and solvent) was injected into the reactor through a gastight syringe (SGE). The flow rate was controlled via a syringe pump (Chemyx) and varied between 0.00625 $mL \cdot min^{-1}$ and 0.1 $mL \cdot min^{-1}$, which corresponds to residence times between 10 minutes and 160 minutes. The end of the reactor was connected to a vial, which could be easily switched to collect different samples for screening of the residence time and reaction temperature.

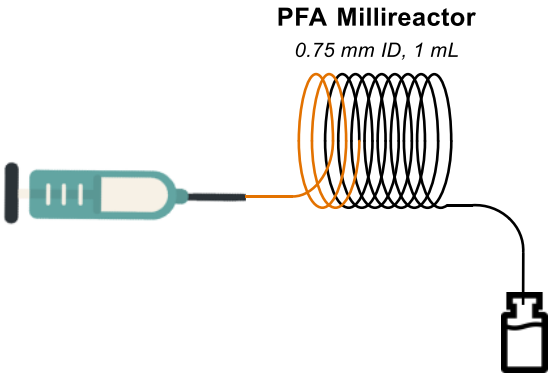

Scheme 1: Schematic representation of the SET-LRP reaction in continuous flow

3.3.2. General method for the synthesis of poly(methyl acrylate) (PMA) in a continuous flow reactor

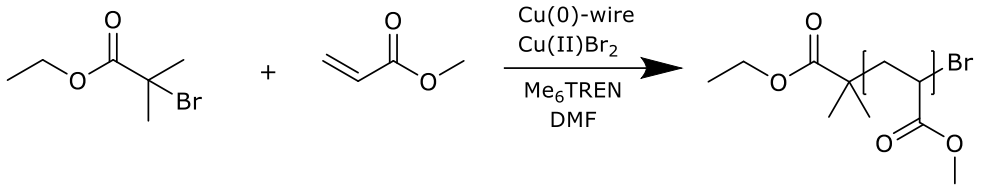

Scheme 2: Synthesis of PMA via SET-LRP in continuous flow

The methyl acrylate monomer (4.75 g, 55.17 mmol, 50 equiv.), the initiator ethyl-2-bromoisobutyrate (EBiB) (0.215 g, 1.1 mmol, 1 equiv.), the ligand tris[2-(dimethylamino)ethyl]amine (Me_6TREN) (0.02 g, 0.088 mmol, 0.08 equiv.) and the catalyst copper(II)dibromide (Cu(II)Br_2) (0.0049 g, 0.022 mmol, 0.02 equiv.) were dissolved in dimethylformamide (DMF) (5 mL). The solution was stirred and purged with nitrogen (N_2) gas for 20 minutes before it was transferred into the syringe. The Cu(0)-wire inside the reactor tubing was activated by flushing the reactor with sulfuric acid (H_2SO_4). Afterwards, the reactor is flushed with N_2-gas and rinsed with DMF. The reagent solution was now pumped into the reactor with the syringe pump and the polymer was formed. The polymer was collected in a vial with a quenching solution of methanol and water with a ratio of 4/1 MeOH/H_2O. The polymer was filtered over a small column with basic alumina to remove the copper and the solvent was evaporated.

3.4. Results and Discussion

3.4.1. Polymerization of methyl acrylate in flow reactors *via* SET-LRP

The PPV containing block copolymer synthesis is already established for batch reactions, but this specific polymerization was not yet performed in continuous flow. PPV block copolymer synthesis would greatly benefit from flow processing since the reaction time could be largely reduced. Moreover, it would be the key piece in the cascade of reactors where the PPV monomer would be transformed into micelles in multiple steps. Hence, block copolymer synthesis in continuous flow reactors will be the focus of this chapter. Since the PPV block copolymerization in batch is performed via SET-LRP, this reaction will also be used for flow polymerization.

First, a benchmark SET-LRP reaction of methyl acrylate (MA) will be examined to find the optimal reaction conditions. The residence time will be varied from 10 minutes till 67 minutes (the flow rate between 0.1 mL·min^{-1} and 0.015 mL·min^{-1}) at room temperature.

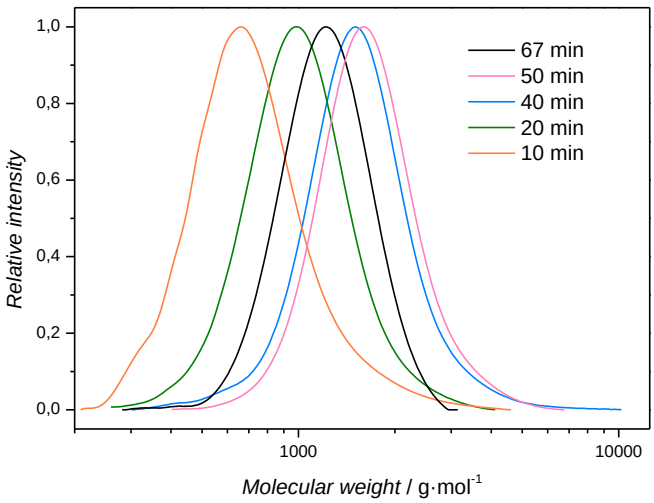

Figure 1: Molecular weight distributions obtained for the SET-LRP reactions of methyl acrylate with different residence times in continuous flow

The reactor setup and reaction conditions are as described in section 3.3.2., with the only difference that here a Cu(0)-wire of 15 cm is used. A Cu(0)-wire length of 15 cm and diameter of 0.22 mm was initially chosen since this resembles the surface area of the shortest Cu(0)-wire used by Percec *et al*.[13] The results presented in Figure 1 and Table 1 show the increase in molecular weight from 640 $g \cdot mol^{-1}$ till 1500 $g \cdot mol^{-1}$ when the residence time is increased from 10 minutes till 50 minutes. Interestingly, at a residence time of 50 minutes, the increase in molecular weight is reduced (only 100 $g \cdot mol^{-1}$ increase compared to 40 minutes residence time). Moreover, at a residence time of 67 minutes, a reduction in molecular weight, towards 1100 $g \cdot mol^{-1}$, is observed. At a residence time of 67 minutes, the flow rate is only 0.015 $mL \cdot min^{-1}$. At these low flow rates, mixing can be poor leading to a lower monomer conversion and a lower molecular weight compared to higher flow rates. The increase in molecular weight was low after 40 minutes. Therefore, 40 minutes was chosen as the optimal residence time for this reactor. There was chosen for the shorter reaction time instead of the slightly higher molecular weight. The dispersities are low for all residence times tested (1.2 for 10 - 40 minutes and 1.1 for 50 and 67 minutes).

Table 1: Overview of the molecular weight of PMA for different residence times

Residence time	M_n	M_w	$Đ$
min	g·mol^{-1}	g·mol^{-1}	
10	640	780	1.2
20	920	1100	1.2
40	1400	1700	1.2
50	1500	1800	1.1
67	1100	1300	1.1

M_n is the number average molecular weight, M_w the weight average molecular weight and $Đ$ represents the dispersity of the molecular weight distribution. Measurements were performed using SEC. The reaction conditions are as described in section 3.3.2.

As mentioned above, the optimal residence time of 40 minutes for a reactor of 1 mL with a 15 cm Cu(0)-wire was obtained. Next, different reactor setups will be examined for the methyl acrylate polymerization *via* SET-LRP in continuous flow, the results are displayed in Table 2. The first reactor tested here had a volume of 0.5 mL, an internal diameter of 0.75 mm and a Cu(0)-wire of 15 cm that was applied in the first part of the tubing. With a residence time of 40 minutes (flow rate is 0.0125 mL·min^{-1}) a conversion of 42% was achieved. The obtained polymer had a molecular weight of 1300 g·mol^{-1} and a dispersity of 1.2.

In order to increase the monomer conversion, the reactor volume was expanded to 1 mL. Subsequently, the conversion increased towards 58% after 40 minutes of residence time (flow rate is 0.025 mL·min^{-1}). A molecular weight of 1800 g·mol^{-1} and a dispersity of 1.2 was achieved. Next, the monomer conversion was further increased by inserting a longer Cu(0)-wire (35 cm) into the tubing

with a volume of 1 mL. A molecular weight and conversion increase towards 2300 g·mol^{-1} and 62% respectively, was observed. A monomer conversion of 62% after 40 minutes of residence time is a good outcome, but performing the polymerization in a Cu(0)-reactor could improve the reaction even more. Therefore, a Cu(0)-tubing reactor with a diameter of 1 mm and a volume of 6.5 mL was investigated. First, the polymerization was tested with a residence time of 40 minutes (flow rate is 0.1625 mL·min^{-1}), but unfortunately a monomer conversion of only 12% was achieved with a molecular weight of 470 g·mol^{-1}. Since the reactor has a volume of 6.5 mL, the flow rate is quite high to obtain a residence time of 40 minutes in comparison with the other reactors of 0.5 mL and 1 mL. At these high flow rates, the reagents have less time to interact with the Cu(0)-tubing. Therefore, a longer residence time of 260 minutes (flow rate is 0.025 mL·min^{-1}) was examined, which led to a monomer conversion of 63% and a molecular weight of 2200 g·mol^{-1}. These values are in the same range as the results of the polymerization in the 1 mL reactor with extra Cu(0)-wire and in comparison with the 60% conversion Haddleton *et al.* obtained. But, since the residence time of the Cu(0)-reactor is much longer than the one of the 1 mL reactor, 260 minutes vs 40 minutes respectively, the 1 mL reactor with the 35 cm Cu(0)-wire is the optimal reactor for the polymerization of methyl acrylate *via* SET-LRP.

Table 2: Overview of the different reactor designs tested for the polymerization reaction of MA

Reactor Volume mL	Residence time min	*Cu(0) source*	M_n g·mol^{-1}	M_w g·mol^{-1}	*Đ*	*Conversion* %
0.5	40	15 cm Cu(0)-wire	1300	1500	1.2	42
1	40	15 cm Cu(0)-wire	1800	2200	1.2	58
1	40	35 cm Cu(0)-wire	2300	2700	1.2	62
6.5	40	Cu(0)-tubing	470	550	1.2	12
6.5	260	Cu(0)-tubing	2200	2500	1.2	63

M_n is the number average molecular weight, M_w the weight average molecular weight and *Đ* represents the dispersity of the molecular weight distribution. Measurements were performed using SEC. The conversion is calculated via ^{1}H NMR.

In the next section, different residence times are tested to synthesize polymers with various molecular weights, a summary of the results is presented in Table 3. First, a degree of polymerization (*DP*) of 50 was aimed for, when the polymerization would proceed to full conversion. The results are depicted in Figure 2 and in Table 3 entries 1-4. When the residence time increases from 20 minutes to 160 minutes (flow rates between 0.05 mL·min^{-1} and 0.00625 mL·min^{-1}), the monomer conversion and therefore also the molecular weight increases from 1100 g·mol^{-1} to 2400 g·mol^{-1}. Again, at higher residence times, a retardation in the molecular weight increase is observed. The molecular weight obtained via SEC measurements closely resembles the theoretical molecular weight, calculated from the conversion determined by ^{1}H NMR. There can be noted that the monomer

conversions are lower than the ones of the same reaction conditions in Table 2 entry 3, this is due to the reduced activity of the Cu(0)-wire. The Cu(0)-wire needs to be reactivated again after some time, this activation was not performed before these reactions were executed, but the trend in molecular weight and conversion stays the same.

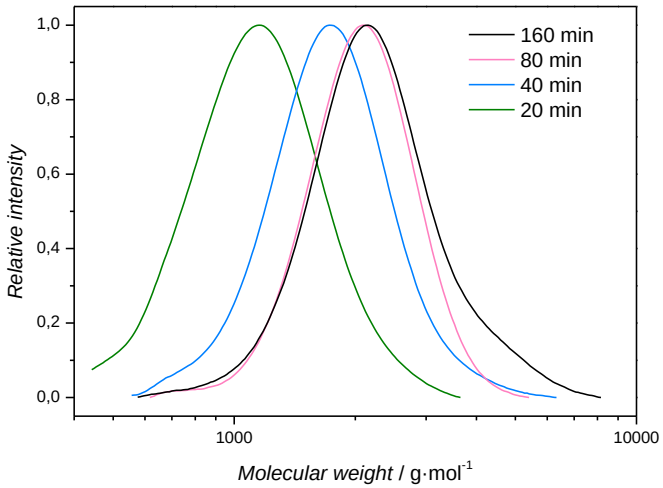

Figure 2: Molecular weight distributions for the different residence times of the polymerization reactions of MA with a targeted *DP* of 50

The same variations are performed for the polymerizations targeting a degree of polymerization of 25, see Table 3 entries 5-7. The variation of the residence times between 20 minutes and 80 minutes (flow rates between 0.050 mL·min^{-1} and 0.0125 mL·min^{-1}) resulted in an increase of the monomer conversion from 33% to 77%. The molecular weight increased from 370 g·mol^{-1} to 1400 g·mol^{-1}, with still a narrow dispersity of 1.1, see Figure 3. There can be observed that the SEC graph of the reaction with 20 minutes of residence time is not 'smooth', this can

be explained by the low concentration of the polymer in the SEC sample since the conversion is only 33% here (the same explanation is valid for Figure 4 later on).

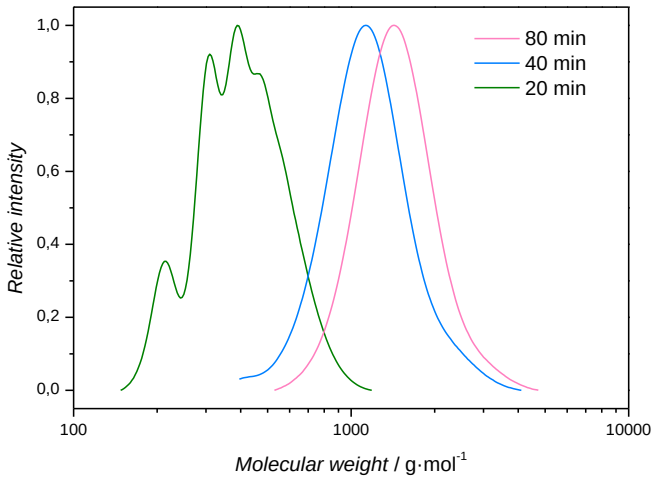

Figure 3: Molecular weight distributions for the different residence times of the polymerization reactions of MA with a targeted *DP* of 25

Table 3: Overview of the molecular weight and conversion of the SET-LRP of MA with a different target degree of polymerization (*DP*)

Entry	*DP*	Residence time	M_n	M_w	*Đ*	Conversion	$M_{n,T}$
		min	g·mol^{-1}	g·mol^{-1}		%	
1	50	20	1100	1200	1.2	20	900
2	50	40	1600	1800	1.1	37	1700
3	50	80	2000	2100	1.1	47	2100
4	50	160	2100	2400	1.2	62	2800
5	25	20	370	420	1.1	33	780
6	25	40	1100	1200	1.1	59	1400
7	25	80	1400	1500	1.1	77	1800
8	10	20	450	510	1.1	47	490
9	10	40	630	700	1.1	71	750

All above presented reactions are performed in a 1 mL reactor with 35 cm Cu(0)-wire, *DP* is the targeted degree of polymerization, M_n is the number average molecular weight, M_w the weight average molecular weight and *Đ* represents the dispersity of the molecular weight distribution. Measurements were performed using SEC. The conversion is calculated via ^{1}H NMR. $M_{n,T}$ is the theoretical molecular weight calculated via ^{1}H NMR. The reaction conditions are as described in section 3.3.2.

Lastly, a degree of polymerization of 10 was targeted, which corresponds to a molecular weight of 1050 g·mol^{-1}, when the polymerization would reach full conversion. Two reactions were performed, whereof the results are shown in Figure 4 and Table 3 entries 8 and 9. The first reaction had a residence time of 20 minutes which resulted in a monomer conversion of 47% and a molecular weight of 450 g·mol^{-1}. A residence time of 40 minutes gave a monomer conversion of 71% and a molecular weight of 630 g·mol^{-1}. The theoretical molecular weight, 490 g·mol^{-1} and 750 g·mol^{-1} respectively, resembles the molecular weight obtained *via* SEC very well.

Overall, there can be concluded that when a higher degree of polymerization is targeted, a longer residence time is required to obtain reasonable conversions.

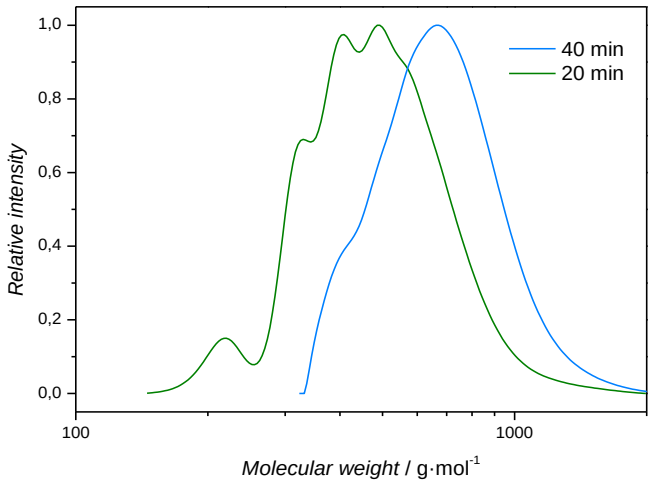

Figure 4: Molecular weight distributions for the different residence times of the polymerization reactions of MA with a targeted *DP* of 10

In literature, the polymerization of MA *via* SET-LRP is mostly performed in DMSO, but since the PPV block copolymer synthesis is performed in DMF, the benchmark polymerization is also performed in DMF. Nevertheless, the comparison is made between the reaction performed in DMSO and DMF to identify the difference in conversion when different solvents are used. Figure 5 shows the difference in molecular weight distributions for the polymerization of MA in DMSO and DMF. After 20 minutes of residence time, a conversion of 28% and 22% is achieved for the polymerizations in DMSO and DMF, respectively. The corresponding molecular weights with a targeted *DP* of 60, are 1600 g·mol^{-1} and 900 g·mol^{-1} for DMSO and DMF polymerizations, respectively. Like expected from literature, the polymerization proceeds faster in DMSO than in DMF. Therefore, the SET-LRP reactions in DMF will be performed at elevated temperature to increase the reaction kinetics.

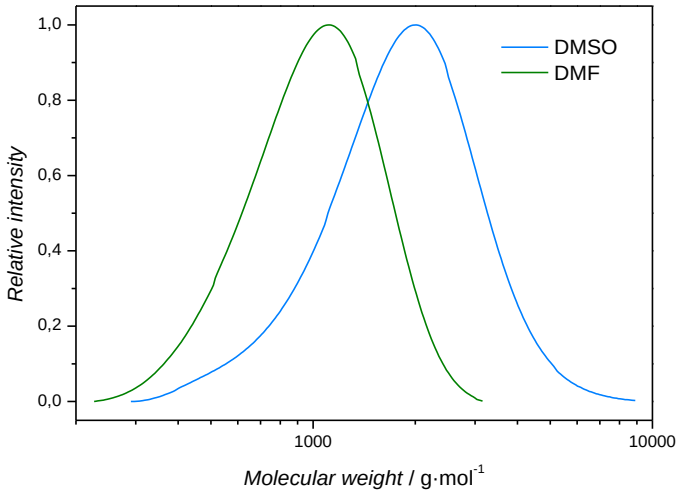

Figure 5: Molecular weight distributions of the polymerization of MA in DMSO and DMF

3.4.2. High temperature SET-LRP of methyl acrylate

In the previous section was identified that the SET-LRP of MA advances faster in DMSO than in DMF. But, since DMF is required for the block copolymerization of PPV, this is still the solvent that will be used further. Therefore, the reaction kinetics was further increased, by performing the polymerization at elevated temperatures.

Different temperatures were tested for the SET-LRP reaction of methyl acrylate in continuous flow. The 1 mL reactor with a 35 cm Cu(0)-wire was used with a residence time of 20 minutes (flow rate is 0.050 mL·min^{-1}) and a targeted degree of polymerization of 60. Figure 6 shows the increase of the molecular weight, when the temperature is increased from room temperature to 75 °C, more details are given in Table 4. Remarkably, when the temperature is further increased to 100 °C, the molecular weight decreases. This can be caused by chain transfer reactions, which have a higher activation energy than propagation reactions and become therefore more abundant at higher temperatures.[14] At 75 °C, a conversion of 67% is achieved in only 20 minutes of residence time, at room temperature it would take over 160 minutes to reach such conversions. Performing the SET-LRP reactions at higher temperatures clearly increases the rate of the polymerization.

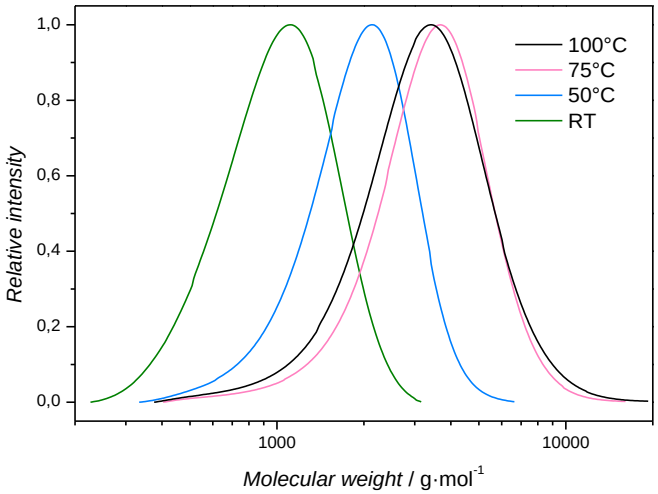

Figure 6: Molecular weight distributions obtained for the SET-LRP reactions of MA with different reaction temperatures in continuous flow

Table 4: Overview of the molecular weight obtained for the SET-LRP reactions of MA with different reaction temperatures in continuous flow

Temperature °C	M_n g·mol^{-1}	M_w g·mol^{-1}	$Đ$	Conversion %	$M_{n,T}$ g·mol^{-1}
R.T.	900	1100	1.2	22	1200
50	1700	2100	1.2	46	2500
75	3000	3700	1.3	67	3600
100	2800	3600	1.3	63	3400

R.T. is the room temperature. The targeted *DP* is 60 and the residence time is 20 minutes for all the reactions displayed in this table.

3.4.3. Block copolymer synthesis of MDMO-PPV and PMA *via* SET-LRP in continuous flow reactors

In the previous section, a reasonable conversion of 67% is obtained for the MA polymerization at 75 °C with a residence time of only 20 minutes. These results are consistent with the 60% conversion Haddleton *et al.* showed for the same flow rate of 0.05 mL·min^{-1} at room temperature, but with 120 minutes of reaction time. These results will now be translated to the block copolymerization of the precursor MDMO-PPV and MA. A *DP* of 100 was targeted for the PPV block copolymerization to see an extension more easily because the molecular weight of the PPV block was already quite high (8600 g·mol^{-1}). This reaction follows the same mechanism as the polymerization of MA with EBiB, since MDMO-PPV has the required bromine group which serves as the initiator to start the polymerization, see Scheme 3. Upon heating, the precursor block copolymer can be eliminated and the conjugated block copolymer is obtained.

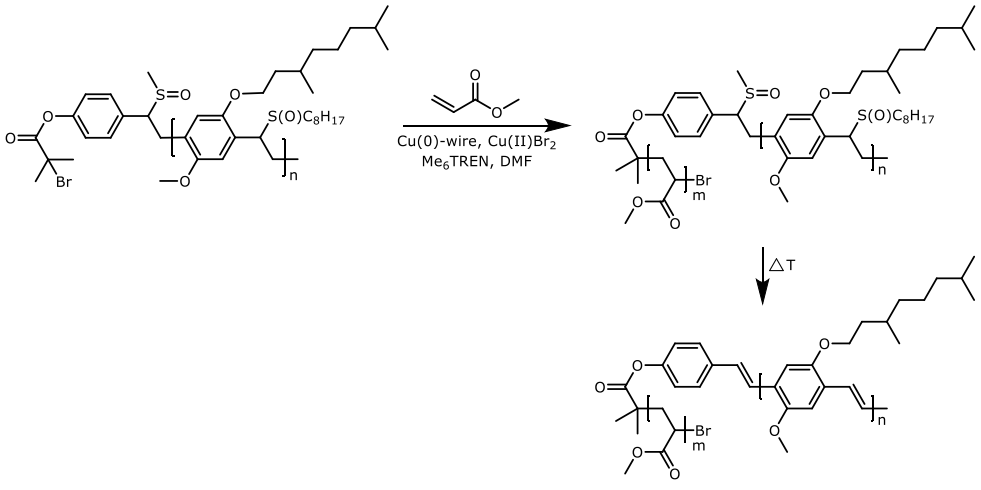

Scheme 3: SET-LRP of the precursor MDMO-PPV and MA into the precursor PPV-*b*-PMA block copolymer

The molecular weight distribution of the obtained block copolymer was measured using SEC and is displayed in Figure 7 and Table 5. The SEC graphs do not show any elongation of the polymer chain, but this doesn't mean the block copolymer formation failed. Moreover, this trend is observed before for this kind of polymerizations and especially for PPV polymers.[1] It can be explained by the low change in hydrodynamic volume when the block copolymer is formed due to the rod-coil like block copolymer, a more detailed explanation is given in chapter 2. Since the ^{1}H NMR of the crude mixture after the block copolymerization showed a methyl acrylate monomer conversion of 70% (Figure 8) and no other ATRP initiator (and source of Br) was present, the probability that the block copolymer is formed is reasonably high. Nevertheless, the formation of a polymer blend or block copolymer cannot be distinguished from these analysis methods. A solid confirmation for the existence of a block copolymer is self-assembly, this will be further elucidated in chapter 4.

Table 5: Overview of the molecular weight obtained for the SET-LRP of PPV and MA in continuous flow

	M_n g·mol^{-1}	M_w g·mol^{-1}	$Đ$	Conversion %	$M_{n,T}$ g·mol^{-1}
Precursor PPV	8600	11200	1.29		
PPV-*b*-PMA	7700	9300	1.22	70	14600

The polymerization is performed at 75 °C. The targeted *DP* is 100 and the residence time is 20 minutes.

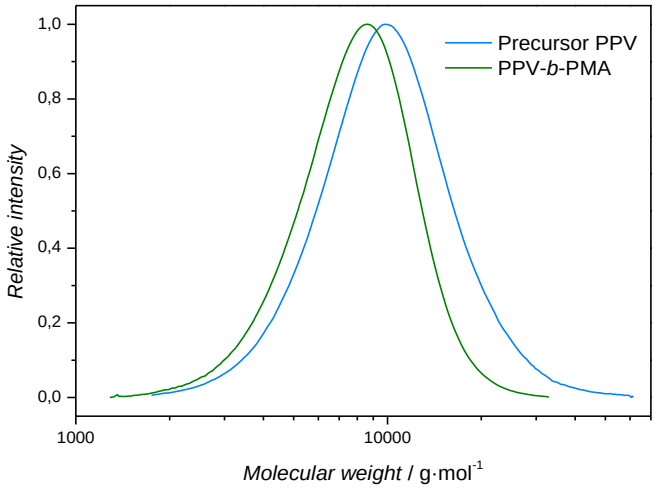

Figure 7: Molecular weight distributions of the PPV homopolymer and the PPV-*b*-PMA block copolymer

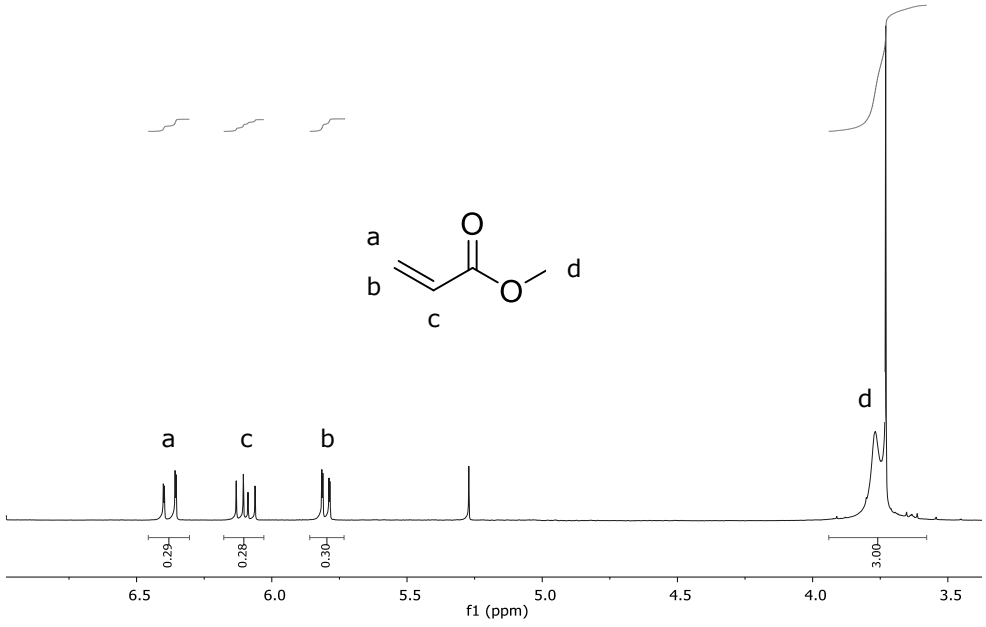

Figure 8: ^{1}H NMR zoom-in on the acrylate peaks of the crude mixture after the block copolymerization of PPV and MA *via* SET-LRP in a continuous flow reactor

3.5. Conclusions

The SET-LRP reaction of methyl acrylate (MA) in DMF was performed in custom-made flow reactors with a Cu(0)-wire inserted. Reasonable monomer conversions up until 77% could be achieved with degrees of polymerizations ranging from 10 till 60. Depending on the targeted *DP*, the residence times were varied from 20 minutes till 160 minutes. When a higher degree of polymerization was targeted, a longer residence time was necessary to reach high monomer conversions. The residence time could be largely reduced by increasing the reaction temperature to 75 °C with maintained polymer properties. Lastly, block copolymer synthesis was performed in this continuous flow reactor and PPV-*b*-PMA was obtained. The PMA homopolymers and PPV-*b*-PMA block copolymer are synthesized via SET-LRP in continuous flow reactors with a residence time of only 20 minutes.

3.6. References

[1] K. Verstraete, N. Zaquen, T. Junkers, *Polym. Chem.* **2020**, 11, 7094-7103.

[2] L. Hontis, V. Vrindts, L. Lutsen D. Vanderzande, J. Gelan, *Polymer* **2001**, 42, 5793.

[3] L. Hontis, V. Vrindts, D. Vanderzande, L. Lutsen, *Macromolecules* **2003**, 36, 3035.

[4] N. Zaquen, H. Lu, T. Chang, R. Mamdooh, L. Lutsen, D. Vanderzande, M. Stenzel, T. Junkers, *Biomacromolecules* **2016**, 17, 4086.

[5] N. Zaquen, J. Vandenbergh, M. Schneider-Baumann, L. Lutsen, D. Vanderzande, T. Junkers, *Polymers* **2015**, 7, 418-452.

[6] G. Lligadas, S. Grama, V. Percec, *Biomacromolecules* **2017**, 18, 1039-1063.

[7] V. Percec, T. Guliashvili, J. Ladislaw, A. Wistrand, A. Stjerndahl, M. Sienkowska, M. Montiero, S. Sahoo, *J. Am. Chem. Soc*. **2006**, 128, 14156-14165.

[8] V. Percec, A. V. Popov, E. Ramirez-Castillo, M. Monteiro, B. Barboiu, O. Weichold, A. D. Asandei, C. M. Mitchell, *J. Am. Chem. Soc*. **2002**, 124, 4940–4941.

[9] G. Lu, Y. Li, H. Gao, H. Guo, X. Zheng, X. Huang*, J. Polym. Sci., Part A: Polym. Chem*. **2013**, 51, 1099–1106.

[10] A. G. West, B. Hornby, J. Tom, V. Ladmiral, S. Harrisson, S. Perrier, *Macromolecules* **2011**, 44, 8034.

[11] N. Chan, M. F. Cunningham, R. A. Hutchinson, *Macromol. Rapid Commun*. **2011**, 32, 604–609.

[12] J. A. Burns, C. Houben, A. Anastasaki, C. Waldron, A. A. Lapkin, D. M. Haddleton, *Polym. Chem*. **2013**, 4, 4809-4813.

[13] N. H. Nguyen, M. E. Levere, V. Percec, *J. Polym. Sci., Part A: Polym. Chem.* **2012**, 50, 860-873.

[14] W. A. Braunecker, K. Matyjaszewski, *Prog. Polym. Sci*. **2007**, 32, 93–146.

Chapter 4

Micellar Self-assembly in Continuous Flow Reactors

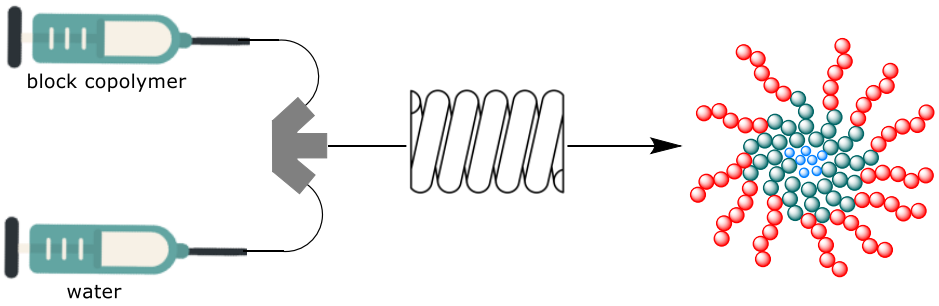

A. Buckinx, K. Verstraete, E. Baeten, R. F. Tabor, A. Sokolova, N. Zaquen, T. Junkers, *Angew. Chem., Int. Ed*. **2019**, 58, 13799.

4.1. Abstract

Kinetically stable micelles are formed from block copolymers using continuous flow techniques by turbulent mixing of water with a polymer solution in THF. It is worth noting that when these particles are formed as a result of kinetics they are defined as nanoparticle aggregates, however, in the case of the system discussed here, thermodynamics and kinetics are both influencing the formation of the particle. As a result, both the separate terms micelle and kinetic aggregate are not exclusively correct, for simplicity we will keep referring to the particles as micelles, but this terminology should be kept in mind. PHEA-*b*-PS block copolymers were used as a benchmark for the micelle formation in continuous flow. An optimal reactor volume of 2 mL with a total flow rate of 2 mL·min^{-1} was obtained. Therefore, in only 1 minute of residence time, highly reliable and stable micelles could be synthesized, which were able to encapsulate a payload. Further, PPV-*b*-PHEA micelles could be formed with a number average diameter of 100 nm. Next, the PPV-*b*-P*t*BuA block copolymer, synthesized in chapter 2, is converted into an amphiphilic block copolymer of PPV with poly(acrylic acid) (PAA). Self-assembly of the PPV-*b*-PAA block copolymer in a continuous tubular reactor resulted in micelles with a number average diameter of 170 nm.

4.2. Introduction

The ability to synthesize amphiphilic block copolymers reliably and with high precision is one of the most significant advances in polymer science in the past decades. Numerous methods have been invented, giving access to a multitude of block copolymers with regards to block composition, length, and dispersity.[1-5] If block copolymers are chosen correctly, they self-assemble into structures such as micelles, vesicles and rods, and they can carry a chemical payload. This is of high significance in bioimaging and drug delivery applications. Poly(*p*-phenylene vinylene) (PPV) for example, which is most of the time strongly hydrophobic, can be extended with a water-soluble polymer and amphiphilic block copolymers can be obtained that are able to self-assemble. Previous work has already shown that amphiphilic PPV-containing block copolymers show excellent self-assembly and payload uptake, and that these are ideal inherently fluorescent carriers for potential biomedical application.[6] Such nanoaggregates are able to penetrate cancer cells and release their encapsulated drug payload. Interestingly, the block copolymers show fluorescence, however, when self-assembled, the fluorescence is quenched due to the organization of the conjugated chain segments. Only upon cell uptake the fluorescence becomes visible again. This is a useful feature that can be employed to closely monitor the cell uptake, and later to determine the fate of the micelle materials over a longer period of time. For most to-date studied drug delivery systems similar questions are under investigation, mostly with the drawback that materials themselves are invisible to confocal microscopy – in contrast to the herein proposed PPV. Therefore, dyes are sometimes attached to classical micelles. Yet, they often deplete either quickly under irradiation, or are toxic.

PPV on the other hand has a high light stability, high fluorescence brightness and is non-toxic. Previously, PPV micelles were formed via classical batch micellization. Another method for the synthesis of nanoparticles which offers thermodynamic control over the self-assembled structure is polymer induced self-assembly (PISA). In PISA, a soluble polymer block is chain-extended using a less soluble monomer, forming an insoluble block that results in spontaneous self-assembly during the polymerization process itself.[7,8] While this is a promising method to synthesize self-assembled structures on scale, it is still governed by complex thermodynamic processes. Another method to gain control over the self-assembly process is via kinetic trapping of the block copolymers during self-assembly. However, when compared to well-studied equilibrium molecular self-assemblies, this method has not yet been explored in depth, and it remains to date a challenge to identify generalized procedures.[9] Today, continuous flow techniques are the most promising methods in which kinetic control can be achieved over self-assembly.

Continuous flow synthesis has in the past decade proven to solve problems associated with batch-to-batch variation, and the pharmaceutical industry is a significant driver in the development of continuous flow processes, also owing to the FDA issuing a recommendation for flow production of pharmaceuticals.[10] Towards polymer synthesis, flow approaches have generally been shown to not only give access to upscaled production, but also to improved definition of polymer materials.[11,12,13] Practically any controlled polymerization method that is used in the block copolymer synthesis benefits from flow processing.[14] Moreover the self-assembly of the block copolymers in flow has already been investigated.[15] In these systems, control over flow rates results in a more precise and better controlled process for self-assembly.

In these experiments, the size of polymeric vesicles could be altered from 25 to 49 nm with very narrow size distributions by changing the mixing speed. Additionally, it was shown that thermodynamically unfavorable morphologies were formed during mixing via kinetic trapping.[15,16] No study has, however, been performed yet for the self-assembly of PPV-containing block copolymers in continuous flow reactors.

4.3. Experimental Section

4.3.1. PHEA-*b*-PS block copolymer synthesis in continuous flow reactors

The polymerization of hydroxyethyl acrylate (HEA) in continuous flow was performed according to literature procedures.[1] A tubular reactor of 0.8 ml was employed. A stock solution of 2-(Dodecylthiocarbonothioylthio)propionic acid (DoPAT) (2.337 g, 6.67 mmol, 1 eq.), 1,1'-azobis(isobutyronitrile) (AIBN) (0.055g, 0.33 mmol, 0.05 eq.) and HEA (23.224 g, 0.200 mmol, 30 eq.) was prepared in n-butanol (14.69 mL) to reach a concentration of 3 mol·L^{-1}. Next, the solution was pumped into the reactor via a P 2.1S HPLC Pump (Knauer Azura) at a flow rate of 0.050 ml·min^{-1}, resulting in a residence time of 16 minutes. A backpressure regulator of 100 PSI was added to the end of the reactor to ensure stable flow conditions. A similar reactor setup and a 5 M concentration of solution was used to synthesize a large batch of HEA.

The PHEA-*b*-PS block copolymerization in flow is also performed according to literature procedures.[1] The setup of the polymerization was used and coupled to a second reactor with different reactor length. The reactors were coupled via a T-piece (Vici, ZT1, 0.75 mm), where the inlets were placed at the perpendicular ends to ensure proper mixing. A second monomer solution was prepared consisting of AIBN (0.246 g, 1.5 mmol, 1.95 eq.) and styrene (31.245 g, 300 mmol, 390 eq) in n-butanol (23.75 mL) as the solvent to reach a concentration of 5 mol·L^{-1}, CH_2Br_2 (13.037 g) was added as the internal standard. A second HPLC pump was used to pump this solution into the reactor. The volume of the second reactor was 8.4 ml with a total flow rate of both pumps of 0.210 ml·min^{-1}.

4.4. Results and Discussion

4.4.1. PHEA-*b*-PS as a model system

In order to tune various reaction conditions, the amphiphilic block copolymer poly(hydroxyethyl acrylate)-*block*-polystyrene (PHEA-*b*-PS), synthesized via RAFT, was chosen as a model system.[1] The number average molecular weight (M_n) of the hydrophilic PHEA block was 1500 g·mol^{-1} (degree of polymerization (*DP*) of 30) with a dispersity of 1.4. The PHEA-*b*-PS block copolymer had an M_n of 4100 g·mol^{-1} (*DP* 120 for PS) with a dispersity of 2.3. To establish a base for comparison, first micelles were formed in conventional batch mode. In a classical batch micelle formation 4 mg of the $PHEA_{30}$-*b*-PS_{120} block copolymer is dissolved in 0.4 mL of organic solvent and 3.6 mL of water is added over 12 hours under heavy mixing.[17] Sizes of around 42 (± 15) nm were observed for classical batch micelles. Most importantly for micelle formation in batch, the high shear forces realized by stirring during the self-assembly process play a crucial role. In flow these shear-forces are created by a micromixer, for example a static mixing tee presented in Figure 1. This mixing device was tested for micelle formation in flow. It has two inlets and one outlet leading to a tubing of 2 mL. Inlet 1 was connected to a syringe containing 10 mg·mL^{-1} of the $PHEA_{30}$-*b*-PS_{100} block copolymer in THF, while the other was connected to a syringe containing water.

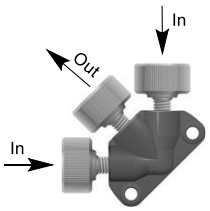

Figure 1: U-466 static mixing tee used in the tubular reactor

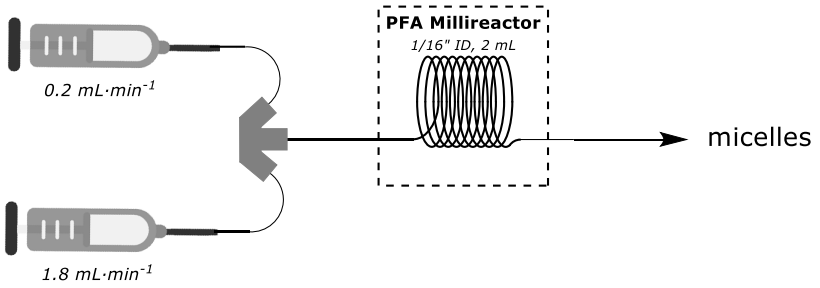

Figure 2: Schematic representation of the flow-reactor setup for the self-assembly of the block copolymers

The outlet of the micromixer was connected to a 2 mL tubular reactor, a schematic representation of the set-up is shown in Figure 2. In principle, a tubular residence unit is not required for micelle formation as self-assembly occurs during mixing. However, preliminary test displayed in Table 1 indicates that removing the tubular reactor from the set-up results in increased particle dispersities indicating that the stabilization time in a tubular reactor compartment positively influences the colloidal stability.

Table 1: DLS results of the micelle formation with varying reactor volume of the PHEA-*b*-PS block copolymer

Reactor Volume	*Intensity D*	*Volume D*	*Number D*	*PDI*
mL	nm	nm	nm	
2	159	100	85	0.14
1	196	176	112	0.16
0.5	150	96	73	0.18
0	163	94	68	0.18

For the first experiments, a THF/water ratio of 10/90 v/v% was used. These mixing ratios result in an asymmetrical mixing profile inside the micromixer since the flow rate of the water was several times higher than that of the organic phase. Residence times between 1 (2 mL·min^{-1}) and 40 min (0.05 mL·min^{-1}) were tested and successful particle formation was verified by DLS analysis. It is worth noting that after micelle formation, samples were left at ambient temperature to evaporate the organic solvent present in the samples. DLS results displayed in Table 2 show relatively constant particle sizes with a slight variation between 61 and 79 nm and dispersities between 0.20 and 0.30 for flow micellization at a variety of flowrates. A total flow rate of 2 mL·min^{-1} (block copolymer flow rate is 0.2 mL·min^{-1} and water flow rate is 1.8 mL·min^{-1}) shows the lowest dispersity of 0.20 and will be considered as the optimal flow rate.

Table 2: DLS results of the micelles when the flow rate is varied

Residence time / min	*Total flow rate** mL·min^{-1}	*Intensity D* nm	*Volume D* nm	*Number D* nm	*PDI*
1	2	134	77	61	0.20
2.5	0.9	161	105	74	0.25
5	0.4	200	255	63	0.30
10	0.2	154	95	71	0.23
20	0.1	187	118	73	0.22
40	0.05	218	191	79	0.25

*A flow rate ratio of THF/water 10/90 v/v% for all experiments was used.

Interestingly, self-assembly in flow has previously been reported to lead to smaller sized nanoparticles as compared to the batch procedure. Our data does not confirm this trend, but we also employed lower overall flow rates, which could lead to larger particle sizes. With our setup, flow rates found in other studies could not be matched. Nevertheless, a comparison of the optimized flow and batch results is shown in Figure 3 for the $PHEA_{30}$-*b*-PS_{100} block copolymers. Ten different samples were made using the optimized batch and flow protocol and analyzed using DLS. The data clearly shows the high reproducibility for micelle formation in flow as compared to batch, which is in correlation with other methods that have been described.

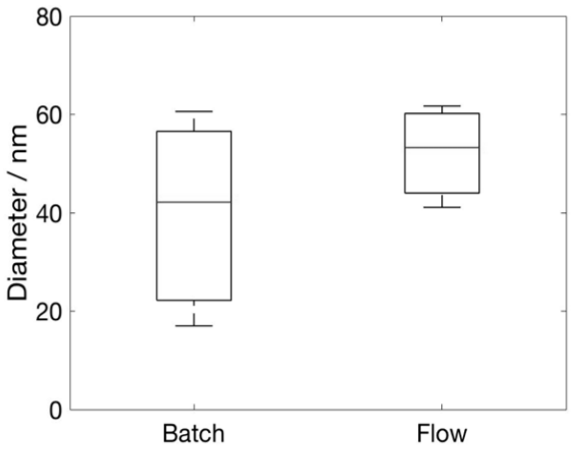

Figure 3: Standard deviation of micelle sizes for batch vs. flow self-assembly of PHEA-*b*-PS block copolymer

Furthermore, high dispersity in amphiphilic block copolymers can result in poorly defined structures as suggested by previous research.[18,19] However, despite the high dispersity after chain extension of the hydrophilic homopolymer, a well-defined self-assembly process was observed in a continuous flow setup with high reproducibility. This reveals another direct advantage of performing self-assembly in continuous flow, where even less defined polymer systems can yield highly precise polymeric nanoparticles. Furthermore, stable micelles were formed in just 1 minute of residence time as compared to the 12 h it takes to form similar micelles with lowered reproducibility in batch. More importantly, in those 12 h in batch, an average of 10 mg of micelles is produced by most standard procedures, while in the same time almost 30 g of micelles can be produced in the continuous process. Additionally, the micelles remained stable after several months of storage. However, a small population of aggregates remain present in all samples measured. This is likely due to hydrogen bonding between the particles due to the presence of the carboxylic acid group from the RAFT-agent at the end of the hydrophilic chain.

4.4.2. Encapsulation of PHEA-*b*-PS micelles with a dye in continuous flow

Next, encapsulation of a dye in flow was also investigated. The dye rhodamine (1 mg·mL^{-1}) was dissolved together with the PHEA-*b*-PS block copolymer (10 mg·mL^{-1}) in THF and mixed with water under the same conditions as the previous micellization procedure. The dye and the block copolymer dissolved in THF are in one syringe and demineralized water is in the other syringe. The water to THF ratio was kept similar (90/10 v/v% respectively) to the experiments described earlier. A residence time of 1 minute was used, this means that the total flow rate was 2 mL·min^{-1}. When the micelles were formed, they were placed in a

dialysis membrane with a pore size M_w < 3 500 g·mol^{-1} and dialyzed against deionized water for 72 h. The data of the successful micelle formation is displayed in Table 3, Figure 4 shows the UV-VIS results of the successful encapsulation of rhodamine into the PHEA-*b*-PS micelles. The maximum absorption wavelength of rhodamine encapsulated into the micelles is λ_{max} = 535 nm.

Table 3: Micelle formation with or without a dye, before and after dialysis

Experimental	*Intensity D* nm	*Volume D* nm	*Number D* nm	*PDI*
PHEA-*b*-PS	134	77	61	0.20
PHEA-*b*-PS + rhodamine before dialysis	73	41	39	0.20
PHEA-*b*-PS + rhodamine after dialysis	79	50	39	0.15

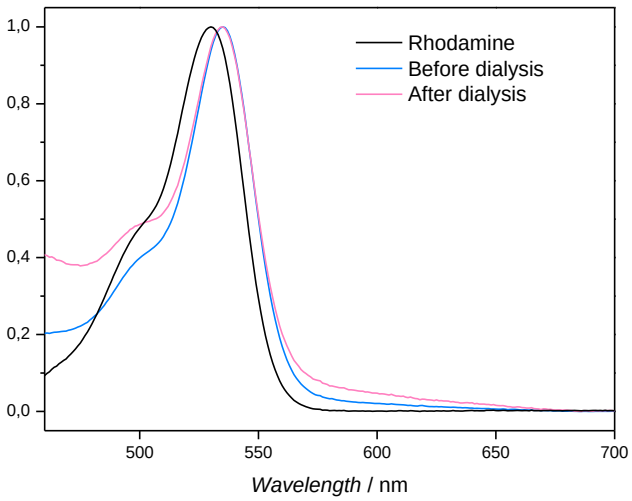

Figure 4: UV-VIS analysis of the PHEA-*b*-PS micelles encapsulated with rhodamine before (blue) and after dialysis (pink) and the UV-VIS spectrum of rhodamine in THF (black)

4.4.3. PPV-*b*-PHEA micelle formation

The successful procedure for the formation of $PHEA_{30}$-*b*-PS_{100} micelles in flow was expanded to the synthesis of poly(*p*-phenylene vinylene)-*block*-poly(hydroxyethyl acrylate) (PPV_4-*b*-$PHEA_{60}$) micelles. The PPV-*b*-PHEA block copolymer was synthesized according to literature procedures.[6] The micelles formed in flow were compared to literature data of classical batch micelle formation. The micellization in batch was carried out by dissolving 2 mg of the PPV-*b*-PHEA block copolymer in 0.4mL of organic solvent (DMF) and 3.6 mL of water was added dropwise over 18 hours under heavy stirring.[6] A number average particle diameter of 156 nm with a dispersity of 0.337 nm was observed for classical batch micelles of the PPV-*b*-PHEA block copolymer. An identical procedure as described for the $PHEA_{30}$-*b*-PS_{100} micelles in flow was then implemented for the PPV-*b*-PHEA micelle formation. Table 4 shows the successful micelles formation in just 1 minute of residence time, with a diameter of 100 nm and dispersity of 0.198, which is in line with the expectations.

Table 4: Micelle formation of the PPV-*b*-PHEA block copolymer

Conc.	*Total flow rate*	*Intensity D*	*Volume D*	*Number D*	*PDI*
$mg \cdot mL^{-1}$	$mL \cdot min^{-1}$	nm	nm	nm	
10	2	200	140	100	0.20

4.4.4. PPV-*b*-PAA micelle formation

In Chapter 2, the successful anionic synthesis of the PPV polymers in continuous flow led to the formation of the PPV-*b*-P*t*BuA block copolymer, but no solid confirmation for the existence of the block copolymer was given yet. This confirmation can be achieved via the self-assembly of the block copolymers.

The PPV-*b*-P*t*BuA block copolymer itself cannot self-assemble into micelles, therefore an amphiphilic block copolymer needs to be synthesized. The amphiphilic block copolymer can be obtained from PPV-*b*-P*t*BuA when the *tert*-butyl acrylate block is hydrolysed into poly(acrylic acid) (PAA). Hydrolysis is performed like explained in earlier research and is further detailed in section 7.2.6.[21] Self-assembly of the obtained amphiphilic block copolymers was again performed in a 2 mL tubular reactor with a static mixing tee. Two gastight syringes were used, the first one contained the PPV-*b*-PAA block copolymer that was dissolved in THF with a concentration of 10 $mg \cdot mL^{-1}$, the second syringe contained water. Both solutions were added to the tubular reactor with a different flow rate (0.2 $mL \cdot min^{-1}$ for the block copolymer solution and 1.8 $mL \cdot min^{-1}$ for water), obtaining a THF/water ratio of 10/90 v/v%. Self-assembly of the block copolymer resulted in PPV-*b*-PAA micelles with an average number diameter of 170 nm and an overall dispersity of 0.23, see Table 5 and Figure 5.

Table 5: Micelle formation of the PPV-*b*-PAA block copolymer

Concentration	*Total flow rate*	*Intensity D*	*Volume D*	*Number D*	*PDI*
$mg \cdot mL^{-1}$	$mL \cdot min^{-1}$	nm	nm	nm	
10	2	361	170	170	0.23

The average diameters are based on the total diameter distributions shown in Figure 5 (this means that also possible aggregates are included, which are more pronounced when intensity averages are considered)

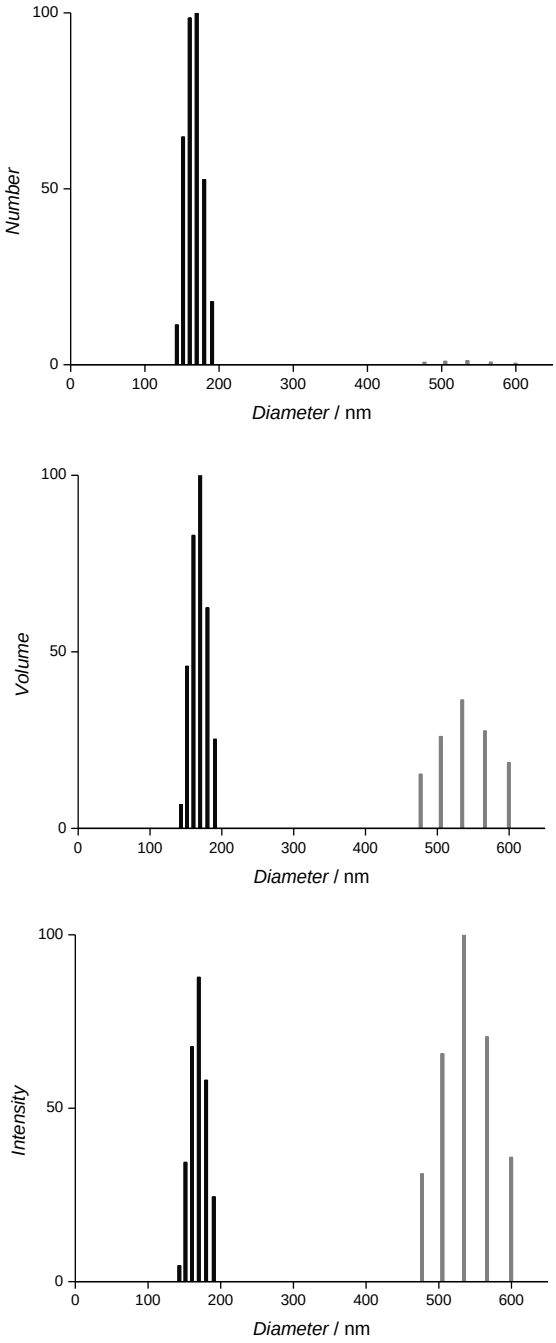

Figure 5: DLS data showing number, volume and intensity diameter distributions of the micelles from PPV-*b*-PAA

These micelle diameters are in the same range as for example the diameter of PPV-*b*-PHEA found in literature, in a tubular flow reactor and in batch for higher dispersity PPV polymers.[20,21] Further, the shift in UV-VIS absorbance upon micelle formation was visible, providing the pro-fluorescence that was employed before in cell uptake studies. The λ_{max} of the micelles was blue shifted to 408 nm (measured in THF as the solvent), which is also within expectation. This makes these micelles excellent candidates for further studies in the field of drug delivery systems. With the new ability to control the length of the polymers better and by being able to influence the dispersity of the PPV block, more detailed studies in the morphology of the obtained micelles can commence, which will be beneficial for cell uptake studies, and for potential drug delivery applications.

4.5. Conclusions

Continuous flow micelle formation was found to yield block copolymer micelles not only in high amounts, but also with increased reliability and lower batch-to-batch variation. Stable PHEA-*b*-PS micelles were formed in only 1 minute, while it would take 12 hours to form similar micelles with lowered reproducibility in batch. Successful encapsulation of the dye rhodamine in the PHEA-*b*-PS micelles was performed. Further, PPV-*b*-PHEA micelles were formed with a number average diameter of 100 nm, likewise in a continuous tubular reactor. Next, the PPV-*b*-P*t*BuA block copolymer could be converted into the amphiphilic PPV-*b*-PAA block copolymer. Due to the good self-assembly properties of this amphiphilic block copolymer, micelles with a number average diameter of 170 nm were obtained. The resulting micelles show a shift in their UV-VIS absorbance, which makes them excellent candidates for the use in the biomedical field as pro-fluorescent drug delivery systems. The formation of well-defined micelles is used to show the well-controlled conditions of the PPV polymerization step.

4.6. References

[1] E. Baeten, J. J. Haven, T. Junkers, *Pol. Chem.* **2017**, 8, 3815-3824.

[2] J. J. Haven, C. Guerrero-Sanchez, D. J. Keddie, G. Moad, S. H. Thang, U. S. Schubert, *Polym. Chem.* **2014**, 5, 5236-5246.

[3] M. Kamigaito, T. Ando, M. Sawamoto, *Chem. Rev.* **2001**, 101, 3689-3746.

[4] C. Barner-Kowollik, S. Perrier, *J. Polym. Sci., Part A: Polym. Chem.* **2008**, 46, 5715-5723.

[5] W. A. Braunecker, K. Matyjaszewski, *Prog. Polym. Sci.* **2007**, 32, 93-146.

[6] N. Zaquen, H. Lu, T. Chang, R. Mamdooh, L. Lutsen, D. Vanderzande, M. Stenzel, T. Junkers, *Biomacromolecules* **2016**, 17, 4086.

[7] M. J. Derry, L. A. Fielding, S. P. Armes, *Prog. Polym. Sci.* **2016**, 52, 1 – 18.

[8] N. Zaquen, J. Yeow, T. Junkers, C. Boyer, P. B. Zetterlund, *Macromolecules* **2018**, 51, 5165 – 5172.

[9] Y. Yan, J. Huang, B. Z. Tang, *Chem. Commun*. **2016**, 52, 11870 –11884.

[10] S. Chatterjee in *IFPAC Annual Meeting*, Baltimore, MD, Vol. 26, **2012**, pp. 34 – 42.

[11] T. Junkers, *Macromol. Chem. Phys.* **2017**, 218, 1600421.

[12] D. Wilms, J. Klos, H. Frey, *Macromol. Chem. Phys*. **2008**, 209, 343 – 356.

[13] T. Junkers, R. Hoogenboom, *Eur. Polym. J*. **2016**, 80, 175 – 176.

[14] C. Tonhauser, A. Natalello, H. Lçwe, H. Frey, *Macromolecules* **2012**, 45, 9551 – 9570.

[15] R. Thiermann, R. Bleul, M. Maskos, *Macromol. Chem. Phys*. **2017**, 218, 1600347.

[16] R. Thiermann, W. Mueller, A. Montesinos-Castellanos, D. Metzke, P. Lçb, V. Hessel, M. Maskos, *Polymer* **2012**, 53, 2205 – 2210.

[17] T. Chang, M. S. Lord, B. Bergmann, A. Macmillan, M. H. Stenzel, *J. Mater. Chem. B* **2014**, *2*, 2883-2891.

[18] A. L. Schmitt, M. H. Repollet-Pedrosa, M. K. Mahanthappa, *ACS Macro Lett*. **2012**, 1, 300 – 304.

[19] K. E. B. Doncom, L. D. Blackman, D. B. Wright, M. I. Gibson, R. K. O_Reilly, *Chem. Soc. Rev*. **2017**, 46, 4119 – 4134.

[20] G. Lligadas, S. Grama, V. Percec, *Biomacromolecules* **2017**, 18, 1039-1063.

[21] I. Cosemans, *Exploring the anionic sulfinyl precursor route towards tailor-made PPV block copolymer materials*, **2013**, PhD thesis, Hasselt University.

Chapter 5

Micelle Purification in Continuous Flow *via* Inline Dialysis

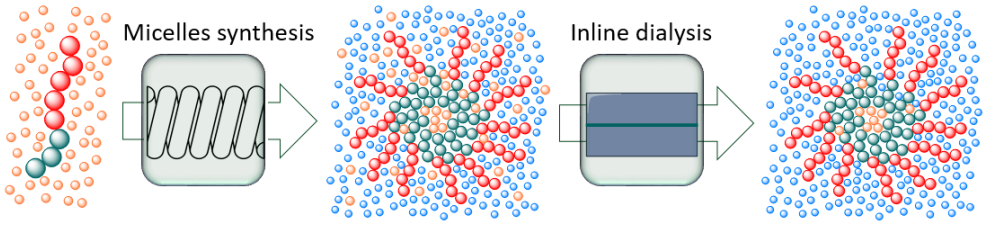

K. Verstraete, A. Buckinx, N. Zaquen, T. Junkers, *Macromolecules* **2021**, 54, 3865-3872.

5.1. Abstract

Micelle solution purification is made available via inline flow dialysis in which micelles are separated from the organic solvent used to dissolve the block copolymers in the self-assembly step. Purification was performed using simple and cost-effective dialysis units employing cellulose membranes. The proposed setup allows to remove THF from a micelle solution within few hours almost entirely in a looped flow system, without significantly changing the micelle size. Purification is found to be independent of the exact flow rates, and only on the circulation time through the dialysis units. The system is not only able to reduce the concentration of the organic solvent, but also water-soluble monomers can be removed. Further, the integration of the method into a full synthesis line to produce encapsulated micelles directly from block copolymer solutions is demonstrated, with a throughput of 1.2 g of micelles per hour.

5.2. Introduction

The ability to self-assemble block copolymers in continuous flow makes it possible to yield kinetically stable micelles not only in high production rates, but also with increased reliability and lower batch-to-batch variation compared to conventional batch-wise methods.[1,2,3] The particle shape and size can be altered by adjusting turbulent mixing conditions of water with the polymer solution in THF, which makes these micelles highly interesting for the use in bioimaging and drug delivery applications.[4,5] It is important to note here that the turbulence is created in the mixer unit of the setup rather than in the small-diameter tubular reactor part, in which flow is typical laminar for polymer solutions. While flow micelle production is highly interesting, the final hurdle to remove any excess of organic solvent remains, which is necessary to make the particles usable for biomedical applications. Since the micelles are formed in continuous flow, the most convenient and practical way to remove the organic solvent is consequently also via inline purification techniques.

Inline purification has already been well investigated in the last decennium in the form of liquid-liquid extraction, which is one of the most used purification techniques in organic synthesis.[6,7,8] This technique relies on the solubility of a compound in two immiscible solvents, where usually a polar and a nonpolar solvent are used. The second step of the extraction is the phase separation, which is, in batch, mostly driven by the difference in density between the two liquid phases used. However, on microscale it is almost impossible to achieve complete phase separation due to the small gravitational forces compared to the surface forces.[9,10] This problem can be overcome by using centrifugal action to separate the two liquids based on their densities, still, disadvantages such as long settling

times can occur with such separation technique.[11] Alternative inline phase separators hence mostly rely on the different wettability properties of the immiscible solvents on a microporous membrane which corresponds to a selective permeability of the membrane. Inline phase separators based on this principle may feature porous capillaries or any other membrane-based separator.[12,13,14] PTFE is frequently used as the membrane for the selective removal of the organic phase. The advantages of membrane phase separators are the wide variety of water immiscible solvents that can be separated and its compatibility with high flow rates which can reduce the workup time of the synthesis.[15]

The purification of a micelle solution is, however, different due to the inherent miscibility of the organic solvent used to trigger the self-assembly of the polymer in water and hence these conventional methods of inline-separation fail. Continuous flow micelle purification therefore needs a different approach than what is available to date. In batch, the purification of a micelle solution with two miscible solvents is typically performed via dialysis. Thereby, a cellulose membrane is used with a pore size small enough (typically below 3500 Da) to not let the species (micelles) diffuse across the membrane but allow small molecules and solvents to pass. The small molecules will diffuse across the membrane via osmosis until equilibrium is reached. The driving force for the diffusion is the concentration gradient at both sides of the membrane. Dialysis of a micelle solution in batch is very time consuming, it often takes up to 48 hours and the water needs to be renewed several times during the process in order to keep the concentration gradient high enough to remove the organic solvent. In a flow process the concentration gradient would naturally be high at all times, since the water phase is constantly renewed, and hence may accelerate the diffusion. The design of a continuous flow dialysis purification system which can be directly

coupled to the self-assembly reactor is hence of very high interest and has the potential to reduce the workup time tremendously. Furthermore, performing the phase separation in flow should reduce the amount of required neat water due to the small internal volume of the flow separator compared to batch.

In this work, the inline osmosis membrane separation for two miscible solvents will be discussed first using a commercially available flow extraction device (Zaiput), which makes use of a PTFE membrane.[11,16,17] PTFE membranes with different pore sizes are examined for the separation of THF out of a micelle mixture in water. Further, a custom-made separation unit is introduced, using a cellulose membrane in comparison. A cascade of five dialysis units is built to analyse the phase separation over multiple membrane units and the concentration of the organic solvent will be measured after each separator unit.

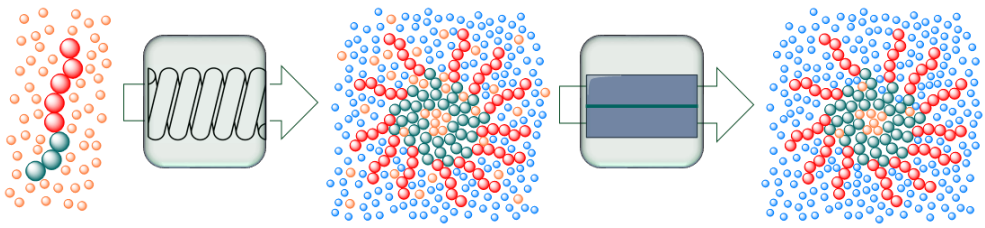

Figure 1: Schematic overview of the micelle formation in flow directly coupled to inline purification. In the first step the micelles are formed by mixing water (blue circles) with a block copolymer-THF solution and in the second step the THF (orange circles) is removed via inline dialysis

Next, to increase the efficiency of organic solvent removal, a looped dialysis system in continuous flow is proposed. This system consists of only two separator units for dialysis in continuous flow. In addition, also the removal of a water-soluble monomer, 2-hydroxyethyl acrylate (HEA), will be examined in the looped dialysis flow reactor to demonstrate that the method is not only useable for micelle purification, but also for removing residual monomer after a flow polymerization. In a final step, the inline purification is tested by telescoped micelle formation and continuous flow looped dialysis. Telescoping refers to coupling of different reactor stages directly without collection or intermediate treatment. PHEA-*b*-PS was chosen as model system in our investigations since it readily forms micelles in a reliable fashion. Further, we have characterized the system previously in detail for the flow mixing and micelle formation, and hence the underlying principles of tuning the flow rate to obtain micelles are already well understood. Generally, flow mixing results in a variation of micelle size distributions and morphologies depending on concentrations and individual flow velocities. This happens due to kinetic freezing of micelle formation on a fast timescale as long as mixing is carried out below the glass transition temperature of the hydrophobic core. Thus, PHEA-*b*-PS is ideal for further studies into the dialysis and purification of micelles. Other polymers and solvents might behave differently in terms of rate of purification and retention of micelle size distributions compared to what we will demonstrate below, yet the general principle is transferable, and has been confirmed in preliminary results that we will discuss in forthcoming studies. The system described will proof to be useful to many researchers that deal with micelle synthesis and require solvent dialysis. The method is low cost and simple to implement, and yet fast to deliver results quickly.

5.3. Experimental Section

5.3.1. Custom-made dialysis units

Figure 2 represents the specialized dialysis system required to perform the inline purification in flow. The system that is used to remove the organic solvent (THF) from the micelles solution (in water) is a custom build dialysis system, with a volume of 0.38 ml (dimensions are 3.8 cm x 1 cm x 0.1 cm). The device consists of two aluminium frames with a chamber in the middle and an O-ring (Viton®, 32mmx2mm, Eriks©) to provide a tight fit between the two parts. A dialysis membrane, with a surface area of 3.8 cm^2, is placed on top of the O-ring, between the two aluminium frames. Despite the PTFE membrane usually used for a liquid-liquid extraction, the membrane used in this dialysis system consists out of regenerated cellulose (Spectra/pore®) with a pore size Mw < 3500 $g \cdot mol^{-1}$.

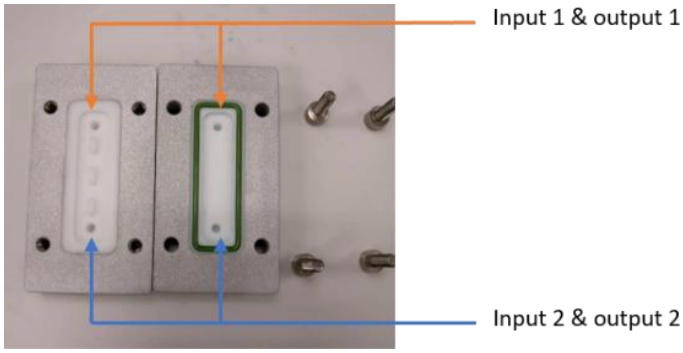

Figure 2: Photo of the opened custom-made dialysis device

5.3.2. Micelle purification using multiple dialysis units

To perform the dialysis in continuous flow, the first dialysis unit was coupled to a syringe containing the micelle solution and the next dialysis units were coupled to each other. The other inputs, on the opposite site of the membrane, were coupled to a syringe with demineralized water. The syringes with the micelle solution and the water were pumped into the system using syringe pumps (Chemyx).

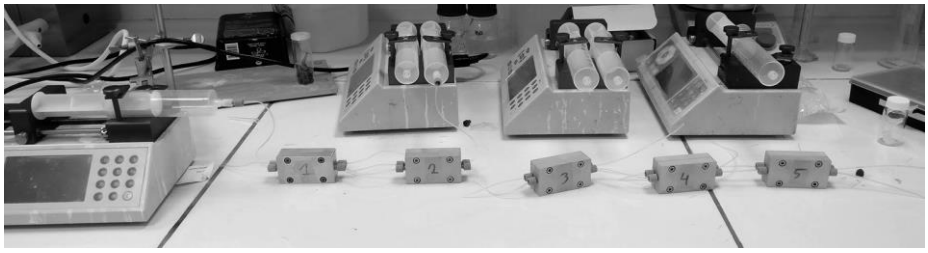

Figure 3: Micelle purification setup with five dialysis units coupled

5.3.3. Block copolymer synthesis

Block copolymer formation of 2-hydroxylethyl acrylate (HEA) and styrene was performed using classical RAFT polymerization. In a round bottom flask, 120 mmol of HEA (13.93 g, 30 equiv.), 4 mmol DoPAT (1.4 g, 1 equiv.) and 0.2 mmol AIBN (33 mg, 0.05 equiv.) were dissolved in 30 mL of n-butanol (4 M). Subsequently, the flask was purged with nitrogen gas for 15 minutes and the solution was left to react for 40 minutes at 100 °C. After the addition of 300 mmol styrene (31.2 g, 75 equiv.) and 1.5 mmol AIBN (0.25 g, 2.7 equiv.) in 70 mL n-butanol, the PHEA-*b*-PS block copolymer was formed.

Table 1: Molecular weight and dispersity of the PHEA homopolymer and PHEA-*b*-PS block copolymer synthesis in batch via RAFT

	M_n g·mol^{-1}	M_p g·mol^{-1}	$Đ$
PHEA	1200	2400	1.4
PHEA-*b*-PS	2300	4900	1.6

M_n shows the number average molecular weight, M_p the molecular weight of the highest peak and $Đ$ represents the dispersity of the molecular weight distribution. Measurements were performed using SEC analysis.

5.3.4. Design of the looped dialysis system

The design of the looped dialysis system is depicted in Scheme 1, A and B are syringe pumps, C is a HPLC pump and D, E, F are switch valves. The procedure for the dialysis in the looped flow system can be divided into three different steps. In the first step, the micelle solution is loaded into the system using pump A, pump B is activated as well enabling the water crossflow and pump C is switched off. The valves are positioned in the way that the micelle solution is pumped through the whole system, the tubing is disconnected at the end of the loop (valve D) in order to let the system stabilize. After the stabilization time (2,5 times the residence time), pump A is switched off, the tubing is connected again at valve D which is switched to the direction of the loop and the HPLC pump C is switched on in order to pump the micelle solution through the looped dialysis system. In the last step, valves E and F are both switched to collect the micelle solution.

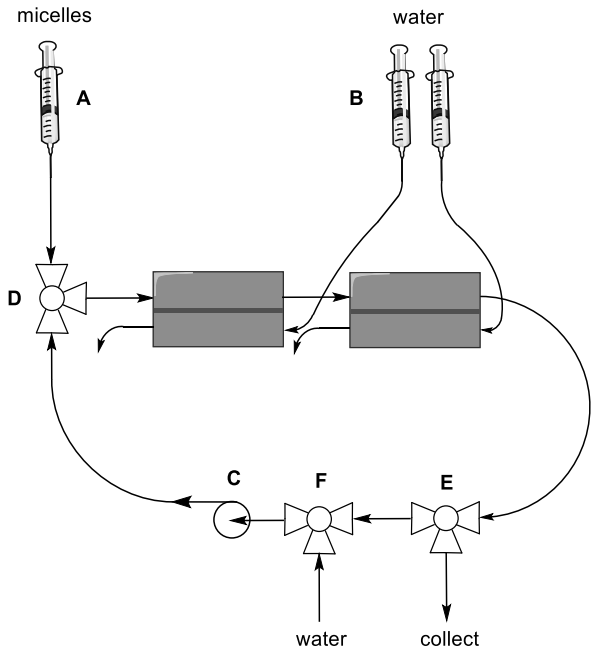

Scheme 1: Design of the looped dialysis system

5.3.5. Micelle formation directly coupled to the inline dialysis

To couple the micelle formation directly to the purification, the setup as detailed in Scheme 2 is used. The micelles are formed according to literature procedures.[1] The most important parts for the micelle formation in flow are the tubular reactor (2 mL PFA tubing, 0.75mm ID) and the static mixing tee (Upchurch scientific, U-466, swept volume of 2.2 µL). One inlet of the micromixer was coupled to a feed of the poly(hydroxyethyl acrylate)-*block*-polystyrene (PHEA-*b*-PS) block copolymer dissolved in THF (10 mg·mL^{-1}) and the other inlet was coupled to a syringe containing only demineralized water. Both solutions are pumped into the reactor with a different flow rate (0.2 mL·min^{-1} and 1.8 mL·min^{-1} respectively), therefore two syringe pumps were required. The outlet of the reactor (A) is directly coupled to valve D and the micelles are pumped into the looped dialysis system. The next steps are as described above at the design of the looped dialysis system.

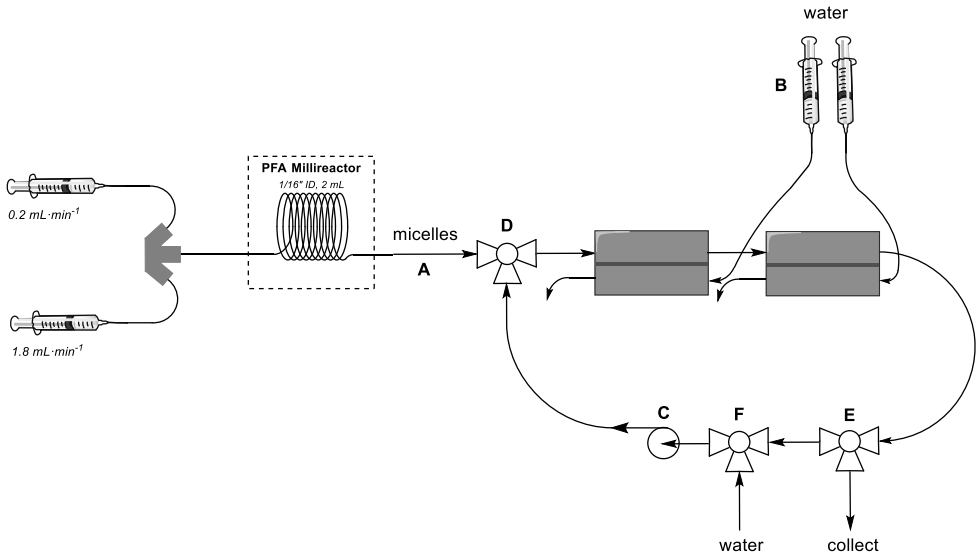

Scheme 2: Micelle formation directly coupled to inline dialysis

5.3.6. Encapsulation and inline purification of PHEA-*b*-PS micelles

The PHEA-*b*-PS micelles were produced with the same reaction conditions as described above. The PHEA-*b*-PS block copolymer (10 $mg \cdot mL^{-1}$) and rhodamine (1 $mg \cdot mL^{-1}$) were dissolved in THF. The dye and the block copolymer dissolved in THF are in one syringe and demineralized water is in the other syringe. The micelle formation and dialysis proceeds as described above, now with a dye encapsulated. The looped dialysis makes sure that the dye which is not encapsulated is dialysed out of the micelle solution together with the THF.

5.4. Results and Discussion

5.4.1. Design of dialysis units

While continuous production of micelles in flow is readily available with conventional HPLC parts, dialysis isn't as straight forwardly applied. Hence the focus on inline dialysis without further discussion on micelle formation in this study. Yet, attention has been paid to the quality of the micelles before and after the inline dialysis via dynamic light scattering (DLS) measurements. As mentioned earlier, conventional biphasic liquid-liquid extraction in continuous flow is already well investigated. Inherently though, for micelle formation, miscible solvents are used, in many cases water and THF. Therefore, another approach to solvent separation is necessary, one that does not rely on spontaneous phase separation. The commercial system often used for liquid-liquid extraction is the so-called Zaiput separator. This flow unit relies on the wettability of a hydrophobic membrane (PTFE) with a certain pore size to induce separation. The membrane will only be wetted with one phase while the other non-wetting phase will be retained. Separation thus relies on the difference in hydrophobicity of the two mixed solvents. In addition to this, the pressure on each side of the membrane is carefully controlled so that only one phase can flow through the pores in the membrane. This type of phase separation was introduced a few years ago and has rapidly become a common method in flow processing, with phase separations being quite efficient, allowing for aqueous extraction of solvent phases inline in coupled flow reactors.

To start, the very same system was tested towards THF removal from micelle solution, hoping the hydrophobicity difference might be large enough to warrant separation. Results indicated though that the membrane used could not selectively

remove THF from the solution. Hydrophobic PTFE membranes with a pore size of 1 micron did not give any selective separation and a micelle solution was collected from both outputs of the Zaiput device. Using hydrophobic membranes with a pore size of 0.2 micron, micelles were retained on one side of the membrane, but also no changes in THF concentration were observed upon ^{1}H NMR analysis, indicating THF was not selectively removed from the solution. While the commercial units are very useful for biphasic liquid-liquid separation, a different system clearly needed to be developed for the removal of the miscible organic solvent THF from an aqueous micelle solution.

Figure 4: A schematic representation of the top view of the device, where in- and output 1 (containing the micelle solution) are separated by the membrane from in- and output 2 (containing water)

A simple, yet specialized dialysis system was built with a cellulose membrane (pore size for cut-off of molecular weights < 3500 Da) to separate the organic solvent from the micelle solution (see Figure 4). A water crossflow is applied as low concentration phase to make the organic solvent diffuse via the membrane. Since the water is constantly replenished, the concentration gradient is high at all times. The use of small pore size membranes prevents micelles from crossing the

membrane, while the organic solvent can cross. The optimal flow rate for the purification of a THF/water mixture (10/90 v/v%) as a proof-of-concept process, was tested at different flow rates using a single dialysis unit. The results displayed in Table 2 show that the optimal THF removal of a system with one dialysis unit is achieved at overall lower flow rates. The lower the flow rate, the more contact time is given for the THF to cross the membrane in a single pass of the device. A lower limit for the flow rate is, however, given to keep a reasonable overall flow rate of the reactor, which would later be defined by the micelle formation itself. A removal of more than 50% as observed in a single pass is, however, a quite reasonable result.

Table 2: Amount of THF remaining in the micelle solution using one pass in a dialysis unit at different micelle solution flow rates. Concentrations of residual THF were calculated from ^{1}H NMR

Micelle solution flow rate* $mL \cdot min^{-1}$	THF remaining %
0.025	37
0.05	54
0.1	68
0.2	72
0.4	87
0.6	94

* The water crossflow rate is always twice the micelle solution flow rate

5.4.2. Calculation of THF concentration *via* ^{1}H NMR

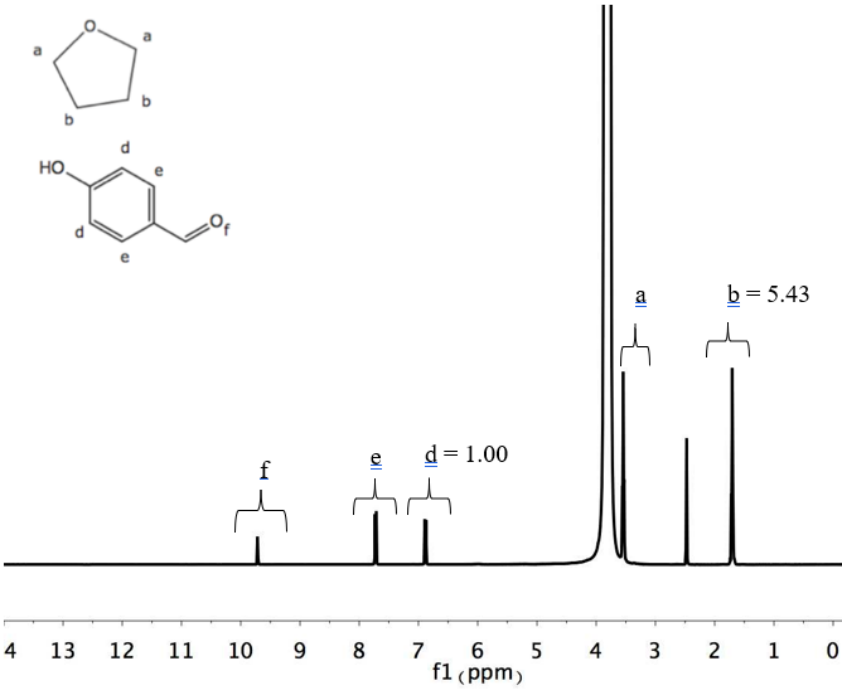

Figure 5: Example of ^{1}H NMR spectrum for THF extraction from a THF/water mixture, the peak at 2.5 is from the solvent DMSO d6 used as a reference. The large peak at 3.33 ppm is due to the water present in the sample

To calculate the concentration of THF after the dialysis, 2.5 mg of 4-hydroxy benzaldehyde (4-HBA) was used as an internal standard for the ^{1}H NMR analysis. To this 0.6 mL of deuterated DMSO was added together with 0.1 mL of the micelle solution. The molar concentration in the ^{1}H NMR sample is thus calculated as:

$$\frac{2.5 \cdot 10^{-3}\ g}{122.12\ g/mol} = 20.47 \cdot 10^{-6}\ mol$$

$$concentration = \frac{20.47 \cdot 10^{-6}\ mol}{0.0007 L}$$

$$M_{4-HBA} = 0.0292\ mol/L$$

Since the signal from the THF peak at 1.7 is caused by 4 protons and the peak of 4-HBA by 2, the following correction is made:

$$M_{H\ 4-HBA} = 2M_{4-HBA} = 0.0585\ \frac{mol}{L} (= 1\ rel)$$

$$5.43\ rel = 0.3177\ \frac{mol}{L}$$

$$5.43\ rel = 0.3177\ \frac{mol}{L} =\ M_{4-THF}$$

$$M_{4-THF} = 4M_{THF}$$

$$M_{THF} = 0.0794\ M$$

Subsequent calculation of the THF concentration in the mixture gives:

$$n_{THF} = 0.0794 \frac{mol}{l} \cdot 0.0007\ l = 0.0556 \cdot 10^{-3}\ mol$$

$$conc_{THF} = \frac{0.0556 \cdot 10^{-3} mol}{0.0001\ l} = 0.556\ M$$

5.4.3. Coupling of dialysis units in series

In order to remove as much of the residual THF (out of a THF/water 10/90 v/v% solution) as possible, multiple dialysis units (up to a set of five) were coupled in series (see Figure 3). This is an alternative to simply building a unit with a larger contact area and allows for more flexibility in reactor design. It should also be noted that the separators are custom-build and were designed keeping biphasic PTFE membrane separation as in the Zaiput devices in mind, which also influenced their size. Regardless, the use of a series of separation units is rather common in continuous flow inline purifications.[18] ^{1}H NMR analysis was performed after each dialysis unit and the progressive results are visualized in Figure 6. A continuous removal of THF is clearly visible with each unit. However, in the beginning of the process, when the THF concentration is the highest, the removal of THF is the

fastest and with a decreasing concentration of THF, also the efficiency of removal decreases with the osmotic pressure. In total, a decrease in THF concentration from 1.03 mol·L^{-1} to 0.21 mol·L^{-1} after using five dialysis units was achieved, thus roughly 80% of the organic solvent. This by itself could be seen as a success, as removal in the units is very fast compared to conventional batch dialysis. Yet, extrapolation of the data in Figure 6 suggests that a very large number of extractors would be required for full removal of all organic solvent. In batch dialysis five steps would typically be sufficient for full removal. Yet, in the flow devices the volume difference between neat water and extracted solution is much smaller, hence explaining the lower efficiency in the total process. It should be noted here that on a production scale, use of ten or more separators would not be a problem, only in R&D settings where larger flexibility is required, this seems unfavourable overall.

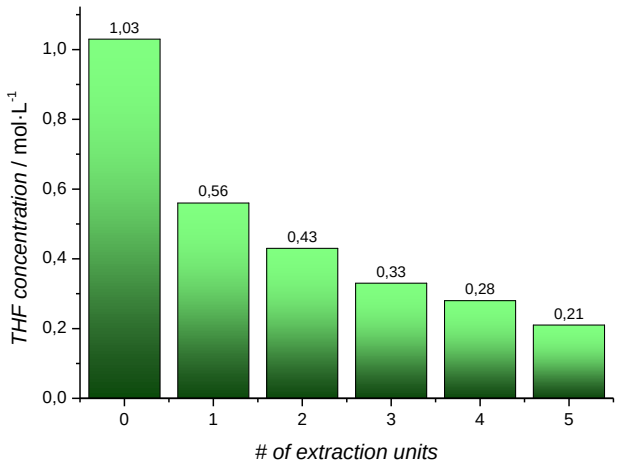

Figure 6: Progressive removal of THF (out of a THF/water 10/90 v/v% solution) with additional separation stages. Concentrations were determined via ^{1}H NMR.

5.4.4. Design of a looped flow reactor

As promising as the decrease in THF concentration of 80% over five dialysis units was, an alternative approach is required in order to decrease the concentration even more in a lab-based setting. Therefore, a looped flow reactor design was constructed, in which the micelle solution is circulated several times over the same separator unit, in this way creating more contact time on the dialysis membrane. A looped flow reactor with five dialysis units would require five syringe pumps in a complete micelle formation and purification process, therefore a less complex design with two dialysis units was constructed to keep the instrumental requirements at minimum (see Scheme 1). The micelle solution is injected into the first dialysis unit which is directly coupled to the second with a short piece of tubing. Next, the loop pump recirculates the solution into the dialysis units. This process can be continued for several hours and the micelle solution can ultimately be collected via a switch valve. Such looped system is not fully continuous but can still be integrated in a continuous process using intermediate collection vessels. This approach is not untypical in flow synthesis.[19] In the first experiments in which THF removal from the micelle solution was performed, the number of loops were counted and rather short dialysis times (between 4 minutes and 40 minutes) were tested. Figure 7 summarizes these investigations and – unsurprisingly – shows similar trends as for the coupled dialysis units, as the number of loops merely mimic a larger amount of separator units in a sequential linear flow setup. The removal of THF is the fastest when the concentration is the highest, and the efficiency reduces with each loop/step. In addition, the same overall effect of the flow rate on the result as in Table 2 is seen as well. A lower flow rate (0.2 $mL \cdot min^{-1}$) removes the THF faster. At the same time, the removal of THF does not influence the micelle size itself. Before flow dialysis, the average micelle

size was determined to 18.4 nm and 17.7 nm (Table 4 (end of chapter), entries 1 and 5). After dialysis particle sizes ranged from 16.1 – 27.6 nm for these experiments (Table 4, entries 1-11). In Figure 14 an example distribution plot of number, volume and intensity particle size distributions, both before and after the dialysis is added. Some variation in size is not unexpected as the removal of THF inherently changes the structure of the micelle to a certain degree.

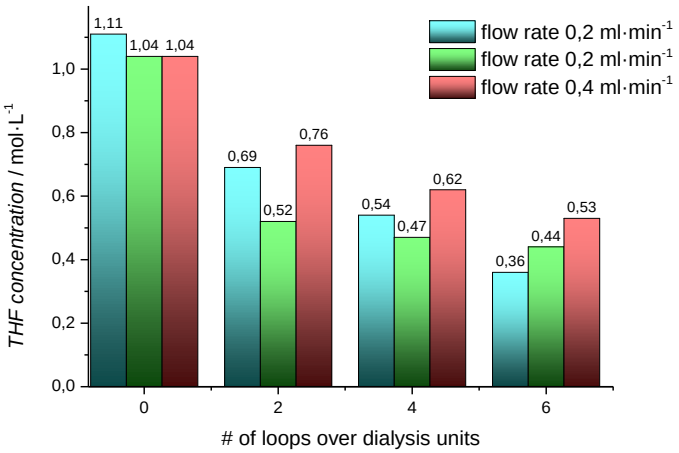

Figure 7: THF removal after several loops over the dialysis units, for a micelle solution flow rate of 0.2 mL·min^{-1} with a water crossflow rate of 0.4 mL·min^{-1} (blue and green bars) and for the micelle solution flow rate of 0.4 mL·min^{-1} with a water crossflow rate of 0.8 mL·min^{-1} (red bars)

5.4.5. Increase of the looping times

The results of these very short loops are not perfectly consistent and the 80% THF removal of the five coupled dialysis units is not achieved yet. Therefore, looping times of several hours were used in order to go to sufficiently low THF concentrations. In Figure 8, longer looping times for the dialysis of THF out of the micelle solution are presented with a micelle solution flow rate of 0.2 mL·min^{-1} and a water crossflow rate of 0.4 mL·min^{-1}. A looping time of one hour corresponds

to about seven loops. Results show that after three hours of dialysis, the THF concentration falls below 10% of the starting concentration and the results are much more reliable than for the shorter loops as depicted in Figure 7. Duplicate measurements gave the same THF concentrations after a defined time with an uncertainty of only 2-3%. Thus, the decrease of the solvent concentration with time can be assumed to be significant and reliable. The second experiment (green bars in Figure 8) was looped for four hours and the THF concentration could be decreased down to 0.02 mol·L^{-1} (1%) and hence almost complete removal. This shows a quite remarkable result. DLS measurements indicated a micelle size between 17.1 nm and 31.6 nm after dialysis (Table 4, entries 12-20). The diameter before dialysis was 17.4 nm and 18.5 nm respectively (Table 4, entries 12 and 17), so again a slight increase in average size was observed. While 4 h seem to be required for full removal, we limited the looping time to 2 h in the following experiments, since this already allows to distinguish the best reaction conditions and saves material in further investigations.

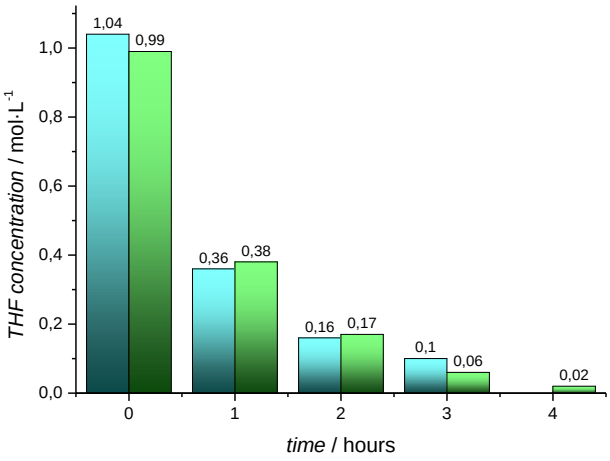

Figure 8: Dependence of THF removal efficiency on looping times, with a micelle solution flow rate of 0.2 mL·min^{-1} and a water crossflow rate of 0.4 mL·min^{-1}

5.4.6. Effect of the micelle solution flow rate

The effect of increasing the flow rate of the micelle solution from 0.2 mL·min^{-1} to 0.4 mL·min^{-1} (the water flow rate from 0.4 mL·min^{-1} to 0.8 mL·min^{-1}) is evaluated again (now for looping times of several hours instead of minutes), since a higher flow rate could be interesting for the coupling of the micelle formation and dialysis later on. As Figure 9 demonstrates, the increase of the flow rate has no effect on the THF removal over a longer period of time, since the micelle solution passes the dialysis units faster when the flow rate is doubled to 0.4 mL·min^{-1}. This is hence no contradiction to the data in Figure 7, where the number of loops over the dialysis unit was counted. So, when the flow rate is higher, less THF is removed per pass. Yet, at constant looping time, the same amount of THF is removed for both flow rates since the number of passes rises proportionally. As expected from literature,[2] the increase of the flow rate has no influence on the THF removal and the average sizes of the micelles stay in the same range (Table 4 entries 18-22: 20.8 nm and 17.1 nm for 0.2 mL·min^{-1}, 20.4 nm and 24.5 nm for 0.4 mL·min^{-1}).

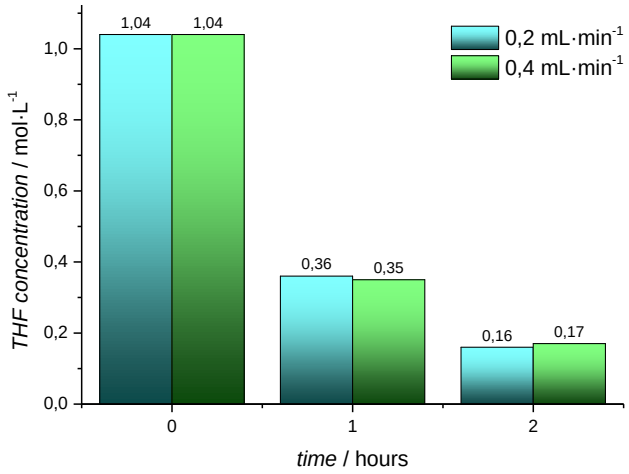

Figure 9: The effect of increasing the micelle solution flow rate from 0.2 mL·min^{-1} to 0.4 mL·min^{-1} (the water crossflow rate from 0.4 mL·min^{-1} to 0.8 mL·min^{-1})

5.4.7. Effect of the water crossflow rate

Another important parameter for the THF removal via dialysis is the water crossflow rate. Therefore, the effect of the water crossflow rate was evaluated in the last step (see Figure 10). Note that up to this point the crossflow rate was always exactly twice the micellar solution flow rate as mentioned above. It may in the first instance be expected that the THF removal would proceed faster when the water crossflow would be increased, because with a faster renewal of the water, a higher concentration gradient is achieved. However, no significant change was seen when performing the experiments. The absence of a more efficient removal at higher flow rates is explained by the fact that the concentration of the removed small molecule – here THF – in the water crossflow is very low at any time. Hence, faster renewal of water does not make much difference, unlike in batch dialysis. In the following experiments, the flow dialysis was also tested for conditions where the water crossflow rate equals the micelle solution flow rate. This is interesting because at longer dialysis times and higher flow rates, significant amounts of water would become necessary and with a lower water crossflow rate the water usage would be highly reduced. As seen in Figure 10, slightly less THF is removed after two hours when the water crossflow rate equals the micelles flow rate. Still, these results are matching the expectations. Again, the change in process has no significant effect on the micelle size (see Table 4 (end of the chapter), entries 17-20 and 23-25), and is in the same range as in the previous experiments, showing that sheer effects do not play a significant role in the extraction/dialysis.

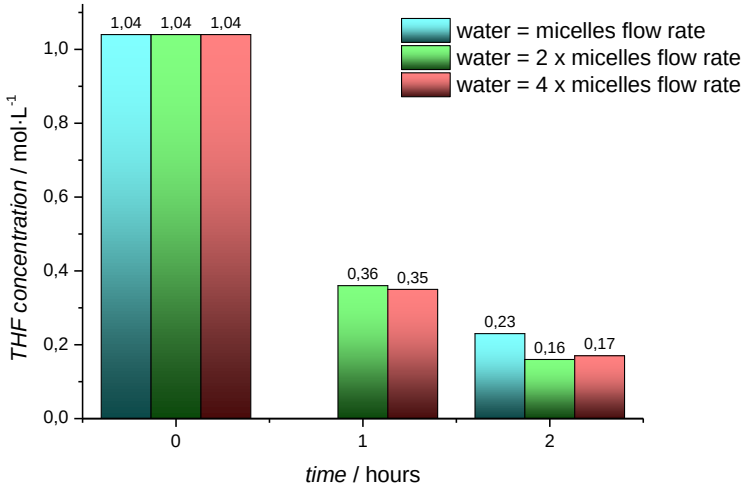

Figure 10: The effect of the water crossflow rate is evaluated for the water flow rate equal, 2x and 4x the micelle solution flow rate of 0.2 mL·min^{-1}

5.4.8. Dialysis of organic molecules

Now that dialysis of an organic solvent in flow is established, dialysis of other organic molecules of interest was tested in a last step. Next to micelle formation, another important application of the dialysis device is to remove residual monomers after a polymerization inline. Specifically, for synthesis of block copolymers, removing residual monomer is crucial to successful block extension. The principle here is the same. Via osmosis, a monomer can be removed in a solution containing polymer that is not able to pass the dialysis membrane and small-sized monomer. To investigate the removal of such residual monomer, a one molar solution (12 v/v %) of 2-hydroxyethyl acrylate (HEA) was added to the micelle solution and then subjected to flow dialysis. It can be observed from Figure 11 that after four hours the HEA concentration is decreased to 0.12 M, which corresponds to 1.4 v/v % of HEA in the total micelle solution (see Table 4

entries 29 and 30 for the diameter of the micelles. This experiment shows that the dialysis system is not only capable of removing the organic solvent out of the micelle solution, but in principle also of the removal of residual monomer. Baxendale *et al.* evaluated the removal of an aqueous soluble monomer, acrylic acid, from the poly(acrylic acid) polymer solution before, using biphasic extraction and employing the insolubility of poly(acrylic acid) in water.[20] They were able to fully purify the polymer solution after 40-60 minutes using three membranes in series, but they also encountered that the extraction rate is dependent on the concentration and volume of the sample. The flow dialysis presents here a convenient alternative that is more broadly applicable since solubility of the polymer does not influence the outcome of the purification. Generally, membrane dialysis can also be used to remove non-water-soluble monomers when being performed with membranes that are stable towards organic solvents. We will investigate this in more detail in future studies.

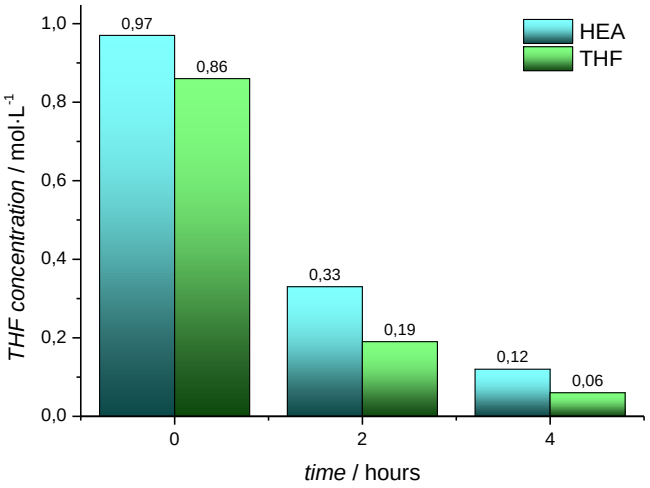

Figure 11: Removal of water-soluble monomer HEA with a micelle solution flow rate of 0.2 mL·min^{-1} and a water crossflow rate of 0.4 mL·min^{-1}

5.4.9. Towards true inline purification

After the underlying effects of flow dialysis had been investigated, and optimal conditions been determined, the flow dialysis was coupled to a full micelle formation process in flow, starting from block copolymer solutions. Using literature procedures, the micelles are often formed with a total flow rate of 2 $mL \cdot min^{-1}$, thus at considerable higher rates than in the experiments described above. However, following the experiments shown in Figure 10, the water crossflow rate was reduced equal to the rate of the micelle solution stream. Before the coupling of the full reactor assembly, we tested the THF removal at 2 $ml \cdot min^{-1}$ in standalone mode. Figure 12 depicts the results for the comparison of the THF removal with a flow rate of 2 $ml \cdot min^{-1}$ with the results of previous experiments (0.2 $ml \cdot min^{-1}$ + 0.4 $ml \cdot min^{-1}$ and 0.2 $ml \cdot min^{-1}$ + 0.2 $ml \cdot min^{-1}$, where the second rate gives the crossflow rate). It is clearly visible that for the experiment with a flow rate of 2 $ml \cdot min^{-1}$ the results are comparable with the results of the other experiments. This is a good confirmation of the trends seen above in that the flow rate influences the removal efficiency per membrane pass, but not over the same total looping time. After two hours a THF concentration of 0.19 $mol \cdot L^{-1}$ was reached which is in line with the expectations and in excellent agreement with all other experiments described herein. DLS measurements show that also at these high flow rates the micelles stay intact, with an average size of 21.9 nm (for 1 h dialysis) and 23.2 nm (for 2 h dialysis), see Table 4 entries 26 and 28, respectively.

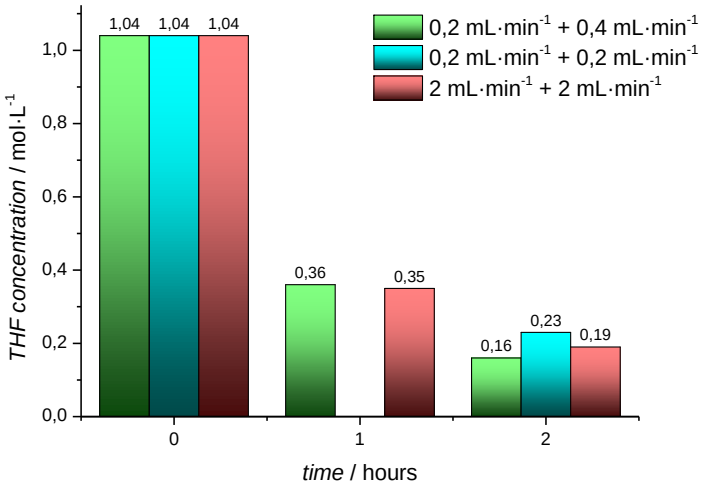

Figure 12: The effect of increasing the flow rate to 2 mL·min^{-1} with the same water crossflow rate. The dialysis with 0.2 mL·min^{-1} for both flow rates was only performed for 2 h circulation time to safe material

5.4.10. Micelle formation with the encapsulation of a model dye directly coupled to the inline dialysis

The ability to form micelles in flow and directly couple it to the inline purification would not only reduce the synthesis time tremendously but also reduce the workload substantially. Thus, in the last step the flow dialysis was integrated into a full micelle synthesis line, including encapsulation of a model payload. The synthesis of purified micelles in one continuous process together with the high stability and good reproducibility that a flow process provides, make such approach very interesting for the use in drug delivery applications. The setup used for the micelle formation in flow was already shown in Scheme 2. The micelles are formed by mixing a PHEA-*b*-PS block copolymer solution in THF and combining it with water in a 10/90 v/v% ratio (generating a THF concentration of 1M). The

micelle solution and water are mixed in a static mixing tee which is connected to a 2 mL reactor. This reaction was stabilized for 3 minutes (3 times the residence time) before it was connected directly to the dialysis system. The total flow rate of the residual micelle solution is 2 $mL \cdot min^{-1}$, therefore the flow rate of the dialysis loop was kept the same at first. After two hours of circulation, the THF concentration was decreased to 0.19 M which is very much alike the results that were obtained from the separate dialysis system in Figure 12. In the next step, the encapsulation of the micelles was evaluated and the looping time was increased to four hours to further reduce the THF concentration. The encapsulation was performed by dissolving rhodamine together with the block copolymer in THF and the micelle formation and purification proceeded the same as before. In this way the dye was encapsulated in the micelles in the first flow stage, and the purification by dialysis removed the residual dye in solution alongside the solvent. The THF concentration was reduced to only 0.05 M, see Table 3, after four hours. The results in Table 3 show that also with a lower flow rate and five hours of dialysis time the residual concentration of THF was 0.04 M. This demonstrates again that the looped dialysis is independent of the flow rate. Moreover, the fact that there is a limit in the THF removal efficiency of the micelle solution may be due to some of the THF being also encapsulated in the micelle core.

The UV-VIS results presented in Figure 13 show the successful encapsulation of rhodamine in the PHEA-*b*-PS micelles for the different dialysis conditions tested. The average sizes of the micelles which encapsulated rhodamine are slightly higher (27.2 – 37.7 nm, Table 4 entries 32-34) than the micelles without the dye (25.2 nm for the coupled system, Table 4 entry 31). The difference between both is not too large though. It should be noted though that this comparison is of qualitative rather than quantitative nature. When synthesizing these micelles in

continuous flow, about 1.2 g of micelles with encapsulated payload are produced in one hour in the present procedure, showing that this approach is able to produce significant amounts of material in short times. With typical batch procedures often only milligram amounts are made, and dialysis would take long time.

Table 3: Micelle formation and dye encapsulation in flow directly coupled to the inline dialysis loop

Micelles flow rate mL·min^{-1}	*Water flow rate* mL·min^{-1}	*Time* h	*THF conc.* M	*Dh** nm	*PDI*	Remarks
2	2	2	0,19	25.2	0.35	
2	2	4	0,05	37.7	0.37	With dye
0.2	0.4	4	0,06	30.4	0.32	With dye
0.2	0.4	5	0,04	27.2	0.30	With dye

**Dh* is the number average hydrodynamic particle diameter

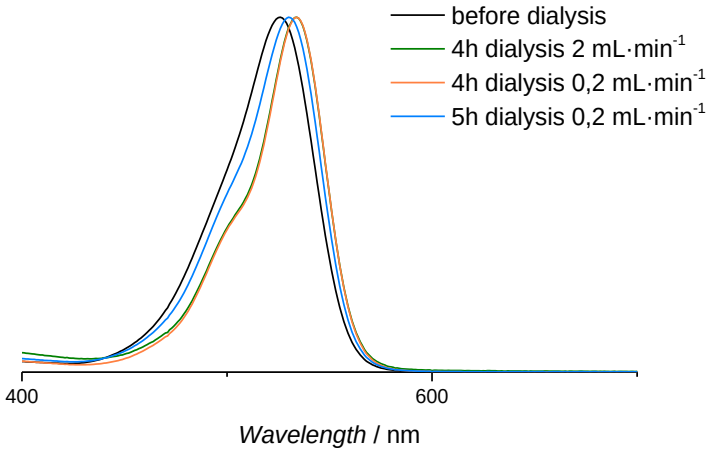

Figure 13: UV-VIS analysis of the PHEA-*b*-PS micelles encapsulated with rhodamine before (black) and after dialysis

Table 4: Mean number diameter optained via DLS for all different dialysis experiments

Entry	Micelle solution	Micelles Flow rate mL·min^{-1}	Water flow rate mL·min^{-1}	Time min	N_{mean} nm	*PDI*	Remarks
1	1	Before dialysis			18.4	0.279	
2	1	0.2	0.4	8	17.9	0.280	
3	1	0.2	0.4	24	25.5	0.278	
4	1	0.2	0.4	40	27.6	0.270	
5	2	Before dialysis			17.7	0.261	
6	2	0.2	0.4	8	16.1	0.256	
7	2	0.2	0.4	24	24.3	0.247	
8	2	0.2	0.4	40	23.4	0.259	
9	2	0.4	0.8	4	23.4	0.272	
10	2	0.4	0.8	12	23.5	0.255	
11	2	0.4	0.8	20	-	-	
12	3	Before dialysis			17.4	0.287	
13	3	0.2	0.4	60	27.9	0.353	
14	3	0.2	0.4	120	18.6	0.294	
15	3	0.2	0.4	180	24.3	0.263	
16	3	0.2	0.4	240	31.6	0.332	

17	4	Before dialysis			18.5	0.297	
18	4	0.2	0.4	60	20.8	0.309	
19	4	0.2	0.4	120	17.1	0.291	
20	4	0.2	0.4	180	22.9	0.334	
21	4	0.4	0.8	60	20.4	0.290	
22	4	0.4	0.8	120	24.5	0.280	
23	4	0.2	0.8	60	25.7	0.366	
24	4	0.2	0.8	120	19.5	0.325	
25	4	0.2	0.2	120	22.0	0.306	
26	4	2	2	60	21.9	0.341	
27	5	Before dialysis			16.6	0.294	
28	5	2	2	120	23.2	0.317	
29	5	0.2	0.4	120	24.5	0.283	+ HEA
30	5	0.2	0.4	240	25.2	0.123	+ HEA
31		2	2	120	25.2	0.345	Coupled
32		2	2	240	37.7	0.365	Coupled + dye
33		0.2	0.4	240	30.4	0.317	Coupled + dye
34		0.2	0.4	300	27.2	0.299	Coupled + dye

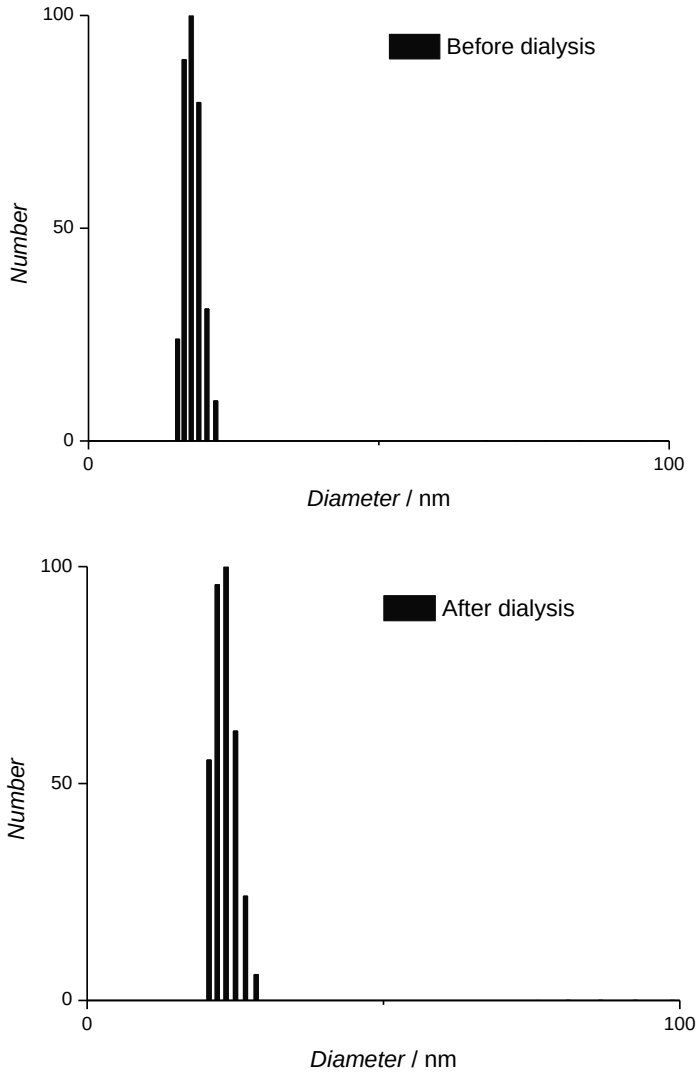
100
50
0
0
100
Number
Diameter / nm
Before dialysis
After dialysis

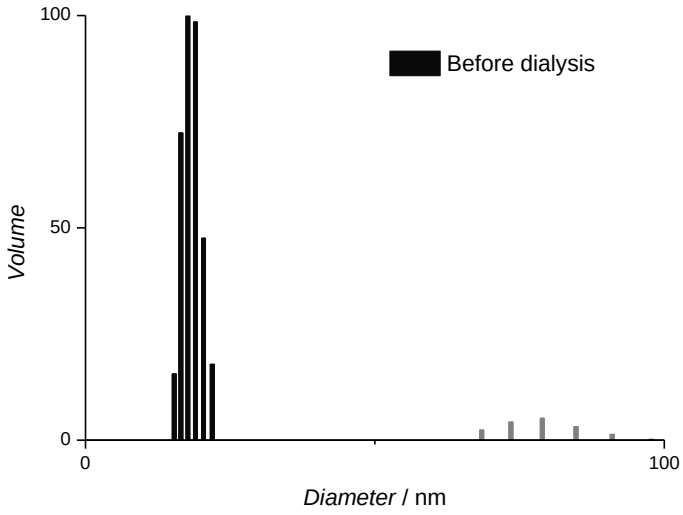
100
50
0
0
100
Volume
Diameter / nm
Before dialysis

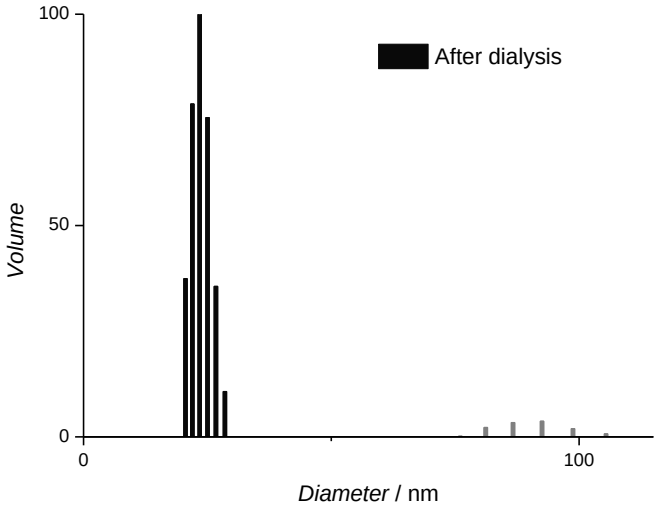
100
50
0
0
100
Volume
Diameter / nm
After dialysis

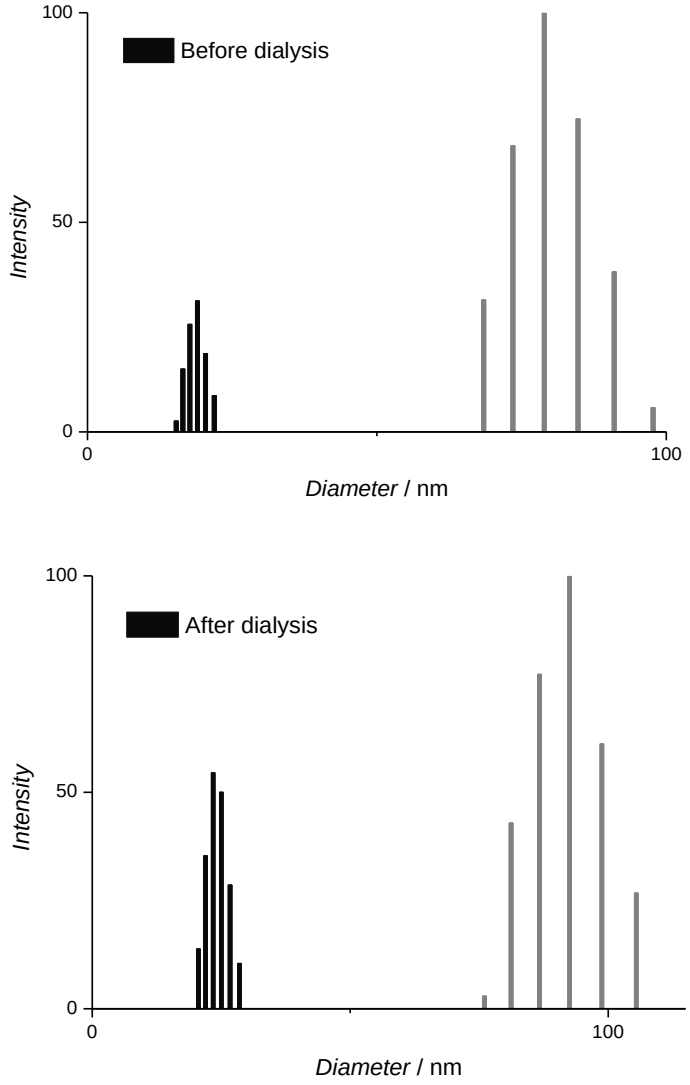

Figure 14: DLS data showing number, volume and intensity average diameter of the micelles before (Table 4 entry 5) and after (40 min) dialysis (Table 4 entry 8)

5.5. Conclusions

An inline purification system for micelle synthesis in continuous flow has been introduced. Micelles are made from mixing solutions of suitable block copolymers in THF with water. Inline flow purification was accomplished via custom-made dialysis units which were operated in a continuous loop. With each pass over the dialysis membrane, small molecules, hence THF is removed from water. Overall, an independency of the purification efficiency from flow rates is observed, and only the total loop time determines the success of the separation. Next to solvent, the system is shown to also remove monomers, as long as they are at least partially water soluble, such as hydroxyethyl acrylate. Flow dialysis seems to have a negligible influence on particle size, as determined from dynamic light scattering monitoring. While this study did not aim at elucidating size distribution and morphology changes that occur during dialysis (and hence removal of solvent that can swell the micelle core), we strongly believe that the increased reliability and reproducibility of our method will pave the way towards such more detailed studies in the future.

Further, it is possible to also purify micelles with an encapsulated payload, in here a dye, which makes the method ready for use in biomedical applications. Overall, the benefit of using flow dialysis is not only that it can be operated semi-continuously, but it is also considerably faster than typical batch methods. Reduction of THF content down to 1% is achieved within 4 h of purification, whereas batch procedures often require days to achieve the same. Further, since flow methods are inherently scalable, they allow for production of encapsulated micelles in significant amounts. Our present, small scale R&D setup allows already to produce up to 1.2 g of micelles per hour.

With the introduction of continuous micelle purification, it is now possible to build setups that can conveniently produce micelles of different shapes, forms and chemical setup. In conjunction with chapter 4 on flow micelle formation itself, the introduction of continuous micelle purification should solve several issues around reproducibility of micelle synthesis, and payload encapsulation. Especially since our setup is easy to use, and also inexpensive, we hope it will find broad use in the community and foster new, exciting developments.

5.6. References

[1] A. Buckinx, K. Verstraete, E. Baeten, R. F. Tabor, A. Sokolova, N. Zaquen, T. Junkers, *Angew. Chem., Int. Ed*. **2019**, 58, 13799.

[2] A. E. Cervera-Padrell, S. T. Morthensen, D. J. Lewandowski, T. Skovby, S. Kiil, K. V. Gernaey, *Org. Process Res. Dev.* **2012**, 16, 888−900.

[3] T. Chang, M. S. Lord, B. Bergmann, A. Macmillan, M. H. Stenzel, *J. Mater. Chem. B* **2014**, 2, 2883 – 2891.

[4] K. Kataoka, A. Harada, Y. Nagasaki, *Adv. Drug Deliv. Rev.* **2001**, 47, 113-131.

[5] H. Cabral, K. Miyata, K. Osada, K. Kataoka, *Chem. Rev.* **2018**, 118, 6844–6892.

[6] K. Benz, K.-P. Jaeckel, K.-J. Regenauer, J. Schiewe, K. Drese, W. Ehrfeld, V. Hessel, H. Loewe, *Chem. Eng. Technol.* **2001**, 24, 11–17.

[7] J. G. Kralj, M. A. Schmidt, K. F. Jensen, *Lab Chip* **2005**, 5, 531–535.

[8] D. A. Wenn, J. E. A. Shaw, B. Mackenzie, *Lab Chip* **2003**, 3, 180–186.

[9] J. G. Kralj, H. R. Sahoo, K. F. Jensen, *Lab Chip* **2007**, 7, 256-263.

[10] J. R. Burns, C. Ramshaw, *Chem. Eng. Commun*. **2002**, 189, 1611–1628.

[11] R. Lebl, T. Murray, A. Adamo, D. Cantillo, C. O. Kappe, *ACS Sustainable Chem. Eng*. **2019**, 7, 20088−20096.

[12] J. H. Bannock, T. W. Phillips, A. M. Nightingale, J. C. DeMello, *Anal. Methods* **2013**, 5, 4991−4998.

[13] T. W. Phillips, J. H. Bannock, J. C. DeMello, *Lab Chip* **2015**, 15, 2960−2967.

[14] A. J. Harvie, J. O. Herrington, J. C. DeMello, *React. Chem. Eng*. **2019**, 4, 1579−1588.

[15] C. I. C. Silvestre, J. L. M. Santos, J. L. F. C. Lima, E. A. G. Zagatto, *Analytica Chimica Acta* **2009**, 652, 54-65.

[16] H. P. L. Gemoets, G. Laudadio, K. Verstraete, V. Hessel, T. Noël, *Angew. Chem. Int. Ed.* **2017**, 56, 7161-7165.

[17] N. Weeranoppanant, A. Adamo, *ACS Med. Chem. Lett.* **2020**, 11, 9-15.

[18] B. Schuur, A. J. Hallett, J. G. M. Winkerlman, J. G. de Vries, H. J. Heeres, *Org. Process Res. Dev.* **2009**, 13, 911–914.

[19] E. Baeten, M. Rubens, K. N.R. Wuest, C. Barner-Kowollik, T. Junkers, *React. Chem. Eng*. **2017**, 2, 826-829.

[20] L. Brocken, P. D. Price, J. Whittaker, I. R. Baxendale, *React. Chem. Eng*. **2017**, 2, 656-661.

Chapter 6

Nanoscale Structural Organization of PPV-containing Block Copolymers for Polymer Light-emitting Diode Applications

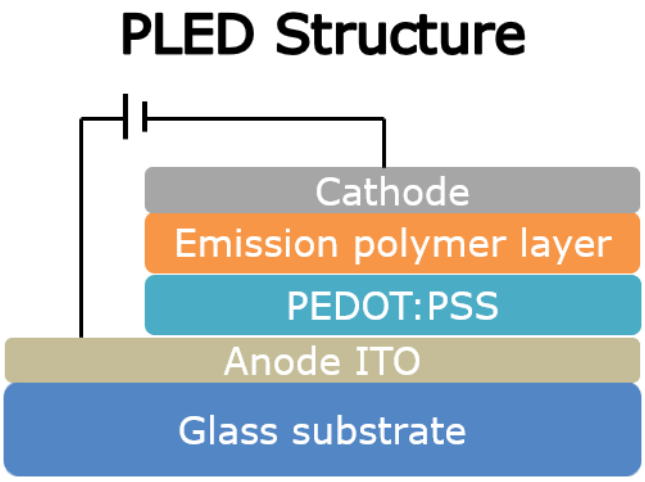

This project was performed in collaboration with Dr. Jasper Michels and the molecular electronics research group of Prof. Paul Blom at the Max Planck Institute for Polymer Research.

6.1. Abstract

The microphase separation of block copolymers containing poly[2-methoxy-5-(3′,7′-dimethyloctyloxy)-1,4-phenylenevinylene] (MDMO-PPV) and butyl acrylate (*n*BuA), butyl methacrylate (*n*BuMA) and tert-butyl acrylate (*t*BuA) is investigated. In contrast with the polymer blends of PPV and these acrylate polymers, their block copolymers cannot macrophase separate since the PPV block is covalently bonded to the polyacrylate, making them suitable for polymer light-emitting diodes (PLED). First, these block copolymers are synthesized via SET-LRP, containing PPV as a first block and *n*BuA, *n*BuMA and *t*BuA as the second block. The corresponding thin-films are spin-coated on a glass substrate and their nanoscale structural organization is examined using atomic force microscopy (AFM), temperature-controlled scanning probe microscopy (SPM) and small-angle x-ray scattering (SAXS).

6.2. Introduction

In the last decades, organic electronics gained a lot of attention due to their low cost, high flexibility and easy processability compared to other semiconducting materials (e.g., crystalline inorganic solids). 1,4-Phenylenevinylene (PPV) materials played a significant role in the development of organic electronics. Moreover, they were the first active materials employed in polymer light-emitting diodes (PLEDs), reported in 1990 by Holmes *et al.*[1] In this case, PPV was applied via spin-coating of the precursor polymer and in a second step the conjugated polymer was achieved after thermal treatment. A dense and uniform PPV thin-film (thickness ~ 100 nm) was achieved. PLED devices were prepared by PPV thin-film deposition on a semi-transparent indium oxide anode layer applied on a glass substrate. Finally, a thin aluminum layer was deposited on top of the conjugated PPV film. Later, PPV monomers with suitable side chains were synthesized to enhance the solubility of the conjugated PPV and to facilitate the synthesis procedure.[2] Polymers such as poly[2-methoxy-5-(2'-ethylhexyloxy)-1,4-phenylenevinylene] (MEH-PPV) and poly[2-methoxy-5-(3',7'-dimethyloctyloxy)-1,4-phenylenevinylene] (MDMO-PPV) became available, which can be easily deposited on substrates *via* various deposition techniques, such as spin-coating[3], dip-coating[4] and inkjet printing[5].

Generally, a PLED is built up of a thin layer of conjugated polymer sandwiched between two electrodes (see Figure 1). At least one of the two electrodes needs to be transparent for the light emission to be visible. Indium-tin oxide (ITO) is generally selected as the anode material for this purpose and is deposited on a transparent glass or plastic substrate. ITO has a relatively high work function close to the polymer's highest occupied molecular orbital (HOMO), promoting hole-

injection into the hole-transporting layer. (The work function expresses the minimum amount of energy there is needed to remove an electron from a solid.) The next layer is often poly(3,4-ethylenedioxythiophene):poly(styrene sulfonate) (PEDOT:PSS) which is a transparent hole-transporting material and simultaneously a buffer layer between the rough ITO layer and the active polymer layer. The hole-transporting material possesses a HOMO in between the polymer's HOMO and work function of ITO. The conjugated polymer layer is established on top of the hole-injection layer *via* spin-coating, and lastly, the cathode is applied as the top layer. The performance of the device is strongly dependent on the cathode since it injects electrons into the active polymer layer when a voltage is applied.[6] A low work function with a small energy difference with respect to the polymer's lowest unoccupied molecular orbital (LUMO) ensures efficient electron-injection into the active polymer layer. One of the downsides related to some low work function cathode metals is their air instability. Therefore, aluminum is often used as the cathode material. Its work function is not very low, but it is relatively stable to air. Another method to prevent corrosion of the low work function materials such as Mg, Li and Ca is by coating them with an air-stable layer of aluminum. In this way, a high electron-transport efficiency and corrosion stable cathode can be guaranteed.

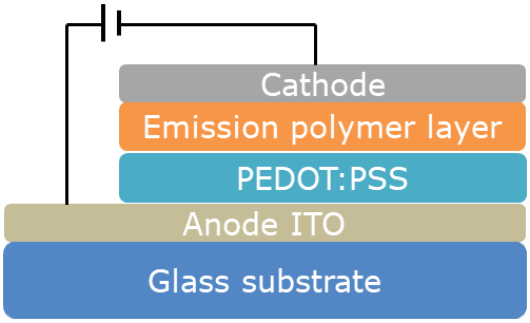

Figure 1: General PLED structure on a glass substrate

When a voltage is applied on the device, the cathode will inject electrons into the active polymer layer. Simultaneously, the anode (ITO) will create holes that are transported by the PEDOT:PSS hole-transporting layer into the polymer layer. The injected holes and electrons diffuse towards the opposite electrodes through the conjugated polymer layer where they will recombine. When the electron-hole pair (exciton) recombines, the exciton will decay and light of a particular color is emitted, determined by the polymer's band gap.[7]

The mobility of holes and electrons in the polymer layer is crucial for the performance of the PLED device. The charge mobility can be interrupted by so-called trap states, which are locations in the polymer layer that restrict the movement of holes and electrons. In the commonly used conjugated polymers for PLEDs, electron transport is limited by trap states caused by chemical impurities or structural defects.[8] The electron hereby falls into an energy level within the bandgap and can in a second step recombine with a hole. This phenomenon is called trap-assisted recombination, which leads to an overall decrease in device performance. Electron-trapping can be minimized by blending the conjugated polymer with an insulating polymer, increasing their contact as much as possible and thereby the PLED efficiency. This is achieved by decreasing both the trap- and transport site density, leading to an increase in the electron current density.[9,10] Unfortunately, due to the immiscibility of both polymers, macrophase separation occurs and trap states are in some cases inevitable. One way to solve this macrophase separation is to increase the amount of insulator polymer until miscibility of both polymers occurs. However, when the volume fraction of the semiconducting polymer is too low, charge transport is reduced tremendously, with a significant current density drop as a result. Consequently, to overcome macrophase separation, the semiconducting and insulator homopolymers are

covalently bonded, forming the corresponding block copolymer. In this way, macrophase separation between the two immiscible polymers is prevented. Still, both covalently bonded blocks tend to demix due to the repulsive interaction between them. As a result, microphase separation can occur, forming microdomains that improve the efficiency of the ion transport within the active layer.[11] The formation of microdomains require enough repulsion between both blocks, since ordering them into microdomains is accompanied by the loss in entropy.[12] The strength of the repulsive interaction is determined by χN, where χ is the Flory-Huggins parameter and N is the number of monomers in the block copolymer. When this number exceeds a critical value, an order-disorder transition will occur and microphase separation is obtained, as presented in Figure 2. The shift towards a disordered phase can be caused by low molecular weight polymers (N is small) or high temperatures (since χ is inversely proportional to the temperature). The microdomain morphology is dependent on the volume fractions (f) of the polymers and can be, for example, spherical (S), cylindrical (C), gyroid (G) and lamellar (L).[13,14] There should be noted that the phase diagram is dependent on the type of block copolymer. This phase diagram could be a tool to determine the morphology, when a certain kind of phase separation is observed in imaging techniques, like AFM.

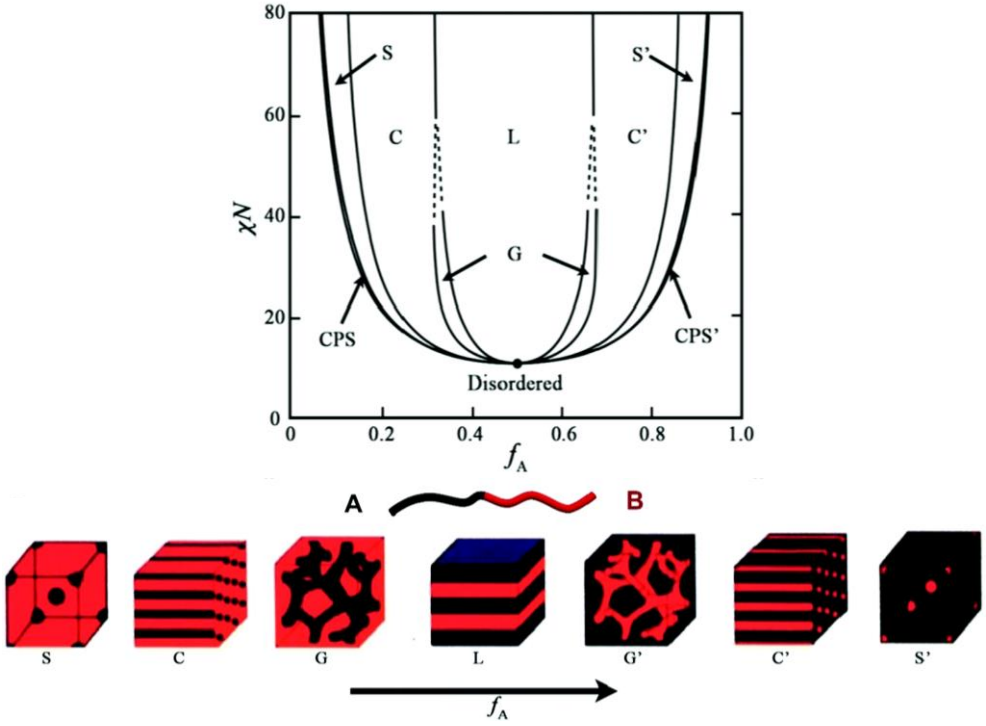

Figure 2: Phase diagram for the microdomain phase separation of block copolymers and their morphologies[14]

Until now, we described the microphase separation of block copolymers in 'bulk', but in PLED applications, there is only a nanolayer of the block copolymer involved. The block copolymers' behavior in thin-films can be different depending on the thickness, synthesis procedure or interactions at the interfaces of neighboring layers. The block copolymer thin-film is generally prepared *via* spin-coating, since this technique is relatively fast and easily applicable. In this technique, the block copolymer is dissolved in a good solvent and is applied on a suitable substrate. The latter is spun at a speed of 1000-5000 rpm to equally distribute the block copolymer over the substrate and evaporate most of the solvent.[15] The thickness

of the film is determined by the spinning rate, the concentration of the polymer in the solvent and the molecular weight of the block copolymer. A thin-film is now deposited on the substrate and due to the repulsion between both parts of the block copolymer, microdomains are formed. In most cases, microdomain formation can take some time and, as a consequence, the thin-film is subjected to an additional annealing step. Annealing can be performed by temperature or solvent vapor treatment. Thermal annealing is performed at temperatures above the polymer's glass transition temperature but below the melting temperature. This temperature needs to be applied long enough to enable microphase separation of the block copolymer. In solvent vapor annealing, the polymer thin-film is brought into an atmosphere filled with solvent vapors. These vapors are adsorbed by the polymer film and enhance the mobility of the different blocks.

The morphology of the microdomains is also strongly dependent on the thickness of the polymer film and the polymer's interface interaction with other layers. The energy at the interface is dependent on the affinity of the different blocks with either the substrate surface or the atmosphere. Each polymer block has mostly also different affinity properties. Therefore, wetting of the polymer sublayers can occur when a block has a more considerable affinity to one of the interfaces. What happens with preferential wetting in lamellar microdomains, is that the same block of the block copolymer will form a layer at the interface between the block copolymer and the substrate or the block copolymer and the air. The lamellar layers of the different blocks will be parallel with the surface.

The size of the microdomains is dependent on the molecular weight of the block copolymer. A symmetric block copolymer, with the simplest lamellar morphology, has microdomains with a size corresponding to the length of two block copolymer molecules in the ordered state, which is called the natural period L_0.[15] When the

film thickness exceeds L_0 (e.g., some hundreds of nanometers to micrometers thick), one can speak of a thick film. Most thick films have cylindrical microdomains, which can be used to form nanopores in template applications.[16] Conversely, when the film thickness is way below L_0, insufficient material is available to from complete layers of the block copolymer. Therefore, sub-monomolecular-thick films, in the form of clusters, are formed.[17] Different morphologies are possible when the film thickness is above the monomolecular layer thickness and just below L_0.[18] In this region, the microdomain formation competes with the surface tension and multiple morphologies can be formed depending on the thickness and annealing procedure.[19]

In this chapter the microphase separation of PPV-acrylate block copolymers is investigated. Various PPV containing block copolymers are spin-coated onto an ITO-containing glass substrate where-after the thickness is determined *via* a scratch test and atomic force microscope imaging is used to visualize the surface morphology.

6.3. Experimental Section

6.3.1. Block copolymer synthesis

The synthesis of the block copolymers was performed as described in literature procedures and is further elucidated in Chapter 7. PPV-*b*-*n*BuA, PPV-*b*-*n*BuMA and PPV-*b*-*t*BuA were synthesized using SET-LRP with *n*-BuA (1.43 g, 1.58 mL, 0.011 mol, 200 equiv.), *n*-BuMA (0.79 g, 0.88 mL, $5.56 \cdot 10^{-3}$ mol, 100 equiv.) and *t*BuA (0.80 g, 0.92 mL, $6.25 \cdot 10^{-3}$ mol, 100 equiv.) as the second block.

6.3.2. Thin-film deposition *via* spin-coating

The block copolymer thin-films will be deposited on Indium-tin-oxide (ITO) covered glass. First, the glass substrates need to be cleaned. This is done by dipping the glass substrate in soap water of 40°C and gently scrubbing it. Next, the substrate is put in water and sonicated for 5 minutes, where-after the same is done for acetone and isopropanol. Lastly, the glass substrate is dried with N_2-gas and cured in the UV-oven for 20 minutes.

Now, a PEDOT:PSS layer can be spin-coated on top of the glass substrate. This was done in a clean room to make sure no dust or other particles could interfere in the PEDOT:PSS layer. The glass substrate was put in the spin-coater with the UV-cured side up and a few drops of the PEDOT:PSS mixture was put through a syringe filter on the substrate. The glass substrate was spin-coated with the PEDOT:PSS layer and afterwards annealed in the oven for 15 minutes at 140 °C. The substrate with the PEDOT:PSS can now be transferred out of the clean room into the glovebox containing a spin-coater. Solutions of the block copolymers in toluene are prepared with different concentrations ranging from 10 $mg \cdot mL^{-1}$ till 20 $mg \cdot mL^{-1}$. These solutions can now be spin-coated on the substrate with the PEDOT:PSS layer and can afterwards be annealed at different temperatures.

6.4. Results and Discussion

6.4.1. Block copolymer synthesis

Various block copolymers containing one PPV block and one acrylate block were synthesized via known procedures for the use in thin-film applications.[20] First, poly[2-methoxy-5-(3′,7′-dimethyloctyloxy)-1,4-phenylenevinylene] (MDMO-PPV) was synthesized via anionic sulfinyl polymerization and in a second step the acrylate block was polymerized via single electron transfer-living radical polymerization (SET-LRP). Butyl acrylate (*n*BuA), butyl methacrylate (*n*BuMA) and tert-butyl acrylate (*t*BuA) were used as the second block to form a rod-coil like block copolymer and counter the stiffness of the PPV rod-like block. Rod-coil like block copolymers are able to self-assemble in different morphologies.[21] The PPV homopolymer chain extensions into the various block copolymers is shown in the size exclusion chromatography (SEC) graphs in Figure 3. The molecular weight increase is clearly visible for the three block copolymers synthesized.

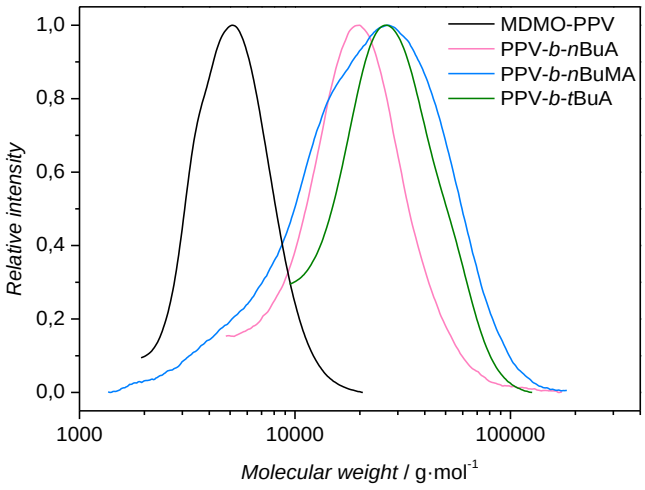

Figure 3: Molecular weight distributions of the PPV homopolymer and the different block copolymers

Remarkably, this is the first and only time in this PhD thesis, that this kind of increase of the molecular weight was visible in SEC for the PPV block copolymers. The fact that much shorter PPV homopolymers are used for the block copolymer synthesis compared to previous chapters, can be an explanation (e.g., the molecular weight of the PPV homopolymer here is 4700 $g \cdot mol^{-1}$ and 8600 $g \cdot mol^{-1}$ in chapter 3). In Table 1, the molecular weight, dispersity and λ_{max} of the PPV homopolymer and various block copolymers are displayed. Their theoretical molecular weight is calculated using the conversion of the acrylate block, measured via ^{1}H NMR. The theoretical molecular weight differs from the molecular weight obtained by SEC, especially for the block copolymer containing *t*BuA. These differences are due to the use of the Mark-Houwink parameters of the PPV homopolymer, which leads to a misinterpretation of the molecular weight of the block copolymer in SEC. Nevertheless, it shows the elongation of the polymer chain with their relatively narrow dispersity of 1.4, 1.8 and 1.3 for the *n*BuA, *n*BuMA and *t*BuA block copolymers respectively. The dispersity of the *n*BuMA block copolymer is slightly higher because it is a methacrylate and it therefore reacts a bit slower than the acrylate polymers used, this resulted in a broader distribution. The λ_{max} of the PPV homopolymer is slightly lower than the normal λ_{max} of 485 nm for conjugated PPV. This difference is caused by the variation in conjugation length around the value of the actual conjugation, which may be induced by the shorter PPV chain.

Table 1: Overview of the molecular weight, dispersity and λ_{max} of the different block copolymers

	$M_{n,T}$ [a] g·mol^{-1}	M_n [b] g·mol^{-1}	M_w [b] g·mol^{-1}	$Đ$	λ_{max} [c]	Conversion[d] %
MDMO-PPV		4700	5600	1.2	465	
PPV-*b*-*n*BuA	20800	16300	23300	1.4	471	63
PPV-*b*-*n*BuMA	18800	15200	28100	1.8	437	99
PPV-*b*-*t*BuA	16900	24000	31000	1.3	451	94

[a] $M_{n,T}$ is the theoretical molecular weight calculated via ^{1}H NMR, [b] M_n is the number average molecular weight, M_w the weight average molecular weight and $Đ$ represents the dispersity of the molecular weight distribution. Measurements were performed using SEC. [c] λ_{max} was determined using chloroform as the solvent. [d] Conversion was determined using ^{1}H NMR.

6.4.2. Thin-film analysis

Three different block copolymers are synthesized that will be tested on their microphase separation. When the ITO-covered glass substrates are cleaned, a PEDOT:PSS layer is applied on the substrate. This layer is, like explained in the introduction of this chapter, a hole-transporting layer in a PLED device. This layer is applied here to resemble the structure of the device and make sure the block copolymer layer is well attached on the relatively rough ITO-covered glass substrate. Since this project was performed in the Max Planck Institute for polymer research in Mainz, the clean room could be used to spin-coat the PEDOT:PSS layer on the substrate. After this layer was formed, the film thickness was measured using a Bruker Dektak XT Profilometer. The film thickness of the PEDOT:PSS layer was 70 nm. In the next step, the block copolymer solutions can

be spin-coated on top of the PEDOT:PSS layer. First, 0.2 mL of a PPV-*b*-*n*BuMA solution with a concentration of 10 mg·mL^{-1} in toluene was spin-coated. The total thickness of the PEDOT:PSS and block copolymer layer was 100 nm, indicating a block copolymer thin-film thickness of 30 nm. Since the preferred film thickness for this kind of materials for PLED devices is between 50 and 100 nm for the block copolymer layer, the concentration was increased to 15 mg·mL^{-1}. The total layer thickness increased to 130 nm, which corresponds to a block copolymer thin-film of 60 nm. This experiment was repeated multiple times for the PPV-*b*-*n*BuMA, PPV-*b*-*n*BuA and PPV-*b*-*t*BuA block copolymers with layer thicknesses between 60 nm and 75 nm, except for the PPV-*b*-*n*BuA block copolymer. This block copolymer seems to stay very soft and the total layer thickness was only 70 nm, so no polymer thin-film was formed. Therefore, the concentration of this block copolymer was increased to 20 mg·mL^{-1}, but unfortunately no change was noticed. Accordingly, the PPV-*b*-*n*BuA block copolymer was not further used.

Atomic force microscopy (AFM) was used to determine the nanoscale structural organization of the block copolymer thin-film. The block copolymer surfaces are visualized by AFM and different annealed and non-annealed samples are compared. Mostly, the microphase separation will be facilitated by thermal annealing, therefore the non-annealed and annealed samples are compared in Table 2 and Table 3 for PPV-*b*-*n*BuMA and PPV-*b*-*t*BuA respectively. (The height/topography images are not represented here since there was completely nothing visible on these images.) The surface is first screened on a 5 µm by 5 µm scale to get a broad view of the microstructure. There can be observed that the surfaces of both block copolymers show almost everywhere the same stiffness, even if only the phase images are represented. The phase images can be used to give an indication of the variations in the local stiffness of the layer, but there is

almost no difference visible for both block copolymers. On the magnified images of both block copolymer thin-films, a very small difference in phase is observed on the annealed samples. Unfortunately, this difference in phase is so small and unpronounced that one cannot speak of a real microphase separation.

Table 2: AFM phase images of the non-annealed and annealed PPV-*b*-*n*BuMA

	Non-annealed	annealed at 150°C	annealed at 180°C
5 µm	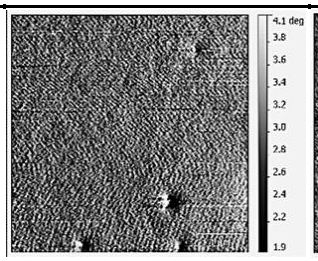	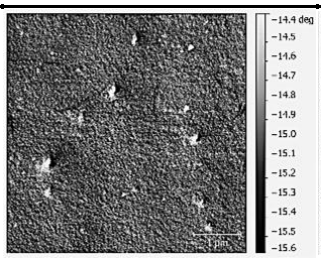	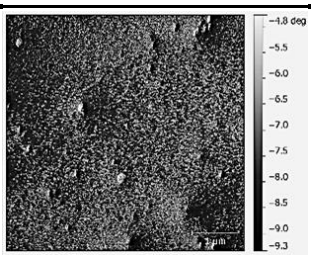
500 nm	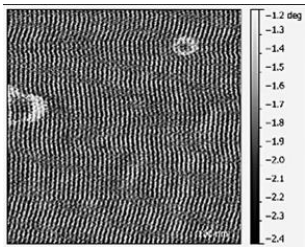	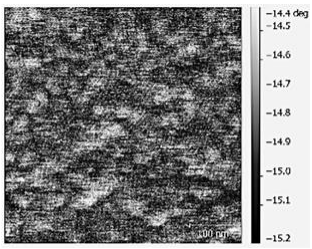	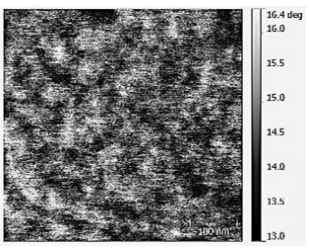

Until now, no clear structural organization could be detected via AFM. A possible explanation for these smooth surfaces could be the formation of a wetting layer at the air-polymer interface, indicating that the same block of the block copolymer forms a layer at the air interface and the other block is not visible. Therefore, more studies will be performed to examine the ordering in the sublayers.

Table 3: AFM phase images of the non-annealed and annealed PPV-*b*-*t*BuA

	Non-annealed	annealed at 150°C	annealed at 180°C
5 µm	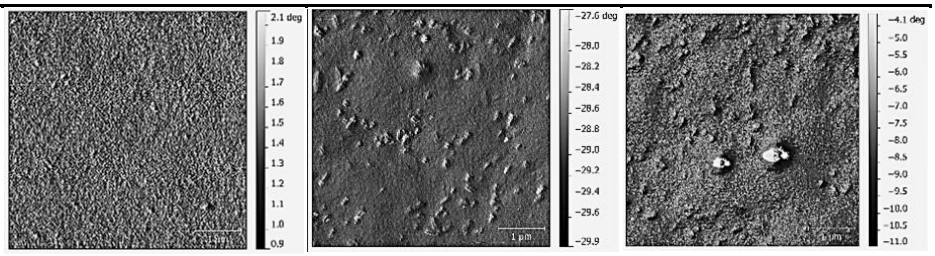		
500 nm	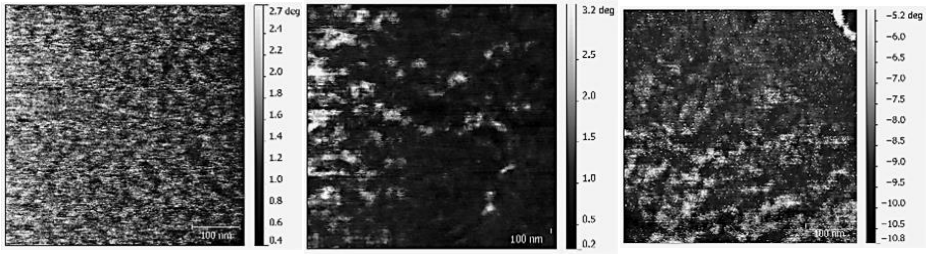		

Since the PPV-*b*-*t*BuA block copolymer showed the most promising results in the AFM images, the following experiments are performed with this block copolymer. Annealing is performed to accelerate structural organization, but if the block copolymer mobility is still very low at these annealing temperatures, no microdomains will be formed yet. Therefore, the mobility of the block copolymer layer is tested at different temperatures using a scanning probe microscope (SPM) equipped with a heating plate. A scratch was made in the block copolymer layer and the behaviour of the edge upon heating was measured. The sample was heated to certain temperatures (took about 10 minutes) and kept at these temperatures for 60 minutes, after which it was cooled down to room temperature (took about 60 minutes) and the SPM measurement could be performed. Figure 4 shows that at room temperature (29.5 °C) the edge of the scratch is very sharp.

In the first heating step, the temperature is increased to 80 °C and a rounding of the edge is observed, indicating that the block copolymer shows mobility at this temperature and starts to flow. When the temperature is further increased, the rounding of the edge becomes more pronounced. The block copolymer clearly moves, even already at 80 °C. Accordingly, the movement of the block copolymer is no restriction for the formation of microdomains.

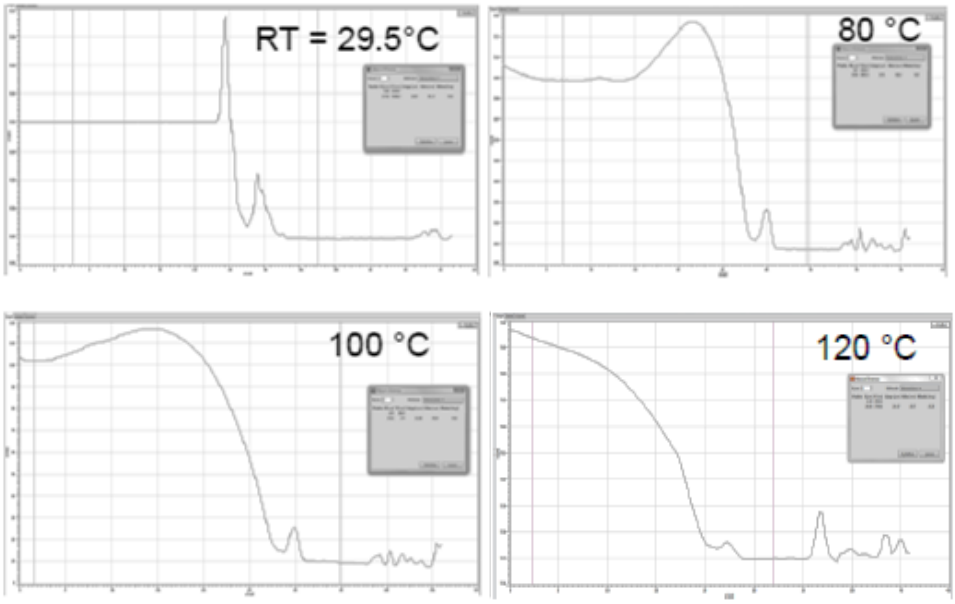

Figure 4: Overview of the SPM results for PPV-*b*-*t*BuA at different temperatures[22]

Since the mobility of the PPV-*b*-*t*BuA block copolymer is no issue, but no pronounced ordering was visible in AFM, further analysis is performed using small-angle x-ray scattering (SAXS). SAXS is an ideal technique to complement the microscopic techniques in visualising nanostructures, since it provides structural information of a large sample area. Figure 5 shows the SAXS results for the non-annealed (blue line) and annealed (orange line) PPV-*b*-*t*BuA block copolymer thin-film. In the non-annealed sample, no scattering signal is detected, meaning there is no sign of ordering. Conversely, the annealed block copolymer sample shows a low intensity peak at approximately 0.47 nm^{-1}. This corresponds to an ordering periodicity of about 13 nm and the relatively broad peak around 1.5 nm^{-1} gives a correlation length of about 130 nm. Comparing these results to other block copolymers showing nanoscale structures, the order in this sample is rather low.[23,24]

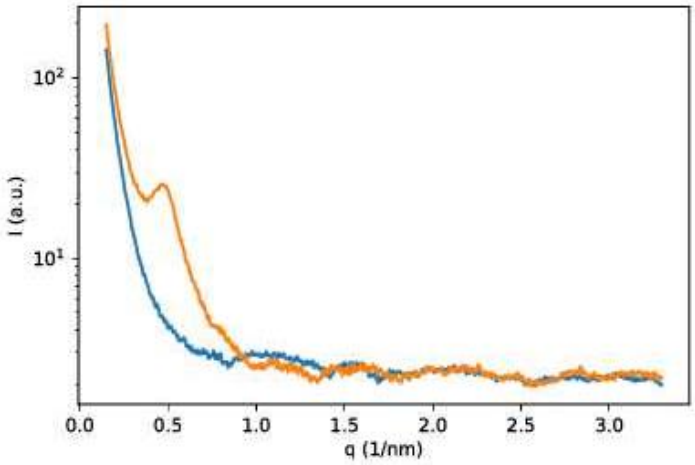

Figure 5: SAXS results of the non-annealed (blue) and annealed (orange) PPV-*b*-*t*BuA block copolymer layer[25]

6.5. Conclusions

Three different block copolymers containing one PPV block and one acrylate block were synthesized to investigate their nanoscale structural behavior in thin-films. Therefore, thin-films of each block copolymer were spin-coated onto a PEDOT:PSS layer, which was deposited on an ITO-containing glass substrate. The nanoscale structural organization was investigated by AFM imaging techniques, but no pronounced ordering was visible. Therefore, the mobility of the PPV-*b*-*t*BuA block copolymer was analyzed using SPM, indicating that the block copolymer shows clear mobility at 80 °C. Subsequently, the ordering of this block copolymer was further examined using SAXS analysis and a minor ordering of about 13 nm was observed. This order is rather low when compared to other block copolymers showing nanoscale structural organization, but nevertheless the device performance of this block copolymer was further investigated at the MPIP in Mainz. Unfortunately, there was no current achieved for the PPV-*b*-*t*BuA block copolymer. A possible explanation could be trapping of the charge carriers by the polymer chains or the distance between the polymer chains is too large because no order was achieved. Interesting for future work would be the variation of the different block lengths of these block copolymers to achieve some ordering and eventually a current applicable for PLED devices. It would be interesting to start with the synthesis of a longer PPV chain, since there is expected that the molecular weight of the PPV polymer is too low to induce charge conduction.

6.6. References

[1] J. H. Burroughes, D. D. C. Bradley, A. R. Brown, R. N. Marks, K. Mackay, R. H. Friend, P. L. Burns, A. B. Holmes, *Nature* **1990**, 347, 539.

[2] M. Kuik, G. A. H. Wetzelaer, H. T. Nicolai, N. I. Craciun, D. M. De Leeuw, P. W. M. Blom, *Adv. Mater.* **2014**, 26, 512–531.

[3] R. H. Friend, R. W. Gymer, A. B. Holmes, J. H. Burroughes, R. N. Marks, C. Taliani, D. D. C. Bradley, D. A. Dos Santos, J. L. Brédas, M. Lögdlund & W. R. Salaneck, *Nature* **1999**, 397, 121–128.

[4] P. Yimsiri, M. R. Mackley, *Chem. Eng. Sci*. **2006**, 61, 3496–3505.

[5] S. C. Chang, J. Liu, J. Bhaeathan, Y. Yang, J. Onohara, J. Kido, *Adv. Mater*. **1999**, 11, 734–737.

[6] M. N. Bochkarev, M. A. Katkova, V. A. Ilichev, A. N. Konev, *Nanotechnol Russia* **2008**, 3, 470–473.

[7] D. X. Yu, *Int. J. Mol. Sci.* **2011**, 12, 1575-1594.

[8] D. Abbaszadeh, A. Kunz, N. B. Kotadiya, A. Mondal, D. Andrienko, J. J. Michels, G.-J. A. H. Wetzelaer, P. W. M. Blom, *Chem. Mater*. **2019**, 31, 6380−6386.

[9] D. Abbaszadeh, A. Kunz, G. A. H. Wetzelaer, J. J. Michels, N. I. Crăciun, K. Koynov, I. Lieberwirth, P. W. M. Blom, *Nat. Mater*. **2016**, 15, 628−633.

[10] A. Kunz, P. W. M. Blom, J. J. Michels, *J. Mater. Chem. C* **2017**, 5, 3042−3048.

[11] L. Leibler, *Macromolecules* **1980**, 13, 1602−1617.

[12] F. S. Bates, G. H. Fredrickson, *Annu. Rev. Phys. Chem*. **1990**, 41, 525−557.

[13] F. S. Bates, G. H. Fredrickson, *Phys. Today* **1999**, *52*, 32-38.

[14] C. Li, Q. Li, Y. V. Kaneti, D. Hou, Y. Yamauchi, Y. Mai, *Chem. Soc. Rev*. **2020**, 49, 4681-4736.

[15] H.-C. Kim, S.-M. Park, W. D. Hinsberg, *Chem. Rev.* **2010,** 110*,* 146–177.

[16] T. Thurn-Albrecht, J. Schotter, C. A. Kastle, N. Emley, T. Shibauchi, L. Krusin-Elbaum, K. Guarini, C. T. Black, M. T. Tuominen, T. P. Russell, *Science* **2000**, 290, 2126-2129.

[17] I. I. Potemkin, M. Möller, *Macromolecules* **2005**, 38, 2999-3006.

[18] T. L. Morkved, H. M. Jaeger, *Europhys. Lett.* **1997**, 40, 643-648.

[19] J. Peng, Y. Xuan, H. F. Wang, Y. M. Yang, B. Y. Li, Y. C. Han, *J. Chem. Phys.* **2004**, 120, 11163.

[20] I. Cosemans, J. Vandenbergh, L. Lutsen, D. Vanderzande, T. Junkers, *Polym. Chem*. **2013**, 4, 3471-3479.

[21] N. Sary, C. Brochon, G. Hadziioannou, R. Mezzenga, *Eur. Phys. J.* **2007**, 24, 379–384.

[22] Rüdiger Berger, Helma Burg and Uwe Rietzler from the MPIP Mainz are thanked for the SPM measurements.

[23] S. Krishnamoorthy, C. Hinderling, H. Heinzelmann, *Mater. Today* **2006**, 9, 40-47.

[24] P. Müller-Buschbaum, *Eur. Polym. J.* **2016**, 81, 470–493.

[25] Markus Mezger and Julian Mars (MPIP Mainz) are thanked for the SAXS analysis

Chapter 7

General Experimental Details, Materials and Characterization

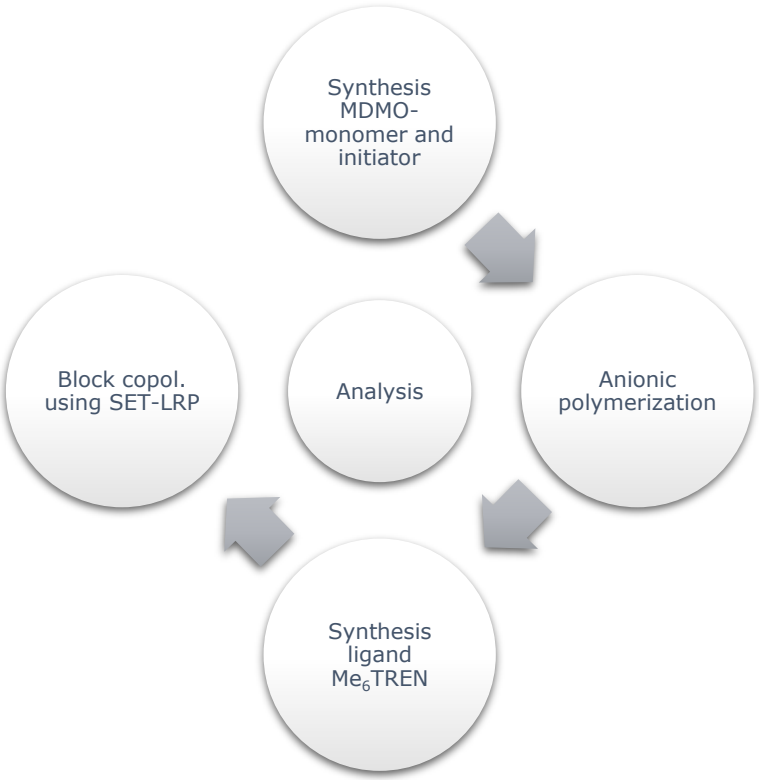

7.1. Materials

All solvents and reagents were purchased from Fisher, Acros, VWR or Sigma Aldrich and were used without further purification. Tetrahydrofuran (THF) and dimethylformamide (DMF) were dried on a MD-SPS 800 system (if indicated as dry solvent). *tert*-Butyl acrylate, *n*-butyl acrylate and *n*-butyl methacrylate were deinhibited over a column with basic alumina prior to use. The PPV premonomer, initiator, (block co)polymer and tris[2-(dimethylamino) ethyl]amine (Me_6TREN) were synthesized as explained below.

7.2. General experimental details

7.2.1. Synthesis of the MDMO sulfinyl premonomer: 1-(Chloromethyl)-5-((3,7-dimethyloctyl)oxy)-2-methoxy-4-((octylsulfinyl)methyl)benzene (MDMO)

The synthesis of the MDMO premonomer was performed as described in literature procedures and is presented in Scheme 1.[1,2] More detail is provided below and characterization of the compounds was performed by NMR.

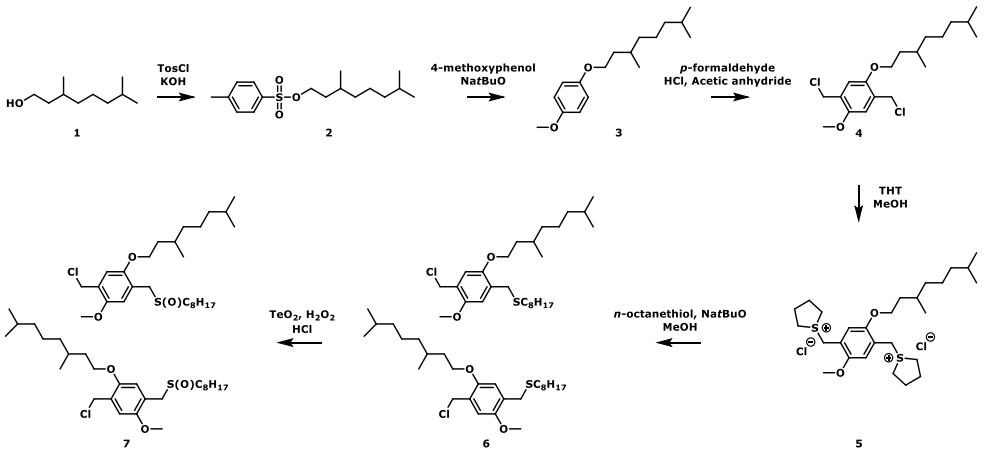

Scheme 1: Synthesis of the MDMO premonomer

Step 1: 3,7-Dimethyloctyl-4-methylbenzene sulfonate [2]

A mixture of 3,7-dimethyloctan-1-ol [1] (115.92 g, 140 mL, 0.732 mol, 1 equiv.) and p-toluenesulfonyl chloride (139,6 g, 0.732 mol, 1 equiv.) in CH_2Cl_2 (500 mL) was cooled with a mixture of $CHCl_3$ and liquid nitrogen. KOH (164.3 g, 2.928 mol, 4 equiv.) was added under nitrogen atmosphere, maintaining a temperature below 5 °C. The mixture was reacted for 3 h at 0 °C after which it was quenched with ice water (500 mL) and extracted with CH_2Cl_2 (3 × 250 mL). The organic layer was dried over anhydrous $MgSO_4$ and filtered. After evaporation of the solvent under reduced pressure, the crude product [2] was obtained as a clear oil. No purification was needed (209.74 g, 91.7%). ^{1}H NMR ($CDCl_3$): δ = 7.74 (m, 2H); 7.30 (m, 2H); 4.01 (m, 2H); 2.39 (s, 3H); 1.59 (m, 1H); 1.42 (m, 3H); 1.06 (m, 6H); 0.79 (m, 9H).

Step 2: 1-((3,7-Dimethyloctyl)oxy)-4-methoxy benzene [3]

A mixture of 4-methoxyphenol (75.75 g, 0.610 mol, 1 equiv.) and sodium *tert*-butoxide (NaO*t*Bu) (70.35 g, 0.732 mol, 1.21 equiv.) in ethanol (600 mL) was stirred at room temperature under nitrogen atmosphere. After 1 h, [2] (209.74 g, 0.671 mol, 1.1 equiv.) was added and the resulting mixture was stirred overnight at reflux temperature (80 °C). Afterwards, the reaction was quenched with H_2O (600 mL) and extracted with CH_2Cl_2 (3 × 250 mL). The organic layer was dried over anhydrous $MgSO_4$, filtered and the solvent was evaporated under reduced pressure to give the crude product as a brown oil. The pure product [3] was obtained by vacuum distillation at 95 °C (127.37 g, 78.9%). ^{1}H NMR ($CDCl_3$): δ = 6.83 (s, 4H); 3.92 (s, 2H); 3.76 (s, 3H); 1.78 (s, 1H); 1.56 (m, 3H); 1.31 (s, 4H); 1.17 (s, 2H); 0.89 (s, 9H). ^{13}C NMR ($CDCl_3$): δ = 154.1 (C4); 152.6 (C4); 115.8

(CH); 115.6 (CH); 67.2 (CH_2); 55.8 (CH_3); 39.2 (CH_2); 37,6 (CH_2); 37,1 (CH_2); 29.2 (CH_2); 28.7 (CH_2); 23.2 (CH_3); 15.24 (CH_3).

Step 3: 2,5-Bis(chloro-methyl)-1-(3,7-dimethyloctyloxy)-4-methoxybenzene [4]

HCl (37%, 312.55 g, 260 mL, 3.175 mol, 6.6 equiv.) was added dropwise at room temperature under nitrogen atmosphere to a stirred mixture of [3] (127.31 g, 0.481 mol, 1 equiv.) and p-formaldehyde (39.76 g, 1.324 mol, 2.75 equiv.). Next, acetic anhydride (491 g, 455 mL, 4.81 mol, 10 equiv.) was added drop wise, without exceeding a temperature of 70 °C. Afterwards, the solution was stirred at 70 °C for 4 h and cooled down to room temperature. H_2O (600 mL) was added to the solution and the resulting precipitate was filtered off and redissolved in CH_2Cl_2 (400 mL). The organic solution was dried over anhydrous $MgSO_4$, filtered and the solvent was evaporated under reduced pressure to give the crude product as a yellow oil. Finally, after recrystallization in hexane, the pure product [4] was obtained as white crystals (136 g, 78.3%). ^{1}H NMR ($CDCl_3$): δ = 6.90 (s, 4H); 4.61 (s, 4H); 4.00 (s, 2H); 3.84 (s, 3H); 1.80 (s, 2H); 1.61 (m, 5H); 1.29 (m, 2H); 1.12 (m, 2H); 0.90 (m 9H); ^{13}C NMR ($CDCl_3$): δ = 19.8 (CH_3); 22.6 (CH_3); 24.6 (CH_2); 27.9 (CH), 30.2 (CH_2), 36.6 (CH_2), 37.4 (CH_2), 39.2 (CH_2), 41.2 (CH_2), 56.4 (CH_3), 67.9 (CH_2), 113.2 (C4), 114.3 (C4), 127.0 (C4).

Step 4: 1,4-Bis(tetrahydrothiopheniomethyl)xylene dichloride [5]

Tetrahydrothiophene (THT) (165.9 g, 166 mL, 1.882 mol, 5 equiv.) was added to a stirred mixture of [4] (136 g, 0.376 mol, 1 equiv.) in MeOH (600 mL). The reaction was reacted for 3 days at room temperature. The solution was precipitated in cold acetone (2 L) under heavy stirring and the resulting precipitate was filtered over a glass filter and washed with cold acetone. After drying under high vacuum, the pure product [5] was obtained as a white solid (92 g, 44.1%). ^{1}H NMR (D_2O): δ = 7.10 (s, 2H); 4.41 (s, 4H); 4.08 (m, 4H); 3.80 (s 2H); 3.40 (d, J = 5.5 Hz, 8H); 2.22 (m, 8H); 1.74 (m, 2H); 1.55–1.37 (m, 3H); 1.18 (m, 6H); 0.84 (d, J = 6.3 Hz, 3H); 0.71 (dd, J = 6.6 and 2.9, 6H). ^{13}C NMR (D_2O): δ = 19.10, (CH_3); 22.07 (CH_3); 24.13 (CH_2); 26.4 (CH); 29.6 (CH); 30.7 (CH_2); 31.3 (CH_2); 37.6 (CH_2); 38.7 (CH_2); 40.9 (CH_2); 43.9 (CH_2); 45.5 (CH_2); 58.6 (CH_3); 70.0 (CH_2); 117.8/118.6 (CH); 121.9/122.4 (C4); 153.7/154.3 (C4).

Step 5: (4-(Chloromethyl)-2-((3,7-dimethyloctyl)oxy)-5-methoxybenzyl)(octyl)sulfane [6]

A mixture of n-octanethiol (24.25 g, 28.8 mL, 0.166 mol, 1 equiv.) and NaOtBu (15.93 g, 0.166 mol, 1 equiv.) in MeOH (400 mL) was stirred at room temperature for 30 min. This mixture was added drop wise to a stirred mixture of [5] (92 g, 0.166 mol, 1 equiv.) in MeOH (550 mL) after which it was reacted for 3 h at room temperature under nitrogen atmosphere. The solvent was removed under reduced pressure and n-octane (100 mL) was added to the mixture. The n-octane was evaporated again under reduced pressure to remove the THT by azeotropic distillation. This procedure was repeated 3-5 times, until all THT was removed. The residue was redissolved in CH_2Cl_2 (350 mL) and extracted with a saturated NaCl:H_2O solution (1:10) (3 × 250 mL). The organic layer was dried over

anhydrous $MgSO_4$, filtered and the solvent was evaporated of under reduced pressure to give the crude product [6] as a white solid (80 g, quantitative yield), which was used immediately (on the same day) in the next synthesis step. ^{1}H NMR ($CDCl_3$): δ = 6.87 (m, 2H); 4.62 (d, J = 2.4 Hz, 2H); 3.99 (m, 2H); 3.84 (m, 3H); 3.70 (d, J = 3.4 Hz, 2H); 2.45 (t, J = 6.8 Hz, 2H); 1.87 (m, 1H); 1.81 (m, 1H); 1.52 (m, 2H); 1.25 (m, 18H); 0.88 (m, 9H).

Step 6: 1-(Chloromethyl)-5-((3,7-dimethyloctyl)oxy)-2-methoxy-4-((octylsulfinyl)methyl)benzene [7]

TeO_2 (3.38 g, 0.0212 mol, 0.125 equiv.) and HCl (2 M, 8.17 mL, 0.204 mol, 1.2 equiv.) were added to a stirred mixture of [6] (80.0 g, 0.170 mol, 1 equiv.) in 1,4-dioxane (800 mL). To start the reaction hydrogen peroxide (H_2O_2) (35%, 29.69 mL, 0.339 mol, 2 equiv.) was added and the reaction was followed on TLC (hexane/EtOAc: 6/4). When all [6] was reacted, the reaction was quenched with a saturated NaCl-solution:H_2O (1:1; 400 mL). Next, the solution was extracted with CH_2Cl_2 (3 × 300 mL), dried over anhydrous $MgSO_4$ and filtered. The solvent was evaporated under reduced pressure to give the crude product as a yellow oil. The pure product [7] was obtained by column chromatography (SiO_2, hexane/EtOAc: 6/4) (80 g, 96.6%). ^{1}H NMR ($CDCl_3$): δ = 7.37 (d, J = 8.0 Hz, 2H); 7.26 (d, J = 8.0 Hz, 2H); 4.55 (s, 2H); 3.91 + 3.93 (dd, JAB = 13.0 Hz, 2H); 2.53 (t, J = 8.0 Hz, 2H); 1.70 (m, 2H); 1.36 (m, 2H); 1.23 (m, 8H); 0.84 (t, J = 6.8 Hz, 3H); ^{13}C NMR ($CDCl_3$): δ = 14.0 (CH_2); 22.4 (CH_3); 22.5 (CH_3); 28.7 (CH); 28.9 (CH_2); 29.1 (CH); 31.6 (CH_2); 45.6 (CH_2), 51.0 (CH_2); 57.6 (CH_3); 129.1 (C4); 130.2 (C4); 130.3 (C4); 137.5 (C4).

7.2.2. Synthesis of the anionic initiator: 4-((methylsulfinyl)methyl)phenyl-2-bromo-2-methylpropanoate

The synthesis of the initiator was performed as described in literature procedures and is presented in Scheme 2.[3] More detail is provided below and characterization of the compounds was performed by NMR.

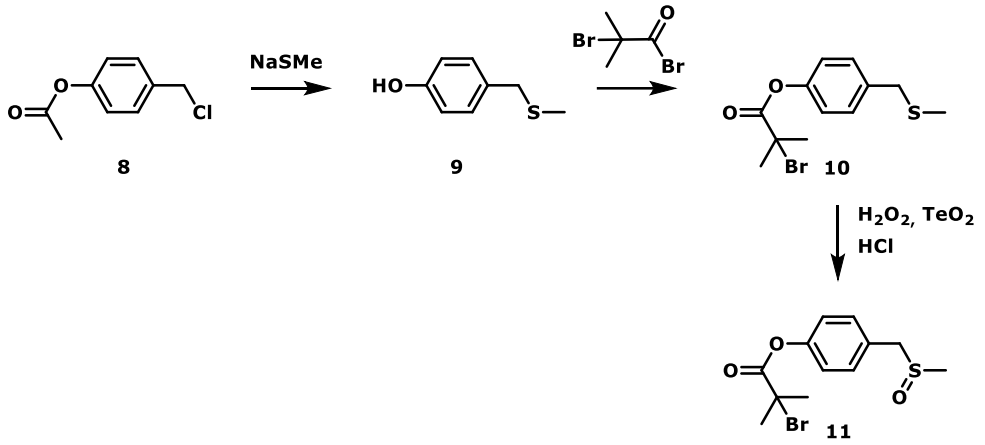

Scheme 2: Synthesis of the anionic initiator

Step 1: 4-((methylthio)methyl)phenol [9]

4-(chloromethyl)phenyl acetate [8] (5.0 g, 0.027 mol, 1 equiv.) was added to a stirred mixture of NaSMe (21% in H_2O, 9.35 g, 0.028 mol, 1.05 equiv.) in EtOH (20 mL) and reacted for 1 h at reflux temperature (80 °C). Potassium hydroxide (KOH) (3.02 g, 0.054 mol, 2 equiv.) was dissolved in H_2O (100 mL) and added to the solution. After 1 h of stirring at room temperature, the solution was acidified with HCl (2 M) to a pH~2. The reaction mixture was extracted with diethyl ether (3 x 100 mL) and the organic layer was dried over anhydrous $MgSO_4$. After filtration, the solvent was evaporated under reduced pressure to give the crude product as an orange oil. The pure product [9] was obtained by column

chromatography (SiO_2, eluent CH_2Cl_2) as a colorless oil (3.08 g, 74%). ^1H NMR ($CDCl_3$): δ = 7.15 (d, *J* = 8.2 Hz, 2H); 6.76 (d, *J* = 8.5 Hz, 2H); 5.28 (s, 1H); 3.60 (s, 2H); 1.97 (s, 3H). ^{13}C NMR ($CDCl_3$): δ = 150.3 (C4); 136.9 (C4); 130.7 (CH); 115.9 (C4); 38.3 (CH_2); 15.5 (CH_3).

Step 2: 4-((methylthio)methyl)phenyl 2-bromo-2-methylpropanoate [10]

To a stirred mixture of [9] (3.08 g, 0.020 mol, 1 equiv.) and pyridine (3.16 g, 3.23 mL, 0.040 mol, 2 equiv.) in dichloromethane (CH_2Cl_2) (150 mL), 2-bromo-2-methylpropanoylbromide (5.97 g, 3.21 mL, 0.026 mol) was added dropwise at 0 °C. The reaction mixture was stirred overnight at room temperature. After which the reaction was quenched with water (150 mL) and extracted with CH_2Cl_2 (3 x 150 mL). The organic layer was dried over anhydrous $MgSO_4$, filtered and the solvent was evaporated under reduced pressure to give the crude product [10] as a yellow oil (7 g, quantitative), no purification was needed. ^1H NMR ($CDCl_3$): δ = 7.32 (d, *J* = 8.6 Hz, 2H); 7.06 (d, *J* = 8.6 Hz, 2H); 2.05 (s, 6H); 1.98 (s, 5H). ^{13}C NMR ($CDCl_3$): δ = 170.2 (C4); 149.6 (C4); 136.2 (C4); 129.9 (CH); 121.0 (CH); 55.2 (C4); 37.5 (CH_2); 30.6 (CH_3); 14.9 (CH_3).

Step 3: 4-((methylsulfinyl)methyl)phenyl-2-bromo-2-methylpropanoate [11]

TeO_2 (0.74 g, $4.62 \cdot 10^{-3}$ mol, 0.2 equiv.) and HCl (2 M, 1.5 mL) were added to a stirred mixture of [10] (7.0 g, 0.023 mol, 1 equiv.) in 1,4-dioxane (100 mL). To start the reaction H_2O_2 (35%, 4.24 mL, 0.046 mol, 2 equiv.) was added and the reaction was followed on TLC ($CHCl_3$/petroleum ether: 6/4). When all [10] was reacted, the reaction mixture was quenched with a saturated NaCl-solution:H_2O (1:1; 100 mL). Next, the solution was extracted with CH_2Cl_2 (3 × 150 mL), dried over anhydrous $MgSO_4$ and filtered. The solvent was evaporated under reduced pressure to give the crude product as a yellow oil. The pure product [11] was obtained by crystallization in hexane/EtOAc (3/1; 3 mL/1 g product) as white crystals (7,5 g, 87%). ^{1}H NMR ($CDCl_3$): δ = 7.33 (d, *J* = 8.2 Hz, 2H); 7.16 (d, *J* = 8.6 Hz, 2H); 2.46 (s, 2H); 2.05 (s, 6H). ^{13}C NMR ($CDCl_3$): δ = 162.7 (C4); 143.5 (C4); 123.8 (CH); 120.2 (C4); 114.3 (CH); 51.9 (CH_2); 47.8 (C4); 29.8 (CH_3); 23.2 (CH_3).

7.2.3. General method for anionic sulfinyl polymerization of MDMO-PPV

The anionic polymerization was performed as described in literature procedures.[4,5] Below, the mechanism is presented in Scheme 3 and the synthesis procedure is further explained.

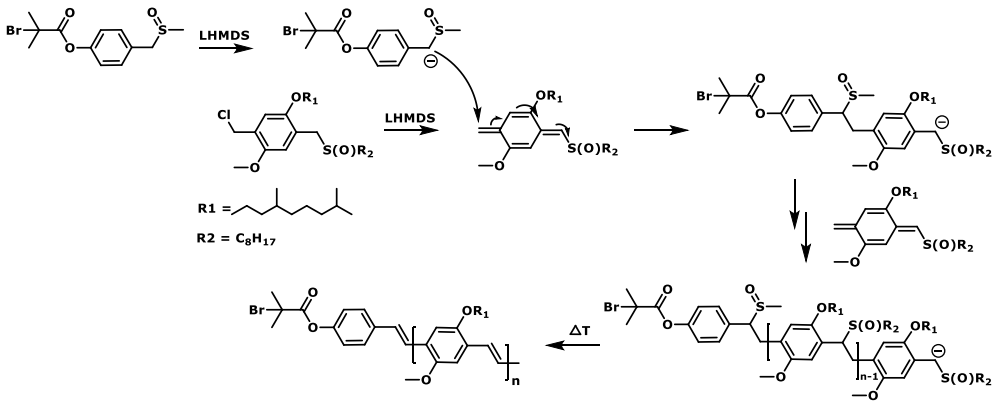

Scheme 3: Mechanism of the anionic sulfinyl polymerization of the MDMO premonomer

The glassware used for the polymerization was dried overnight in an oven and flame dried under vacuum. The MDMO premonomer (0.7 g, 1.437 mmol, 1 equiv.) and the initiator (0.092 g, 0.287 mmol, 0.2 equiv.) are flushed 3 times with N_2-gas and vacuum before they were dissolved in dry THF (32.7 mL) under N_2 atmosphere at 0 °C. To start the polymerization, the base LHMDS (1 M in THF; 1.90 mL, 1.868 mmol, 1.3 equiv.) was added. The reaction mixture was stirred for 15 minutes under N_2 atmosphere at 0 °C, before it was quenched with 50 mL of a 1 M HCl-solution. The reaction mixture was then poured in 50 mL H_2O and extracted with CH_2Cl_2 (3 x 150 mL). The solvent was evaporated under reduced pressure and the precursor polymer was obtained as a yellow sticky oil. To obtain the conjugated polymer, the precursor polymer was dissolved in 40 mL toluene

and stirred for 3 h at reflux temperature (110 °C) under N_2 atmosphere. Afterwards, the reaction mixture was cooled down to room temperature and precipitated in cold MeOH (50 mL). After filtration, the polymer was isolated as a red powder.

7.2.4. Synthesis of the ligand tris[2-(dimethylamino)ethyl]amine (Me_6TREN)

The synthesis of the ligand was performed as described in literature procedures and is presented in Scheme 4.[6] The synthesis procedure is explained in more detail below and characterization of the products was performed *via* NMR.

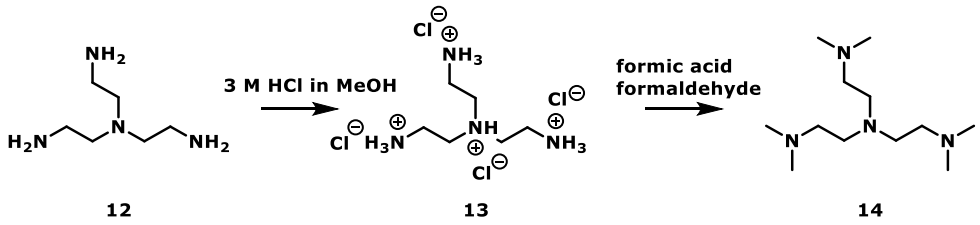

Scheme 4: Synthesis procedure of the ligand Me_6TREN

Step 1: Synthesis of *N,N*-bis(2-aminoethyl)ethane-1,2-diamine [13]

Tris(2-aminoethyl)amine [12] (3.95 g, 4.0 mL, 0.027 mol) is dissolved in 50 mL methanol and 30 mL of 3.0 M HCl in methanol (7.5 mL of 12 M HCl stock solution in 30 mL MeOH) was added dropwise. The reaction mixture was stirred for 1 h at room temperature. The precipitate was filtered and washed 3 times with 50 mL methanol to yield 6.72 g (98% yield) of the product.

Step 2: Synthesis of tris[2-(dimethylamino)ethyl]amine [14]

To a mixture of [13] (6.72 g, 0.026 mol) in 10 mL water, formic acid (50 mL) and formaldehyde aqueous solution (46 mL) were added. The reaction mixture was stirred at reflux temperature (120 °C) for 6 h after which the solvent was removed

under reduced pressure. Next, 100 mL of a 10% NaOH aq. solution was added to the solid residue to achieve a basic solution with a pH>10. The mixture was extracted with diethyl ether (6 x 100 mL) and dried over KOH. The organic solvent was evaporated under vacuum and the product was achieved as a yellow to colorless liquid (6.0 g, 0.026 mol, overall yield 96%). ^{1}H NMR ($CDCl_3$): 2.198 (s, 18H), 2.332-2.369 (m, 6H), 2.560-2597 (m, 6H).

7.2.5. General method for the synthesis of the block copolymer

The synthesis of the block copolymer was performed as described in literature procedures, an example is given here.[7,8] A Schlenk tube was filled with the MDMO-PPV precursor polymer (0.1 g, 1800 g·mol^{-1}, 5.56·10^{-5} mol, 1 equiv.), *n*-butyl acrylate (*n*BuA) (1.43 g, 1.58 mL, 0.011 mol, 200 equiv.) and Me_6TREN (0.028 g, 0.033 mL, 1.22·10^{-4} mol, 2.2 equiv.) dissolved in DMF (1 mL). 5 freeze-pump-taw cycles were performed, where-after the Schlenk tube was transferred into the glovebox. The reaction mixture was transferred into a vial with a stirring bar and Cu(0) (0.004 g, 6.12·10^{-5} mol, 1.1 equiv.) was added. The reaction mixture was stirred for 4 h at room temperature. When the reaction mixture was transferred back out of the glovebox, a ^{1}H NMR sample was taken before the reaction mixture was poured into an Al-tray and the reaction was quenched by the addition of a MeOH/H_2O 4:1 mixture. Next, the polymer was filtered over basic alumina to remove all copper and the solvent was evaporated under vacuum. To obtain the conjugated block copolymer, the precursor block copolymer was dissolved in toluene (40 mL) and stirred for 3 h at reflux temperature (110 °C) under N_2 atmosphere. Afterwards, the reaction mixture was cooled down to room temperature and precipitated in a cold MeOH/H_2O 4:1 mixture. After filtration, the block copolymer was isolated as a red solid.

7.2.6. General method for the hydrolysis of PPV-*b*-P*t*BuA into PPV-*b*-PAA

The hydrolysis of the *tert*-butyl group of the block copolymer was performed as described in literature procedures.[3] The PPV-*b*-P*t*BuA block copolymer (0.1 g, 18900 $g \cdot mol^{-1}$ based on NMR) was dissolved in dry DCM (10 mL) and trifluoroacetic acid (TFA, 16 equiv. relative to the *tert*-butyl acrylate, calculated from NMR results, 0.43 mL) was added. The reaction mixture was stirred overnight at room temperature. The solvent was evaporated and the residue was dissolved in a little bit of THF before it was precipitated in water. After filtration and washing with water, the PPV-*b*-PAA block copolymer was isolated as a red solid.

7.3. Characterization

Proton nuclear magnetic resonance (^1H NMR) spectra were recorded in deuterated chloroform ($CDCl_3$) at room temperature on either a Varian Inova spectrometer at 400 MHz using a 5 mm OneNMR PFG probe (Agilent Technologies Inc, Santa Clara, CA, USA) or on a Jeol 400 Mhz spectrometer. The chemical shifts (δ) are recorded in ppm relative to tetramethyl silane (δ = 0 ppm), referenced to the chemical shift of the residual solvent ($CDCl_3$) resonances (^1H). Spectra were analysed in Mestrenova software.

Size exclusion chromatography (SEC) was used for the analysis of the molecular weight distributions of the polymer and block copolymer samples. The system is a Tosoh EcoSEC HLC-8320GPC, comprising an autosampler, a PSS guard column SDV (50 x 7.5 mm), followed by three PSS SDV analytical linear XL columns (5 µm, 300 x 7.5 mm) and a differential refractive index detector (Tosoh EcoSEC RI) using high-performance liquid chromatography (HPLC) grade tetrahydrofuran (THF) as the eluent at 40 °C with a flow rate of 1 $mL \cdot min^{-1}$. Toluene was used as the flow marker. The SEC system was calibrated using linear narrow polystyrene (PS) standards from PSS laboratories ranging from 474 to 7.5 x 10^6 $g \cdot mol^{-1}$ (PS (K = 14.1 x 10^{-5} $dL \cdot g^{-1}$ and α = 0.70)). Polymer concentrations were in the range of 3-5 $mg \cdot mL^{-1}$. Mark Houwink parameters for plain precursor (α = 0.67605 and K = 0.000142 $mL \cdot g^{-1}$) and conjugated (MDMO)-PPV (α = 0.809 and k = 0.00002 $mL \cdot g^{-1}$) were used. All samples were filtered through a 0.45 µm filter prior to injection.

Ultraviolet-Visible (UV-VIS) spectra were recorded on a Varian Cary 5000 UV-Vis-NIR spectrophotometer (scan rate 600 $nm \cdot min^{-1}$, continuous run from 200 to 800 nm). The samples were measured using chloroform as the solvent.

Attenuated total reflectance - Fourier transform infrared (ATR-FTIR) spectra were collected with a Bruker Tensor 27 FT-IR spectrophotometer (nominal resolution 4 cm^{-1}). Spectra were analysed with OPUS software.

Dynamic light scattering (DLS) was performed using a ZetaPALS equipment (Brookhaven Instruments Cooperation). The average hydrodynamic diameter and the polydispersity index of the nanoparticles were determined in water.

Surface profilometry was measured on a Bruker Dektak XT Profilometer. To determine the film thickness, a scratch was made into the polymer layer and subsequently, the height measuring lever of the profilometer was moved across the scratch. The step height of this scratch, which is the film thickness of the polymer layer was measured.

Atomic force microscopy (AFM) was performed using a Nanoscope Dimension 3100 (Bruker) and a Si tip with an Al backside coating. The measurement was carried out in tapping mode. The three-dimensional (3D) data was processed using the software Gwyddion and the pictures where shown as 2D images.

Scanning probe microscopy (SPM) measurements are performed by Rüdiger Berger, Helma Burg and Uwe Rietzler at the Max Planck Institute (MPIP) for polymer research.

Small angle x-ray scattering (SAXS) measurements are performed and interpreted by Markus Mezger and Julian Mars at the MPIP as well.

7.4. References

[1] F. Louwet, D. Vanderzande, J. Gelan, J. Mullens, *Macromolecules* **1995**, 28, 1330-1331.

[2] H. Becker, H. Spreitzer, K. Ibrom, W. Kreuder, *Macromolecules* **1999**, 32, 4925-4932.

[3] I. Cosemans, J. Vandenbergh, L. Lutsen, D. Vanderzande, T. Junkers, *Polym. Chem.* **2013**, 4, 3471-3479.

[4] I. Cosemans, *PhD thesis*, Universiteit Hasselt **2013**.

[5] N. Zaquen, *PhD thesis*, Universiteit Hasselt **2016**.

[6] L. Feng, J. Hu, Z. Liu, F. Zhao, G. Liu, *Polymer* **2007**, 48, 3616-3623.

[7] I. Cosemans, L. Hontis, D. Van Den Berghe, A. Palmaerts, J. Wouters, T. Cleij, L. Lutsen, W. Maes, T. Junkers, D. Vanderzande, *Macromolecules* **2011**, 44, 7610-7616.

[8] N. Zaquen, P. H. M. Van Steenberge, D. R. D'Hooge, M.-F. Reyniers, G. B. Marin, J. Vandenbergh, L. Lutsen, D. Vanderzande, T. Junkers, *Macromolecules* **2015**, 48, 8294-8306.

Chapter 8

Summary and Outlook

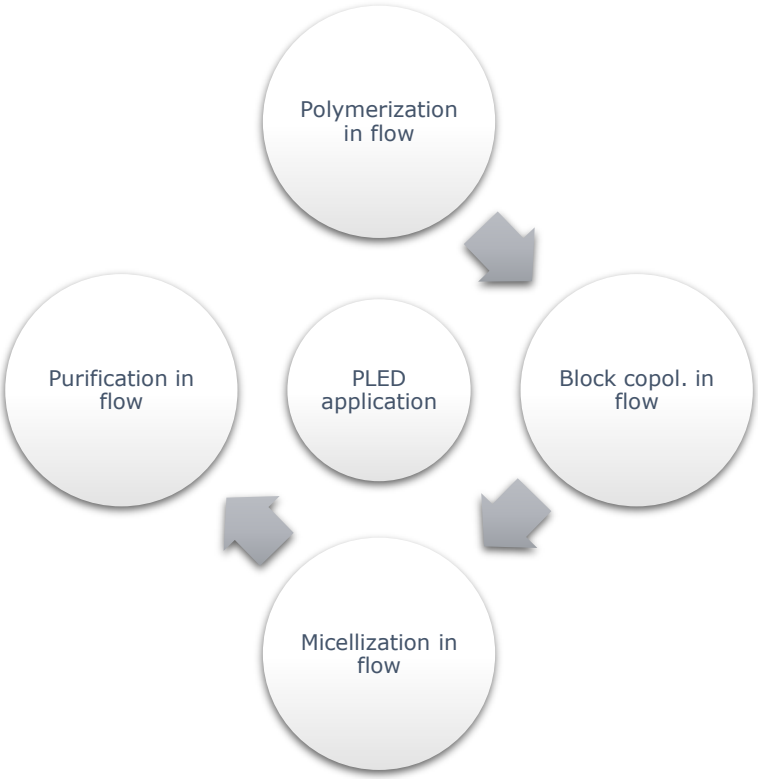

8.1. Summary

Poly(*p*-phenylene vinylene) (PPV) derivatives are well known conjugated polymers with excellent electrical and optical properties, which make them very interesting for the use in electronic applications. Although, PPVs have lost some significance due to the development of new generations of conjugated polymers, they are still one of the most common types of conjugated polymer materials in optoelectronic applications. Their robustness, high reproducibility and controlled synthesis procedures promoted PPVs for the use in a variety of complex polymer architectures. Additionally, their excellent fluorescent and non-toxic properties make PPVs ideal candidates for the use in biomedical applications.

Relatively good control over the synthesis procedure and well-defined end groups of poly[2-methoxy-5-(3',7'-dimethyloctyloxy) -1,4-phenylenevinylene] (MDMO-PPV) were previously achieved by the development of the anionic sulfinyl precursor polymerization. Further improvements towards the control over the molecular weight and dispersity of MDMO-PPV was obtained using continuous flow techniques. Performing the anionic polymerization in continuous tubular reactors under flash chemistry conditions led to the development of low dispersity MDMO-PPV with well-defined end groups. Dispersities of 1.2 could be reached due to very efficient mixing at really low residence times, which would be unachievable in batch reactors.

In a next step, PPV-containing block copolymers were synthesized using single electron transfer-living radical polymerization (SET-LRP) in either batch or flow reactors. In flow reactors, optimal reaction conditions were determined using the polymerization of methyl acrylate (MA) as a benchmark. Ultimately, high temperature SET-LRP was performed for the synthesis of PPV-*b*-PMA block

copolymers with remarkable low residence times. Furthermore, amphiphilic block copolymers could be synthesized, which are able to self-assemble upon the addition of water. These PPV-containing micelles are very appealing for the use in biomedical applications since they can penetrate cells and release their encapsulated payload. Interestingly, the block copolymers show fluorescence, however, when self-assembled, the fluorescence is quenched due to the organization of the conjugated chain segments. Only upon cell uptake the fluorescence becomes visible again since the micelle is decomposed back into the block copolymers. This is a useful feature that can be employed to closely monitor the cell uptake and later to determine the fate of the micelle materials over a longer period. The synthesis of these micelles was performed by turbulent mixing of water and the block copolymer solution in THF, using continuous flow techniques. The ability to self-assemble block copolymers in continuous flow makes it possible to yield kinetically stable micelles not only in high production rates, but also with increased reliability and lower batch-to-batch variation compared to classical batch-wise methods.

Purified micelle solutions became available by the inline dialysis of the organic solvent, used to dissolve the block copolymers. The purification was performed using custom-made dialysis units with a cellulose membrane. A looped flow reactor was constructed wherein, in only a few hours, the organic solvent could be largely reduced, while the quality of the micelles was maintained. Additionally, the water-soluble monomer hydroxyethyl acrylate (HEA) could be removed from the micelle solution and a dye could be encapsulated. The coupling of the micelle formation to its purification in continuous flow make these micelles readily available for the use in biomedical applications.

Lastly, block copolymers were synthesized containing PPV as a first block and butyl acrylate (*n*BuA), butyl methacrylate (*n*BuMA) and tert-butyl acrylate (*t*BuA) as the second block, for the use in polymer light-emitting diode (PLED) applications. The block copolymers were spin-coated on a glass substrate for the formation of thin-films and their nanoscale structural organization is examined. Block copolymers cannot macrophase separate – in contrast with polymer blends – but both covalently bonded blocks tend to demix due to the repulsive interaction between them. As a result, microphase separation can occur, forming microdomains that improve the efficiency of the ion transport within the block copolymer layer. The formation of microdomains require enough repulsion between both blocks, since ordering them into microdomains is accompanied by the loss in entropy. Unfortunately, a rather low microscale order was identified, therefore no further investigations were performed on these block copolymers for PLED devices.

8.2. Outlook

8.2.1. Optimized monomer structures for biomedical applications

This and previous work already showed that amphiphilic PPV-containing block copolymers show excellent self-assembly and payload uptake, and that these are ideal inherently-fluorescent carriers for biomedical application. Such micelles are able to penetrate into cancer cells and release their encapsulated drug payload. While experiments proof that delivery to the cell works well and that unloaded micelles are not cytotoxic, not much is known about the fate and transport of the micelles in and around the cell before and after payload delivery. Additionally, the block copolymers show fluorescence, however, when self-assembled, the fluorescence is quenched due to the organization of the conjugated chain segments. Only upon cell uptake the fluorescence becomes visible again. This is a useful feature that can be employed to determine the fate of the micelle materials over a longer period of time.

So far, only a proof-of-concept study is provided for the PPV block copolymers and non-optimized monomer structures have been used. Further development of the concept to a mature technique is required. To reach this aim, novel phenylene vinylene (pre-)monomers that are specifically designed for biomedical use should be synthesized. With these novel materials at hand, micellation accompanied with cell tests will aid in the elucidation of the transport mechanism of the micelles into the cells as well as the fate of their decomposition products over a longer period of time. Such tests are of high importance for the general understanding of processes *in vivo, but* will also provide a basis for advanced use (and hence valorization) of the PPV-based micellar drug delivery platform.

There is a need to design new monomers with a broader fluorescence range and a higher quantum yield compared to MDMO-PPV used in this work. One way to achieve this aim is to build-in aromatic rings in the side chains, enabling delocalization of the electrons in the polymer chain, such as in poly[2,5-bis(2',5'-bis(2''-ethylhexyloxy)phenyl)-p-phenylene vinylene] (BBEHP-PPV) or to build-in an additionally fluorophore in the side chain. BBEHP-PPV is expected to lead to increased quantum yields, due to the presence of aromatic rings in the side chain, enabling delocalization of the electrons. The pendent aromatic rings with the hydrocarbon side chains encapsulate the polymer backbone, which provides a protective layer that will prevent self-quenching and increase the resistance to photo-bleaching. In addition, the long hydrocarbon side chains ensure solubility of the monomer in organic solvents and easy work up during the synthesis.
Another interesting monomer to investigate would be an amide-functionalized PPV because of the expected interesting self-assembly behavior, caused by the hydrogen bonds present, which ultimately will lead to more stable micelles.

8.2.2. Continuous flow synthesis

In this work the synthesis of the PPV polymer, block copolymer and micelles in flow is discussed for all these steps separately. It would be interesting to investigate the possibility to couple the separate synthesis steps and make a cascade of multiple reactors. A first step would be to synthesize the block copolymer in a coupled process, which would require three reactors in a cascade. The first reactor will be fed with the premonomer and base solutions, after which the PPV prepolymer is formed. This prepolymer is used as a new feeding stream together with the feeding stream of the vinylic comonomer, starting the SET-LRP chain extension. Lastly, a third reactor is coupled to perform the elimination

reaction at elevated temperatures. The coupling of reactors is not that straightforward as one would think since for each step in this cascade different solvents are used, which implies that the cascade would also involve some solvent switchers/evaporators. Eventually, the micelle formation and dialysis could be added to the cascade to make the process complete. In this way, five different reactors would be coupled in a cascade, starting from monomers and ending up with purified micelles.

8.3. Samenvatting

Poly(*p*-fenyleenvinyleen) (PPV) derivaten zijn bekende geconjugeerde polymeren met uitstekende elektrische en optische eigenschappen, die hun erg interessant maken voor het gebruik in elektronische toepassingen. Hoewel PPV's wat aan belang hebben verloren door de ontwikkeling van nieuwe generaties van geconjugeerde polymeren, zijn ze nog altijd een van de meest voorkomende soorten van geconjugeerde polymere materialen in opto-elektronische toepassingen. Hun robuustheid, hoge reproduceerbaarheid en gecontroleerde synthese procedures bevorderde PPV's voor het gebruik in een verscheidenheid aan complexe polymeerarchitecturen. Bovendien maken hun uitstekende fluorescerende en niet-toxische eigenschappen PPV's ideale kandidaten voor het gebruik in biomedische toepassingen.

Relatief goede controle over de synthese procedure en goed gedefinieerde eindgroepen van poly[2-methoxy-5-(3',7'-dimethyloctyloxy) -1,4-phenylenevinylene] (MDMO-PPV) werden eerder bereikt door de ontwikkeling van de anionische sulfinyl precursorpolymerisatie. Verdere verbeteringen in de controle van het molecuulgewicht en de dispersiteit van MDMO-PPV werden verkregen met behulp van flowreactoren. Het uitvoeren van de anionische polymerisatie in flowreactoren leidde tot de ontwikkeling van lage dispersiteit MDMO-PPV met goed gedefinieerde eindgroepen. Dispersiteiten van 1.2 konden worden bereikt door het zeer efficiënt mengen bij zeer lage verblijftijden, hetgeen niet haalbaar zou zijn in batchreactoren.

In een volgende stap werden de PPV-bevattende blokcopolymeren gesynthetiseerd met behulp van single elektron transfer-living radicaal polymerisatie (SET-LRP) in batch- of flowreactoren. In flowreactoren werden de

optimale reactieomstandigheden bepaald door de polymerisatie van methylacrylaat (MA) te gebruiken als ijkpunt. Uiteindelijk werd de SET-LRP-reactie op hoge temperatuur uitgevoerd voor de synthese van de PPV-*b*-PMA blokcopolymeren met opmerkelijk lage verblijftijden. Bovendien werden amfifiele blokcopolymeren gesynthetiseerd, die zelf-assembleren na toevoeging van water. Deze PPV-bevattende micellen zijn zeer interessant voor het gebruik in biomedische toepassingen, omdat ze in cellen kunnen doordringen en hun ingekapselde lading kunnen vrijgeven. Interessant is dat de blokcopolymeren fluorescentie vertonen, maar wanneer ze zelf-assembleren, wordt de fluorescentie verminderd door de organisatie van de geconjugeerde ketensegmenten. Pas bij de cel opname wordt de fluorescentie weer zichtbaar, aangezien de micel weer wordt afgebroken tot de blokcopolymeren. Dit is een handige functie die kan worden gebruikt om de cel opname nauwlettend te volgen en om later het lot van de micelmaterialen over een langere periode te bepalen. De synthese van deze micellen werd uitgevoerd door het uitvoerig mengen van water en de blokcopolymeeroplossing in THF, met behulp van flowreactoren. Het zelf-assembleren van blokcopolymeren in flowreactoren, maakt het mogelijk om kinetisch stabiele micellen te produceren, niet alleen met hoge productiesnelheden, maar ook met verhoogde betrouwbaarheid en lagere batch-tot-batch-variatie in vergelijking met klassieke batchgewijze methoden.

Gezuiverde miceloplossingen werden beschikbaar door de inline dialyse van het organische oplosmiddel, dat werd gebruikt om de blokcopolymeren op te lossen. De zuivering werd uitgevoerd met op maat gemaakte dialyse-eenheden met een cellulosemembraan. Er werd een doorstroomreactor geconstrueerd waarin, in slechts enkele uren, het organische oplosmiddel grotendeels kon worden

verwijderd, terwijl de kwaliteit van de micellen behouden bleef. Bovendien kon het in wateroplosbare monomeer hydroxyethyl acrylaat (HEA) uit de miceloplossing worden verwijderd en kon een kleurstof worden ingekapseld. De koppeling van de micelvorming aan de zuivering in flowreactoren maakt deze micellen gemakkelijk beschikbaar voor gebruik in biomedische toepassingen.

Ten slotte werden blokcopolymeren gesynthetiseerd met PPV als een eerste blok en butylacrylaat (nBuA), butylmethacrylaat (nBuMA) en tert-butylacrylaat (tBuA) als het tweede blok, voor gebruik in polymere licht emitterende diode (PLED) toepassingen. De blokcopolymeren werden door middel van spincoating op een glazen substraat aangebracht voor de vorming van dunne films en hun nanoschaal structurele organisatie werd onderzocht. Blokcopolymeren kunnen macroscopisch niet fase scheiden - in tegenstelling tot polymeermengsels - maar beide covalent gebonden blokken hebben de neiging om te ontmengen vanwege de afstotende interactie daartussen. Als resultaat kan microscopische fasescheiding optreden, waarbij microdomeinen worden gevormd die de efficiëntie van het ionentransport binnen de blokcopolymeerlaag verbeteren. De vorming van microdomeinen vereist voldoende afstoting tussen beide blokken, aangezien het ordenen van microdomeinen gepaard gaat met verlies aan entropie. Helaas werd een tamelijk lage microschaalorde waargenomen, waardoor er geen verder onderzoek gedaan werd naar deze blokcopolymeren voor PLED-apparaten.

List of Abbreviations

°C	degrees Celsius
ΔT	elevated temperature
α	Mark-Houwink constant
κ	Mark-Houwink constant
λ	wavelength
λ_{max}	wavelength at maximum absorbance
ρ	density
μ	viscosity
δ	chemical shift
χ	Flory-Huggins parameter
^1H	proton
AFM	atomic force microscopy
AIBN	1,1'-azobis(isobutyronitrile)
ATR	attenuated total reflectance
ATRP	atom transfer radical polymerizations
BEH-PPV	poly[2,5-bis(2'-ethylhexyloxy)-1,4-phenylenevinylene]
Br	bromine
Ca	calcium
$CDCl_3$	deuterated chloroform
CH_3	methyl
CH_2Br_2	dibromomethane
CH_2Cl_2	dichloromethane
$CHCl_3$	chloroform
CN-PPV	poly[(2,5-dicyano)-1,4-phenylenevinylene]

CPM-PPV	poly[2-methoxy-5-(carboxypentyloxy)-1,4-phenylenevinylene]
Cu	copper
Cu(II)Br_2	copper(II) dibromide
d	dimensions
D	diameter
Đ	dispersity
Da	dalton
DLS	dynamic light scattering
DMF	dimethylformamide
DMSO	dimethyl sulfoxide
DNA	Deoxyribonucleic acid
DoPAT	2-(Dodecylthiocarbonothioylthio)propionic acid
DP	degree of polymerization
EBiB	ethyl-2-bromoisobutyrate
E_g	bandgap
equiv	equivalents
EtOAc	ethyl acetate
EtOH	ethanol
eV	electron volt
f	volume fractions
FDA	food and drug administration
FET	field-effect transistors
FT-IR	Fourier transform infrared spectroscopy
h	hour
HEA	hydroxyethyl acrylate

HCl	hydrochloric acid
H_2O	water
H_2O_2	hydrogen peroxide
HOMO	highest occupied molecular orbital
H_2SO_4	sulfuric acid
I	initiator
ID	internal diameter
ITO	indium-tin oxide
k_{act}	activation rate constant
k_d	decomposition rate constant
k_{deact}	deactivation rate constant
k_i	initiation rate constant
KOH	potassium hydroxide
k_p	propagation rate constant
k_t	termination rate constant
k_{tr}	chain transfer rate constant
L	ligand
L_0	natural period
LED	light-emitting diode
LHMDS	lithium bis(trimethylsilyl)amide
Li	lithium
LiF	lithium fluoride
LUMO	lowest unoccupied molecular orbital
M	molar
MA	methyl acrylate

MDMO-PPV	poly[2-methoxy-5-(3',7'-dimethyloctyloxy)-1,4-phenylenevinylene]
MEH-PPV	poly[2-methoxy-5-(2'-ethylhexyloxy)-1,4-phenylenevinylene]
MeOH	methanol
Me_6TREN	tris[2-(dimethylamino)ethyl]amine
Mg	magnesium
$MgSO_4$	magnesium sulfate
Mhz	megahertz
min	minute
M_n	number average molecular weight
$M_{n,T}$	theoretical molecular weight
Mt	metal
M_w	weight average molecular weight
N	number of monomers in the block copolymer
N_2	nitrogen
NaCl	sodium chloride
NaOH	sodium hydroxide
NaOtBu	sodium *tert*-butoxide
NaSMe	sodium thiomethoxide
*n*BuA	butyl acrylate
*n*BuMA	butyl methacrylate
NIR	near infrared
N_{mean}	number mean diameter
NMP	nitroxide-mediated polymerizations
NMR	nuclear magnetic resonance

OD	outer diameter
OLED	organic light emitting diode
OPV	organic photovoltaics
p	monomer to polymer conversion
P	polymer
PAA	poly(acrylic acid)
PAV	poly(arylene-vinylene)
PBA	poly(butyl acrylate)
PCBM	Phenyl-C61-Butyric acid Methyl ester
PEDOT	poly(3,4-ethylenedioxythiphene)
PEEK	poly(ether ether ketone)
PEG	poly(ethylene glycol)
PEGMA	poly(ethylene glycol methyl ether methacrylate)
PFA	perfluoro alkoxy
PHEA	poly(2-hydroxyethyl acrylate)
PHPMA	poly(2-hydroxypropyl methacrylate)
PI	polyisoprene
PISA	polymer induced self-assembly
PLA	poly(lactic acid)
PLED	polymer-based light emitting diode
PMA	poly(methyl acrylate)
PMMA	poly(methyl methacrylate)
P_n^*	polymer radical
P_n-X	dormant polymer
ppm	parts per million
PPV	poly(*p*-phenylene vinylene)

PS	polystyrene
PSI	pound-force per square inch
PSS	poly(styrene sulfonate)
P*t*BuA	poly(*tert*-butyl acrylate)
PTFE	polytetrafluoroethylene
QD	quantum dots
R	radical
RAFT	reversible addition-fragmentation chain transfer
R&D	research and development
RDRP	reversible-deactivation radical polymerization
Re	Reynolds number
ROMP	ring opening metathesis polymerization
RT	room temperature
SAXS	scanning probe microscopy
sec	second
SEC	size exclusion chromatography
SET-LRP	single electron transfer living radical polymerization
SiO_2	silicon dioxide (silica)
SPM	scanning probe microscopy
St	styrene
*t*BuA	*tert*-butyl acrylate
TeO_2	tellurium dioxide
THF	tetrahydrofuran
THT	tetrahydrothiophene
TLC	thin layer chromatography
UV-VIS	ultraviolet-visible

v	flow rate
v/v%	volume/volume percent
X	chain transfer agent or halogen
X_n	number average degree of polymerization

Publications and Personal Contribution

Publications

A. Buckinx, K. Verstraete, E. Baeten, R. F. Tabor, A. Sokolova, N. Zaquen, T. Junkers, *Kinetic control of aggregation shape in micellar self-assembly, Angew. Chem., Int. Ed*. **2019**, 58, 13799.

- Synthesis of PPV micelles
- Writing supporting information

K. Verstraete, N. Zaquen, T. Junkers, *Flash-synthesis of low dispersity PPV via anionic polymerization in continuous flow reactors and block copolymer synthesis, Polym. Chem.*, **2020**, 11, 7094-7103.

- Article writing
- All synthetic work, characterization and analysis

K. Verstraete, A. Buckinx, N. Zaquen, T. Junkers, *Micelle purification in continuous flow via inline dialysis, Macromolecules* **2021**, 54, 8, 3865-3872.

- Article writing
- Synthetic work, characterization and analysis

Conferences: poster presentations

K. Verstraete, A. Buckinx, E. Baeten, N. Zaquen, T. Junkers, *Robust block copolymer micelle formation and in-line purification in continuous flow,* Annual Meeting of the Belgian Polymer Group, May 2018, Blankenberge.

K. Verstraete, N. Zaquen, T. Junkers, *Poly(p-Phenylene Vinylene) (Block Co)Polymers via Anionic Polymerization / SET-LRP in Continuous Tubular Reactors*, Annual Meeting of the Belgian Polymer Group, May 2019, Houffalize.

K. Verstraete, N. Zaquen, T. Junkers, *Novel PPV Block Copolymers from Continuous Tubular Reactors Designed for Biomedical Use,* Chemistry Conference for Young Scientists (ChemCYS), February 2020, Blankenberge.

Dankwoord

Beste lezers, we naderen het einde van deze thesis, wat ook meteen het einde van mijn doctoraat betekend. Een vreemd gevoel, bijna niet te vatten dat dit hoofdstuk al bijna om is. Deze 4 jaar zijn werkelijk omgevlogen en nu is het moment gekomen om jullie allemaal in de bloemetjes te zetten, want jullie hebben stuk voor stuk bijgedragen om mijn doctoraat tot een goed einde te brengen.

First, I would like to thank my promotor Tanja. Without you and the PhD project you were offering, I would never even have started a PhD. But off course, starting was one thing, finishing was still far away. Thanks to your confidence in me and the project I was able to persevere in more difficult times and finally bring this chapter in my life to a good end. Although you were most of the time on the other side of the world with 8 to 10 hours of a time difference, you kept involving the 'PRD UHasselt branch' and always made time whenever we needed you. It was not always easy for both sides, but I am grateful this worked out really well and that is all thanks to your efforts.

Graag wil ik ook mijn copromotor, Dirk, bedanken voor al de hulp bij de monomeersynthese. Je wist altijd wel raad, niemand die zoveel afweet van PPV's als jij. Bedankt om me erop te wijzen initiatief te nemen en te blijven vragen om hulp (ook al vraag je dit aan een zeer drukbezet persoon).

Neomy, jou wil ik ook ontzettend hard bedanken voor alle hulp doorheen heel mijn doctoraat. Je bleef altijd meedenken, ik kon je allerlei vragen stellen, zelfs al had je het heel druk met andere projecten (aan de andere kant van de wereld) of had

je zelfs een nieuwe job. Dank je voor de talrijke meetings en verbeteringen, ongelofelijk hoe jij je blijft inzetten terwijl je het zelf al ontzettend druk hebt. Ik wil je echt heel erg bedanken, want dat is niet vanzelfsprekend wat jij gedaan hebt!

Ik wil graag alle juryleden bedanken om mijn thesis te lezen en deel te nemen aan mijn verdediging, dit wordt van harte geapprecieerd. Jasper, jou wil ik ook persoonlijk bedanken voor de leuke samenwerking en tijd in het MPIP in Mainz. Ik heb heel wat bijgeleerd en erg genoten van de warme ontvangst in je onderzoeksgroep.

Ik wil de universiteit bedanken voor de financiering van mijn doctoraat de afgelopen 4 jaar. With this I would also like to thank Laurence for the budgetary aspects.

Aan al mijn OBPC-collega's, bedankt voor de fijne tijd samen! Het was een plezier om met jullie in het labo te staan en op 'de grote bureau' te zitten, het verveelde er nooit. In het bijzonder wil ik graag alle PRD-leden bedanken zowel in Hasselt als in Australië voor de fijne tijd en samenwerkingen. Verder mijn speciale dank aan Evelien (de 'manager' van de grote bureau, je stond altijd klaar voor iedereen en extra dank om in mijn jury te zitten!), Tom C. (om de 'nieuwe manager' te worden en zoveel extra's op je te nemen), Pieter (om heel het labo draaiende te houden), Sam (voor het organiseren van de gezamenlijke activiteit en het etentje), Paul-Henry (bedankt voor je humor, maar ook voor de diepzinnige gesprekken en het nalezen van een hoofdstuk!), Martijn (bedankt om lab verantwoordelijke te zijn!), Wouter (dankzij jou bleef de glovebox operationeel, merci!).

Een hele grote dankjewel aan alle collega's van de C108A! Bij jullie bloeide ik open en kon ik mezelf zijn. Heel erg bedankt allemaal voor de fijne gesprekken die ik met iedereen gehad heb, ik ga jullie heel erg missen! Bedankt Erika, Svitlana, Lowie, Greg, Jeroen V, Jeroen DN, Sofie, Bryn, Apostolos, Mariana, Mahsa.
Ik wil ook de Belgische PRD-collega's in Australië extra bedanken voor de fijne momenten en in het bijzonder Axel, merci voor de goede en fijne samenwerking bij onze gezamenlijke projecten en het nalezen van de thesis hoofdstukken.

Speciale dank aan de laatste PRD'ers aan de UHasselt, Greg en Lowie. Toen we nog met z'n drietjes waren, was het wel een raar gevoel, het einde was echt nabij… Greg, bedankt voor je ongelooflijke vriendelijkheid, je aanstekelijke positiviteit, alle cadeaus die je voor iedereen kocht, je (sportieve) motivatie en het nalezen van bijna mijn volledige thesis! Lowie, bedankt voor het organiseren van groepsuitjes, de extra overnachting + brouwerijtoer in Houffalize en de steun de laatste maanden wanneer we in hetzelfde schuitje vertoefde. We moeten snel nog eens een Chouffke gaan drinken!
Ook wil ik Sofie extra bedanken en niet alleen voor het nalezen van mijn introductie. Als eerste AFP'er hebben we je proberen te betrekken bij onze groepsactiviteiten, want we hadden je er maar al te graag bij! Bedankt voor je positiviteit en gezelligheid, het is zeer aangenaam om in je gezelschap te vertoeven, dus blijf zeker wie je bent!
Ook Elien wil ik graag bedanken voor de gezellige babbeltjes op de bureau of in de gang en voor het organiseren van de supertoffe wandeling! Ik hoop dat we dit nog vaker kunnen doen.

De studenten Axel, Dries en Nele die ik heb mogen begeleiden, heel erg bedankt voor jullie inzet en fijne samenwerking!
Gunter en Koen, ik wil jullie heel erg bedanken voor het zeer zorgvuldig meten van de vele NMR's en voor de extra aandacht die jullie geven aan speciale metingen. Huguette, jou wil ik bedanken voor de uitleg bij de UV-VIS, fluorescentie en FT-IR metingen.

Tenslotte wil ik mijn familie en vrienden bedanken voor de jarenlange steun bij mijn studies en de interesses die steeds weer getoond werden. Mama en papa, jullie wil ik in het bijzonder bedanken, want zonder jullie steun was ik nooit zover geraakt. Ik ben jullie zo ontzettend dankbaar voor alle kansen die ik van jullie gekregen heb! Ook Gunter, mijn lieve broer(tje), harde werker en creatieveling, bedankt om er altijd te zijn (en voor de lekkere pralines, ideaal voor tijdens het schrijven 😉)!
Dries, jij komt helemaal achteraan het rijtje, maar je weet wat dat betekent… Bedankt liefje om er altijd voor mij te zijn en om me te steunen wanneer ik na 5 jaar studies er nog 4 jaar aan vast ging breien. Je staat altijd voor me klaar, als het even wat moeilijker gaat met een dikke knuffel of wanneer we iets te vieren hebben met een glaasje bubbels. Bedankt voor alles!

Bedankt allemaal!!